Investigation on the physical properties of unconventional nematic liquid crystals

A Thesis submitted to University of Hyderabad for the award of the degree of

Doctor of Philosophy

in Physics

by

Paladugu Sathyanarayana
(07PHPH08)

School of Physics

University of Hyderabad

December 2012

Family & Friends

Declaration

I, Paladugu Sathyanarayana, hereby declare that the work presented in this thesis has been carried out by me under the supervision of Dr. Surajit Dhara, School of Physics, University of Hyderabad, Hyderabad, India, as per the Ph.D. ordinances of the University. I declare, to the best of my knowledge, that no part of this thesis has been submitted for the award of a research degree of any other University.

(Paladugu Sathyanarayana)
Reg. No: 07PHPH08.

Certificate

This is to certify that the thesis work entitled **Investigation on the physical properties of unconventional nematic liquid crystals** being submitted to the University of Hyderabad by **Paladugu Sathyanarayana** (Reg. No. 07PHPH08), for the award of the degree of Doctor of Philosophy in Physics, is a record of *bonafide* work carried out by him under my supervision.

The matter embodied in this report has not been submitted to any other University or Institution for the award of any degree or diploma.

<div align="right">

Dr. Surajit Dhara,
Thesis Supervisor,
School of Physics,
University of Hyderabad.

</div>

Dean,
School of Physics,
University of Hyderabad.

A word of Gratitude

During the past five years at the university, I had the chance to meet lots of new and interesting people. Through discussions with people in my surroundings I was able to gain new insights and ideas or overcome problems I had encountered in the course of my work. Sometimes the interactions were not exclusively work-related and in those times I enjoyed the company of these people. All of them helped me in a certain way. Therefore, it is impossible to thank every single one personally. Nevertheless, a few people deserve a personal thank you.

First and foremost I would like to thank my thesis advisor Dr. Surajit Dhara. His direction and knowledge were an invaluable part of this process. I admire his candour about my strengths and weaknesses.

I am grateful to Prof. V. S. S. Sastry and Prof. K. P. N. Murthy for many valuable academic discussions and suggestions. I take this opportunity to thank Prof. S. N. Kaul, Prof. S. R. Shenoy, Prof. M. Sivakumar and Prof P. K. Suresh for theoretical course-work at the beginning of my research career. I am grateful to Prof. S. Dutta Gupta and Dr. S. Srinath for helping me in various ways.

I thank Prof. Ivan Smalyukh for giving me an opportunity to attend I-CAMP'12 summer school. I also thank all the collaborators for providing the samples.

I have been fortunate to have Dr. T. Arun Kumar as my senior. He has given me invaluable feedback and has helped refine my work. I learned many scientific aspects as well as about various other techniques from him.

I would like to extend my warm thanks to all my other lab-mates M. Eswara Reddy, J. Ananthaiah, B. Uday Kumar and Venkata Sai for their assistance. I wish all the best to young juniors M. V. Rasna, Rasmita Sahoo and K. P. Zuhail.

I am happy to acknowledge Dr. Trivikram Rao, Dr. Sai Preeti, Dr. Jayasri, Dr. Rajeswari and Kamala Latha for their support and guidance.

I thank former Deans, Prof. Vipin Srivatsava and Prof. C. Bansal and present Dean, Prof. S. P. Tewari, for providing needful facilities, and all the other faculty members of School of Physics for their enlightening suggestions.

Preface

Liquid Crystal Displays (LCDs) play significant role in display information. There are various types of LCDs available in the market. Almost all liquid crystal displays use nematic liquid crystal mixtures and plenty of scopes are there to improve them. Effective liquid crystal mixture should show chemical and photochemical stability, wide temperature range of operation, low viscosity, optimized electric and optical parameters and ability to be oriented by solid surfaces. To fulfil these requirements, it is necessary to understand the relation between physical properties and the structure of molecules. The electrooptic properties of liquid crystals strongly depend upon the viscoelastic properties. Elastic constants are molecular parameters and describes the restoring forces in a liquid crystalline medium when an external field distorts the medium from its ground state, whereas rotational viscosity describes the rotation of molecule around an axis perpendicular to the local director. Several molecular structures were designed to cover a wide range of elastic properties. In the past few years, bent-core liquid crystals have created immense interest in the scientific community because they show several new liquid crystalline phases along with some known phases of calamitic liquid crystals. Concomitantly efforts are made to synthesize liquid crystal with unconventional shapes like, V, W, T etc. Many physical properties of these new liquid crystals are not yet understood. This thesis is an attempt to study the structure-property correlation of unconventional nematic liquid crystals. We have constructed experimental setup to measure various physical parameters of liquid crystal mixture of rod-like and bent-core molecules, pure bent-core molecules, hockey stick shaped (asymmetric bent-core) and T-shaped molecules.

The **first chapter** consists of a brief introduction to the liquid crystals and the physical properties that are relevant in later chapters. We also discuss about various alignment of liquid crystals in cells in this chapter.

The **second chapter** consists of all experimental techniques used for measuring the physical properties of liquid crystals. All the phase transitions are observed using optical polarizing microscope. Experimental techniques used for measurements of sample thickness (d), birefringence (Δn), dielectric constants ($\varepsilon_{||}$, $\varepsilon_{\perp}$), splay (K_{11}) and bend (K_{33}) elastic constants, rotational viscosity (γ_1) and flexoelectric coefficients are

explained briefly.

In the **third chapter** we study the temperature dependence of birefringence (Δn), splay (K_{11}), bend (K_{33}) elastic constants and rotational viscosity (γ_1) of various concentrations of the above mixture. We found that K_{11} and Δn remains almost constant for all the concentrations, whereas K_{33} is always lower than K_{11} and further decreases with increasing concentration of bent-core compound in the mixtures. Apart from a large jump in Δn at the nematic-isotropic transition (NI) a significant jump in Δn at the nematic-smectic transition (NS) is also observed that increases with increasing mol % of the bent-core compound in the mixtures. Rotational viscosity increases by a factor of four when the concentration of the bent-core compound is increased from 0 to 10 mol %. The results are discussed on the basis of their structural similarity and mutual alignment in the nematic phase.

The **fourth chapter** consists of measurements of the temperature variation of physical properties in ambient-temperature nematic liquid crystal mixture of bent-core (BC) and rod-like molecules (5CB). We measured temperature dependence of birefringence (Δn), static dielectric constants ($\varepsilon_{||}$) and ($\varepsilon_{\perp}$), splay (K_{11}) and bend (K_{33}) elastic constants, rotational viscosity (γ_1) and diffusion coefficients ($D_{||}$ and $D_{\perp}$) of a microsphere. Both Δn and $\varepsilon_{||}$ decrease rapidly with increasing BC concentration, whereas $\varepsilon_{\perp}$ remains almost constant. At a shifted temperature (e.g., $T - T_{NI} = -10$ °C, where T_{NI} is isotropic-nematic transition temperature), K_{11} increases by $\sim 50\%$ and K_{33} decreases by $\sim 80\%$ compared to pure 5CB when the BC concentration is increased to ~ 43 mol %. Viscosities parallel and perpendicular to the director ($\eta_{||}$, $\eta_{\perp}$) which are nearly equal to the Miesowicz viscosities η_2 and η_3, respectively, were obtained by $D_{||}$ and $D_{\perp}$ using the Stokes-Einstein relation. Both the viscosities at room temperature increase by 60 and 50 times, respectively, whereas γ_1 increases by 180 times (at ~ 43 mol %) compared to the corresponding values of pure 5CB. The stiffening of K_{11} and exorbitantly large enhancement in all the viscosities at a higher mol % of bent-core compound indicates that the viscoelastic properties are highly impacted by the presence of smectic clusters of BC molecules that result from the restricted free rotation of the molecules along the bow axis in the nematic phase. A possible attachment model of smectic type clusters of BC molecules surrounding the microparticle

is presented.

In the **fifth chapter** we study the physical properties of a *pure* bent-core nematic liquid crystal. We show that in the vicinity of the nematic-isotropic transition temperature K_{33} is proportional to the square of the order parameter. In the nematic range K_{11} increases monotonically with decreasing temperature, whereas K_{33} is practically independent of temperature and is smaller than K_{11}. K_{33} exhibits a pretransitional slow divergence toward the smectic transition temperature and becomes slightly larger than K_{11}. The small K_{33} is explained on the basis of strong coupling of the bent shape of the molecules with the bend distortion. Measurement of the rotational viscosity is performed by measuring the decay time of the optical phase retardation of the sample. In the nematic phase, $\gamma_1 \simeq 0.25$ Pa s (e.g., at $T - T_{NI} \simeq -35\,°\text{C}$), which is only slightly larger than the values known for several conventional calamitic nematic liquid crystals. γ_1 starts to increase rapidly below a reduced temperature, $T - T_{NI} \simeq -45\,°\text{C}$ showing the effect of short-range smectic fluctuations. The temperature dependence of γ_1 far from the nematic to smectic-C transition temperature is fitted well with the Osipov-Terentjev theory.

The **sixth chapter** consists of measurement of birefringence, dielectric constant, splay and bend elastic constants and rotational viscosity in the nematic phase (N) of a hockey stick-shaped compound exhibiting smectic-A (SmA) and anticlinic smectic-C (SmC_a) phase transitions at lower temperature. It is found that the physical properties are significantly different than calamitics and partially similar to the bent-core liquid crystals. It exhibits the positive dielectric and the negative elastic anisotropy. The optical and the thermal measurements show that all the transitions are first order. The rotational viscosity is comparatively higher than that of calamitic liquid crystals and exhibits weak pre-transitional divergence. The temperature dependent static dielectric measurements indicate antiparallel correlation of both the longitudinal and the transverse components of dipole moments in the two smectic phases. The parallel component of the dielectric constant exhibits a single Debye type relaxation in all the phases. The activation energy in the nematic, SmA and SmC_a phases are comparatively larger than that of the respective phases of calamitic liquid crystals and can partially be attributed to the higher rotational viscosity of the hockey stick-shaped

molecules.

The **seventh chapter** consists of measurement of splay K_{11} and bend K_{33} elastic constants in the nematic phase of a liquid crystal with T-shaped molecules. We find that the ratio, K_{33}/K_{11} is $\simeq 1$ in the entire nematic range except very close to the nematic to SmA (SN) transition. Both K_{33} and K_{11} show pretransitional divergence as the SN transition is approached from higher temperature. The ratio, K_{33}/K_{11} suggests that the length L to effective width D ratio i.e., L/D is significantly smaller due to the presence of long and flexible lateral group, compared to that of rigid rodlike molecules. It is argued that apart from the extra contribution to the elasticity the long and flexible lateral group also has a significant contribution to the suppression of the splay fluctuations at the onset of smectic short-range fluctuations. The structure of the SmA phase is also investigated using small angle X-ray diffraction, and a possible arrangement of the molecules in the SmA layer is proposed.

In the last chapter (**eighth chapter**) we study the temperature variation of flexo-elastic coefficient (e^*/K) of a host calamitic liquid crystal (RO) and its mixture with two guest bent-core (BC-120 and BC-60) liquid crystals. These bent-core (BC) molecules have different core structures and their bent angles are $\theta \simeq 120°$ and $\simeq 60°$ respectively. We find that e^*/K is independent of temperature and decreases rapidly with increasing concentration of BC-120 molecules and changes sign from positive to negative. In mixtures with BC-60, e^*/K is always positive and its concentration dependent variation is not unique. At 7 mol % it is significantly large (3 times) near the nematic-isotropic transition and decreases strongly with reducing temperature. Dielectric measurement suggests antagonistic orientation of the dipole axes (arrow axes) of the two BC molecules in the host liquid crystal and based on this the opposite sign of e^*/K is explained.

Contents

List of Figures

List of Tables

List of Symbols

List of symbols frequently used in this thesis

N	Nematic phase
SmA	Smectic-A phase
SmC	Smectic-C phase
SmC$_a$	Anticlinic smectic-C phase
$\hat{n}$	Liquid crystal director
S	Scalar order parameter
ITO	Indium tin oxide
$\Delta\Phi$	Optical phase difference
n_o	Ordinary refractive index
n_e	Extraordinary refractive index
$n_{\parallel}$	Refractive index parallel to $\hat{n}$
$n_{\perp}$	Refractive index perpendicular to $\hat{n}$
$\Delta n = n_e - n_o$	Birefringence
$\varepsilon_{\parallel}$	Dielectric constant parallel to $\hat{n}$
$\varepsilon_{\perp}$	Dielectric constant perpendicular to $\hat{n}$
$\Delta\varepsilon = \varepsilon_{\parallel} - \varepsilon_{\perp}$	Dielectric anisotropy
$\langle\varepsilon\rangle = (\varepsilon_{\parallel} + 2\varepsilon_{\perp})/3$	Average dielectric constant

$\varepsilon_{\circ}$	Vacuum permittivity
ε'	Real part of complex permittivity
ε''	Imaginary part of complex permittivity
$\varepsilon^* = \varepsilon' + i\varepsilon''$	Complex permittivity
$\varepsilon'_{\|\|}$	Real part of complex permittivity parallel to $\hat{n}$
$\varepsilon''_{\|\|}$	Imaginary part of complex permittivity parallel to $\hat{n}$
K_{11}, K_{22}, K_{33}	Splay, Twist and Bend elastic constants
K	Average elastic constant
γ_1	Rotational viscosity coefficient
η_1, η_2, η_3	Miesowicz viscosity coefficients
$\eta_{\|\|}$	Passive viscosity coefficient parallel to $\hat{n}$
$\eta_{\perp}$	Passive viscosity coefficient perpendicular to $\hat{n}$
$D_{\|\|}$	Self-diffusion coefficient parallel to $\hat{n}$
$D_{\perp}$	Self-diffusion coefficient perpendicular to $\hat{n}$
T	Absolute temperature
T_{NI}	Nematic-isotropic phase transition temperature
T_{SN}	Nematic-smectic-A phase transition temperature
NI	Nematic-isotropic phase transition
NS	Nematic-smectic-A phase transition
θ	Tilt angle (polar)
φ	Twist angle (azimuthal)
γ^E	Molecular polarizability
$\gamma^E_{\|\|}$	Molecular polarizability parallel to $\hat{n}$
$\gamma^E_{\perp}$	Molecular polarizability perpendicular to $\hat{n}$
$\Delta\gamma^E = \gamma^E_{\|\|} - \gamma^E_{\perp}$	Molecular polarizability anisotropy
$\langle \gamma^E \rangle = (\gamma^E_{\|\|} + 2\gamma^E_{\perp})/3$	Average molecular polarizability
$\tau_{\circ}$	Relaxation time
$\vec{P}$	Flexoelectric polarization vector
e_1	Flexoelectric splay coefficient

e_3	Flexoelectric bend coefficient
e^*	$e_1 - e_3$
$\vec{E}$	Electric field vector
$\vec{D}$	Electric displacement vector
λ	Wavelength
ω	Angular frequency
I	Intensity
f_s	Surface energy density
f_{el}	Elastic distortion energy density
V	Voltage
γ	$\varepsilon_{||}/\varepsilon_{\perp} - 1$
κ	$K_{33}/K_{11} - 1$
V_{th}	Freedericksz threshold voltage
r	Radius
τ, t	Time
α	McMillan parameter
β	Exponent in Haller extrapolation
DSC	Differential scanning calorimetry
BC	Bent-core molecules
RO	Rod-like molecules (calamitic liquid crystal)

1

Introduction

1.1 Liquid crystals

L IQUID CRYSTAL is an intermediate state of matter between that of a crystalline solid and an isotropic liquid. Liquid crystals possess many of the mechanical properties of liquid, e.g., high fluidity, inability to support shear, formation, and coalescence of droplets. At the same time they exhibit crystalline properties such as anisotropy in their optical, electrical, and magnetic properties [1, 2]. Liquid crystals were discovered by an Austrian botanist Fredrich Reinitzer in 1888. They are found among organic compounds with molecular shape anisotropy. They are classified into two types namely thermotropic and lyotropic. Thermotropic liquid crystals exhibit mesophases as a function of temperature whereas lyotropic liquid crystals exhibit mesophases as a function of its concentration in solvent [3, 4]. Conventional liquid crystals are mostly made of rod and disc-like molecules. In this thesis we report on the physical properties of some unconventional thermotropic liquid crystals.

1.2 Types of liquid crystals

Shape anisotropy is an essential requirement for exhibiting liquid crystalline phase. Depending on the shape of the molecules, thermotropic liquid crystals are classified into three categories [5, 6]. (i) Calamitic, (ii) Discotic and (iii) Bent-core liquid crystals. They are basically composed of rod-like, disc-like and bent-core molecules, respectively. Schematic representation of these molecules are shown in figure 1.1.

(i)   (ii)   (iii)
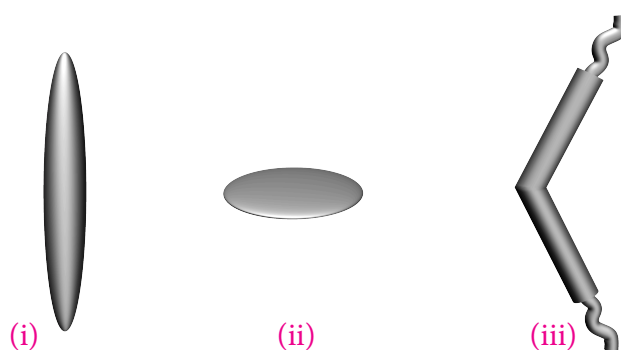
Figure 1.1: *Schematic representation of (i) Calamitic, (ii) Discotic and (iii) Bent-core molecules.*

1.2.1 Calamitic liquid crystals

A typical calamitic liquid crystal consists of rigid core with flexible side chains. The physical properties are widely influenced by the nature of the core and the side chains. There are different liquid crystal phases (*mesophases*) formed by calamitic mesogens.

1.2.1.1 Nematic phase

The uniaxial nematic (N) phase is the simplest phase among all the known mesophases. The word nematic comes from the Greek word *nema*, which means thread. Thread like structures are seen when we observe nematic phase under polarizing microscope. In the nematic phase molecules have no positional order but they tend to align with their long axes parallel to each other in a particular direction. The direction is called
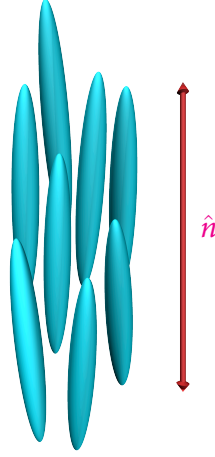
Figure 1.2: *Schematic representation of the molecular arrangement of rod-like molecules in the nematic phase, where $\hat{n}$ is the director.*

director, represented by $\hat{n}$ which is apolar in nature i.e. $\hat{n}$ and $-\hat{n}$ are equivalent. Since there is no long-range correlation between the centres of mass of the molecules they can translate freely.

1.2.1.1.1   Order parameter

The order parameter is a measure of order in the relevant phases. In nematic liquid crystal the orientational order parameter describes the average orientation of the long axes of the molecules with respect to the director. To define the local orientation at a point $\vec{r} = (x, y, z)$, following de Jeu [4], let us assume that the molecule is a rigid rod with a unit vector $\hat{a}$ along the long axis. Now consider the thermal average of the relevant tensor that are composed into $\hat{a}$, over a microscopic volume around $\vec{r}$. The first choice is a vector order parameter $\langle \hat{a} \rangle$, where the angular brackets denote the ensemble average. The unit vector $\hat{a}$ will be zero in the nematic phase because $\hat{n}$ and $-\hat{n}$ are physically equivalent. The next choice of order parameter is a second rank tensor S, the elements of which are given by

$$S_{\alpha\beta} = \langle a_\alpha a_\beta \rangle - \frac{1}{3}\delta_{\alpha\beta} \qquad \alpha, \beta = x, y, z \qquad (1.1)$$

The addition of Kronecker delta ensures that $S_{\alpha\beta}$ is zero in the isotropic phase where $\langle a_\alpha^2 \rangle = \frac{1}{3}$. The tensor order parameter is symmetric and traceless and has five independent elements. In the principal coordinate system the above tensor can be written in diagonal form. For the uniaxial case, the most general form of order parameter field in the nematic phase is given by

$$S_{\alpha\beta}(\vec{r}) = S\left(n_\alpha(\vec{r})n_\beta(\vec{r}) - \frac{1}{3}\delta_{\alpha\beta}\right) \tag{1.2}$$

where S is a measure of the degree of alignment of the long axis of the molecules along $\hat{n}(\vec{r})$ and the expression in the parenthesis describes the spatial variation of $\hat{n}(\vec{r})$ from point to point. $\hat{n}$ is independent of $\vec{r}$ in a well-aligned nematic. For cylindrically symmetric molecules the scalar order parameter is defined as [1]

$$S = \frac{3\langle \cos^2\theta - 1\rangle}{2} \tag{1.3}$$

where the angular brackets represent the ensemble average and θ is the angle made by the molecule with the director. In a perfectly aligned sample $S = 1$, whereas in the isotropic phase $S = 0$. Usually the value of S in a nematic liquid crystal varies from $\simeq 0.3$ to 0.8 with temperature. The order parameter can be directly related to certain experimentally determined quantities, for example diamagnetic and dielectric anisotropy, birefringence etc [3].

1.2.1.2 Cholesteric phase

Cholesteric phase is observed when the molecules are chiral or chiral dopant is added to nematic liquid crystals. Along with long-range orientational order, spacial variation of director also exists which causes helical structure. If we move along helix axis the local director rotates. A full rotation of $\hat{n}$ is completed by a distance p, called pitch. The repetition period is $p/2$ since $\hat{n}$ and $-\hat{n}$ are equivalent. A schematic representation of

the molecular arrangement of rod like molecules in the cholesteric phase is shown in figure 1.3.
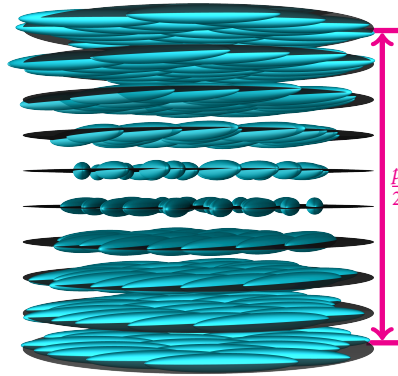
Figure 1.3: *Schematic representation of the molecular arrangement of rod-like molecules in the cholesteric phase. Half pitch is indicated by p/2.*

1.2.1.3 Smectic phases

In smectic phases the molecules form layered structures. These phases show orientational order along with some positional order. The molecules are preferably pointing in one direction, just like in the nematic phase. In the layer the centres of mass of the molecules are random i.e. liquid-like. There are several different types of smectic mesophases.

1.2.1.3.2 Smectic-A (SmA)

In smectic-A phase the long axes of molecules are parallel to the layer normal $\hat{z}$. The interlayer attractions are relatively weak and the layers can slide over one another relatively easily and each layer behaves as a two dimensional liquid [2]. If the molecules are symmetric and non-polar, in the smectic-A phase the layer spacing (d) is approximately equal to the molecular length (l). A schematic representation of the molecular arrangement of rod-like molecules in the SmA phase is shown in figure 1.4.
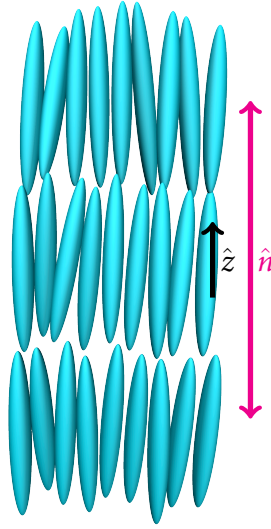
Figure 1.4: *Schematic representation of the molecular arrangement of rod-like molecules in the SmA phase, where $\hat{n}$ is the director and $\hat{z}$ is layer normal.*

1.2.1.3.3 Smectic-C (SmC)

In smectic-C phase the long axes of the molecules make an angle with the layer normal $\hat{z}$. The tilt angle θ (polar) reduces the layer thickness. The azimuthal angle φ does not affect the layer thickness. So at any temperature, the amplitudes of θ fluctuations of the director are small compared to those of the φ fluctuations. A schematic representation of the molecular arrangement of rod-like molecules in the SmC phase is shown in figure 1.5.

1.2.1.3.4 Anticlinic smectic-C (SmC$_a$)

In anticlinic smectic-C phase the long axes of molecules make an angle with the layer normal $\hat{z}$ similar to SmC but the angle changes its sign as we move from layer to layer. A schematic representation of the molecular arrangement of rod-like molecules in the SmC$_a$ phase is shown in figure 1.6.
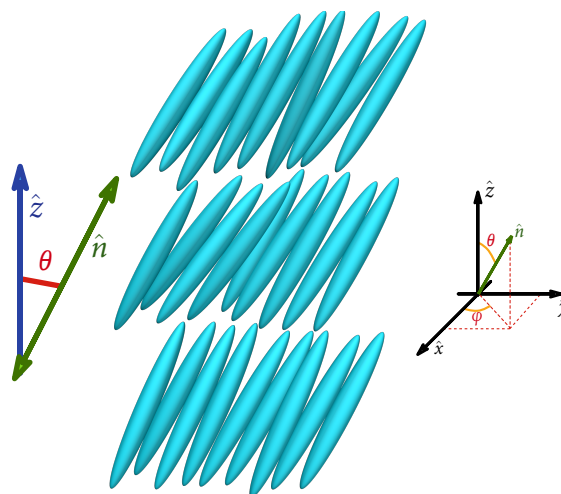
Figure 1.5: *Schematic representation of the molecular arrangement of rod-like molecules in the SmC phase, where $\hat{n}$ is the director and $\hat{z}$ is layer normal.*
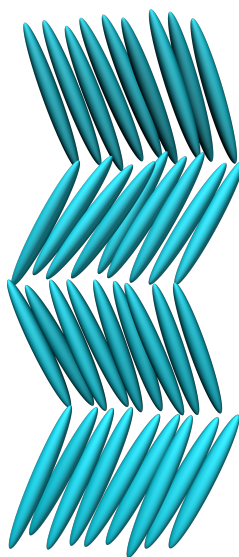
Figure 1.6: *Schematic representation of the molecular arrangement of rod-like molecules in the SmC_a phase.*

1.2.1.3.5 Smectic-C* (SmC*)

If a smectic-C phase is composed of chiral molecules, the chiral interactions lead to the formation of helical structure and the phase is called smectic-C* (SmC*). The helix is formed by precession of the tilt direction about an axis perpendicular to the layer with a characteristic pitch. The helix can be either right or left handed depending on the

chirality of the constituent molecules. The helix of the smectic-C* can be unwound either by surface interactions or by the application of strong electric or magnetic fields. The tilt angle θ (polar) remains the same whereas the azimuthal angle φ varies as we move from layer to layer. A schematic representation of the molecular arrangement of rod-like molecules in the SmC* phase is shown in figure 1.7.
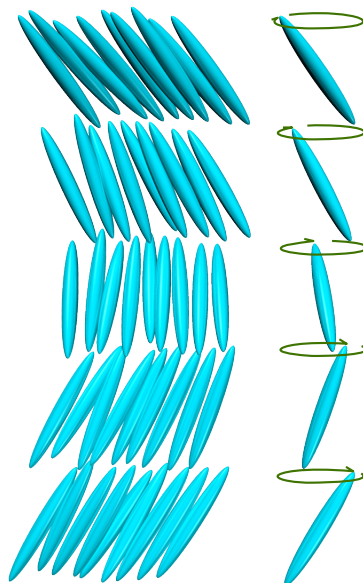
Figure 1.7: *Schematic representation of the molecular arrangement of rod-like molecules in the SmC* phase.*

1.2.2 Discotic liquid crystals

The liquid crystals composed of disc-like molecules are called discotic liquid crystals. Discotic liquid crystals usually consist of a rigid, flat core unit and flexible side chains, which are surrounding this core [7].

1.2.2.1 Nematic discotic phase

The nematic phase for discotic liquid crystals is quite similar to the one for calamitic mesogens. Again, there is only orientational order. The nematic phase is less common

in discotic liquid crystals, as the discotic molecules have a great tendency of assembling in columns, forming columnar phase. A schematic representation of the molecular arrangement of disc-like molecules in the nematic phase is shown in figure 1.8.
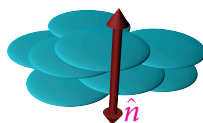
Figure 1.8: *Schematic representation of the molecular arrangement of disc-like molecules in the nematic phase, where $\hat{n}$ is the director.*

1.2.2.2 Columnar discotic phase

In columnar discotic phases the cores of molecules are aligned in columns, surrounded by the side chains. These columns can then be arranged in various ways, for example in a hexagonal or a rectangular lattice. A schematic representation of the molecular arrangement of disc-like molecules in the columnar hexagonal phase is shown in figure 1.9.
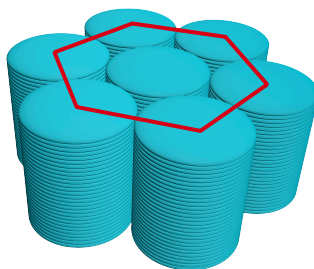
Figure 1.9: *Schematic representation of the molecular arrangement of disc-like molecules in the hexagonal columnar phase.*

1.2.3 Bent-core liquid crystals

Liquid crystals exhibited by bent-core molecules show various mesophases and they are mostly different from the ones exhibited by rod-like and disc-like molecules [8]. The new phases exhibited by them are labelled as B_n phases [9, 10]. The letter B stands

for banana or bent-core or bow shaped molecules, and the suffix 'n' corresponds to the sequence of discovery of different phases. Occasionally the bent-core molecules also show nematic and smectic phases.

1.2.3.1 B_1 phase

In this phase the bent-core molecules are arranged in a 2D rectangular columnar structure. It has two lattice parameters a and b as shown schematically in figure 1.10. This phase is observed in compounds with relatively short alkyl chains. Aromatic cores and alkyl chains of the molecules overlap only near column boundaries. Recently, it has been shown that B_1 phase can exhibit several sub-phases which sometimes show switching properties.
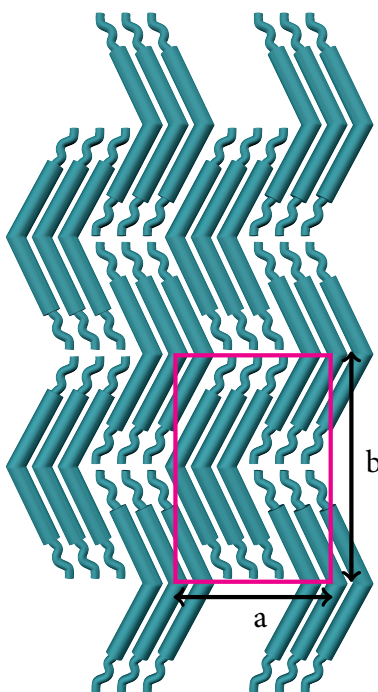
Figure 1.10: *Schematic representation of the molecular arrangement of bent-core molecules in the B_1 phase.*

1.2.3.2 B$_2$ phase
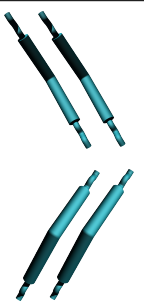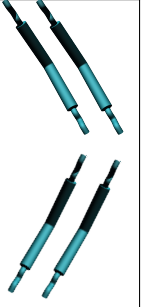
In this phase molecules form polar and chiral layer structures. These structures arise as molecular bows point in the same direction in one layer (giving rise to layer polarization) and molecular long-axis tilted from the layer normal, as in the case of SmC phase. This phase is observed in compounds with long alkyl chains. The layer has no mirror plane and becomes chiral even though the molecules are achiral. As the symmetry is broken spontaneously, structures of opposite chirality are equally probable [11]. B$_2$ phase is identical as SmCP phase (P stands for polar). There are two macroscopic racemic layer structures (SmC$_S$P$_A$ and SmC$_A$P$_F$) and two macroscopic chiral structures (SmC$_A$P$_A$ and SmC$_S$P$_F$), each showing two enantiomeric structures as shown in table 1.1 [11]. A schematic representation of the molecular arrangement of bent-like molecules in the B$_2$ phase is shown in figure 1.11.
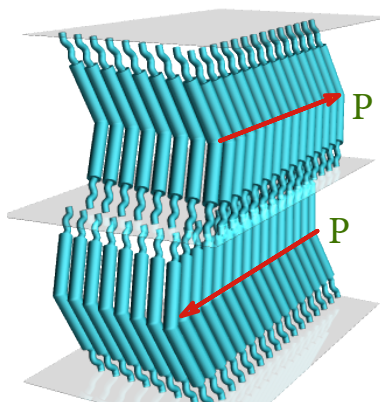
Figure 1.11: *Schematic representation of the molecular arrangement of bent-core molecules in the B$_2$ phase.*

1.2.3.3 B$_6$ phase

In this phase the molecules form an intercalated fluid lamellar (smectic) structure with layer spacing equal to half the length of the molecules with short chains. Cores and chains overlap significantly. A schematic representation of the molecular arrangement of bent-like molecules in the B$_6$ phase is shown in figure 1.12. This phase is

SmCP phase	Antiferroelectric		ferroelectric	
C: tilted	SC	AC	SC	AC
SC: Syn-clinic				
AC: Anticlinic	SmC_SP_A	SmC_AP_A	SmC_SP_F	SmC_AP_F

Table 1.1: *Side view of bent-core molecules in a layer structure.*

observed in compounds with very short alkyl chains and they have weak transverse anti-ferroelectric order. The molecules do not switch under an electric field.
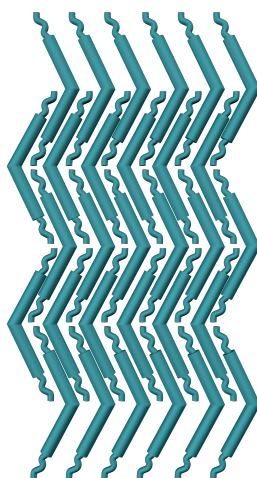
Figure 1.12: *Schematic representation of the molecular arrangement of bent-core molecules in B_6 phase.*

1.3 Physical properties

In this section, we discuss some physical properties, that are measured in the later chapters.

1.3.1 Optical properties

1.3.1.1 Refractive index

Refractive index is the property of a material that determines the relative speed of light in the material. In the case of liquid crystals, the speed of light for polarisation parallel to the director is different from that for the perpendicular direction. The uniaxial nematic phase has two principal refractive indices called n_e and n_o. The suffixes 'e' and 'o' stand for extraordinary and ordinary rays respectively. For a nematic, $n_e = n_{||}$ and $n_o = n_{\perp}$, where the parallel and perpendicular directions are defined in relation to the director. The average value of the refractive indices in the nematic phase is given by

$$\langle n^2 \rangle = \frac{1}{3}(n_{||}^2 + 2n_{\perp}^2). \tag{1.4}$$

1.3.1.2 Birefringence

The birefringence is given by

$$\Delta n = n_e - n_o = n_{||} - n_{\perp} \tag{1.5}$$

which is usually positive and varies from 0.01 to 0.2 [4, 12]. The optical anisotropy $\Delta n = n_{||} - n_{\perp}$ is defined by electronic polarizability anisotropy ($\Delta \gamma^E = \gamma_{||}^E - \gamma_{\perp}^E$), measured parallel and perpendicular to the long molecular axis. However, Δn is used to estimate the orientational order in liquid crystals using the relation

$$S \approx \frac{\Delta n}{\Delta n_{\circ}} \tag{1.6}$$

where $\Delta n_{\circ}$ is the birefringence in fully aligned state when $S = 1$.

1.3.2 Dielectric properties

1.3.2.1 Dielectric constant

Dielectric constant is a measure of the response of materials to an external electric field. It depends on the intrinsic properties of the materials like distribution of the charges in the molecules as well as the intermolecular interactions. For liquid crystals which consist of non-polar molecules, the dielectric constant arises due to induced polarization whereas for liquid crystals with polar molecules dielectric constant arises not only from induced polarization but also from permanent dipoles which orient themselves parallel to the field.
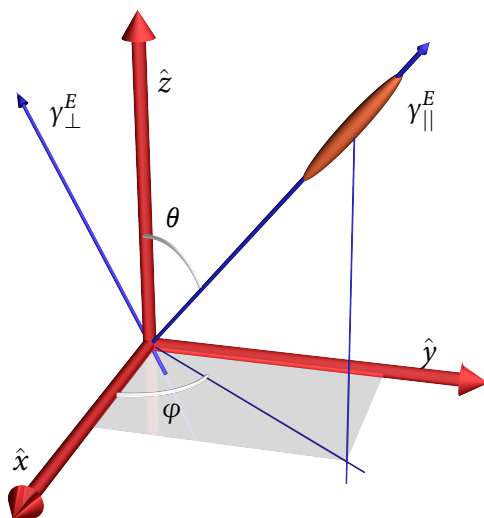
Figure 1.13: *Schematic representation of the principal components of the polarizabilities of liquid crystal.*

In liquid crystals, the dielectric constants $\varepsilon_{||}$ and $\varepsilon_{\perp}$ are measured with electric field parallel and perpendicular to the director ($\hat{n}$) respectively. The dielectric anisotropy is given by $\Delta\varepsilon = \varepsilon_{||} - \varepsilon_{\perp}$. These dielectric constants depend on orientational order (S) of liquid crystal, the angle β between the molecular dipole and the axis of the maximum polarizability of the molecule, the average molecular polarizability $\langle \gamma^E \rangle = (\gamma_{||}^E + 2\gamma_{\perp}^E)/3$, and its anisotropy $\Delta\gamma^E = \gamma_{||}^E - \gamma_{\perp}^E$.

Maier and Meier's theory [13] gives the following expressions for the dielectric constants

$$\varepsilon_{||} = 1 + \frac{4\pi\rho}{M} N_A h F \left[\langle \gamma^E \rangle + \frac{2\Delta\gamma^E}{3}S + F\frac{\mu^2}{3k_BT}\left(1 - (1 - 3\cos^2\beta)S\right) \right] \qquad (1.7)$$

$$\varepsilon_{\perp} = 1 + \frac{4\pi\rho}{M} N_A h F \left[\langle \gamma^E \rangle - \frac{\Delta\gamma^E}{3}S + F\frac{\mu^2}{3k_BT}\left(1 + \frac{1}{2}(1 - 3\cos^2\beta)S\right) \right] \qquad (1.8)$$

where M is molar weight, $h = 3\langle\varepsilon\rangle/(2\langle\varepsilon\rangle + 1)$ is the cavity field factor, $F = 1/(1 - f\langle\gamma^E\rangle)$ where $f = (\langle\varepsilon\rangle - 1)/[2\pi a^3(2\langle\varepsilon\rangle - 1)]$ is the reaction field factor for spherical cavity and $a^3 = 3(\mu/4\pi)N_A\rho$ is the cavity volume. From equations 1.7 and 1.8 the average dielectric constant $\langle\varepsilon\rangle = (\varepsilon_{||} + 2\varepsilon_{\perp})/3$ is given by

$$\langle\varepsilon\rangle = 1 + \frac{4\pi\rho}{M} N_A h F \left[\langle\gamma^E\rangle + F\frac{\mu^2}{3k_BT} \right] \qquad (1.9)$$

and dielectric anisotropy is given by

$$\Delta\varepsilon = \varepsilon_{||} - \varepsilon_{\perp} = \frac{4\pi\rho}{M} N_A h F \left[\Delta\gamma^E - F\frac{\mu^2}{2k_BT}(1 - 3\cos^2\beta) \right] S. \qquad (1.10)$$

The relative magnitude of the two terms within the square brackets of equation (1.10) determines the sign of $\Delta\varepsilon$. When $\beta < 55°$, the two terms add up and the compound exhibits a positive dielectric anisotropy. For $\beta \sim 55°$, the second term vanishes and only $\Delta\gamma^E$ contributes to $\Delta\varepsilon$. For $\beta > 55°$, $\Delta\varepsilon > 0$ or < 0, depending on whether the dipolar contribution is less or more than the contribution due to polarisability anisotropy.

When a time-varying electric field is applied to the dielectric medium, a complex dielectric permittivity describes the phase lag between the displacement $\vec{D} = \varepsilon^*\vec{E}$ and the external field $\vec{E}$ in the dispersion region of orientation polarizability. The complex permittivity ε^* is given by

$$\varepsilon^* = \varepsilon' - i\varepsilon'' \qquad (1.11)$$

where ε' and ε'' are, respectively, the real and imaginary parts of ε^*. They are given by

$$\varepsilon' = \varepsilon(\infty) + \frac{\varepsilon(0) - \varepsilon(\infty)}{1 + \omega^2 \tau_D^2} \tag{1.12}$$

$$\varepsilon'' = \frac{[\varepsilon(0) - \varepsilon(\infty)]\omega\tau_D}{1 + \omega^2 \tau_D^2} \tag{1.13}$$

where $\varepsilon(\infty)$ is the permittivity at the high frequency limit, $\varepsilon(0)$ is the static, low frequency permittivity, ω is angular frequency and τ_D is the characteristic relaxation time of the medium. The dielectric losses are given by

$$\tan\varphi = \frac{\varepsilon''}{\varepsilon' - \varepsilon(\infty)} = \omega\tau_D. \tag{1.14}$$

These dielectric losses cause electric current even in a purely insulating medium where there are no free charge carriers. The magnitude of the electrical conductivity caused by dielectric losses is given by $\sigma_D = \varepsilon_\circ \varepsilon'' \omega$.

1.3.3 Viscoelastic properties

The viscoelastic properties of liquid crystals are very important. These properties mainly determine the behaviour of liquid crystals in external electric or magnetic fields. The controlling voltage, steepness of the transmission-voltage curve, response time, etc. depends on the viscoelastic properties.

1.3.3.1 Curvature elastic constants

A nematic liquid crystal possesses curvature elasticity. In a uniformly orientated, mono-domain sample of nematic liquid crystal, the director $\hat{n}$ is independent of r. When a distortion is induced and the derivatives of $\hat{n}(r)$ exist, an elastic restoring torque comes into play tending to restore $\hat{n}(r)$ to the undistorted state. Any deformation can be considered to be a combination of three basic curvature deformations.

These are called splay, twist and bend and the deformation free energy density is defined as [1, 2, 14],

$$g = \frac{1}{2}\left[K_{11}(\nabla \cdot \hat{n})^2 + K_{22}(\hat{n} \cdot \nabla \times \hat{n})^2 + K_{33}(\hat{n} \times \nabla \times \hat{n})^2\right] \qquad (1.15)$$

where K_{11}, K_{22} and K_{33} are the splay, twist and bend elastic constants respectively. The constants are positive and usually $K_{33} > K_{11} > K_{22}$ in rod-like molecules. The typical magnitudes of these constants are $\sim 10^{-12}$ N. A schematic representation of the splay, twist and bend deformations is shown in figure 1.14.
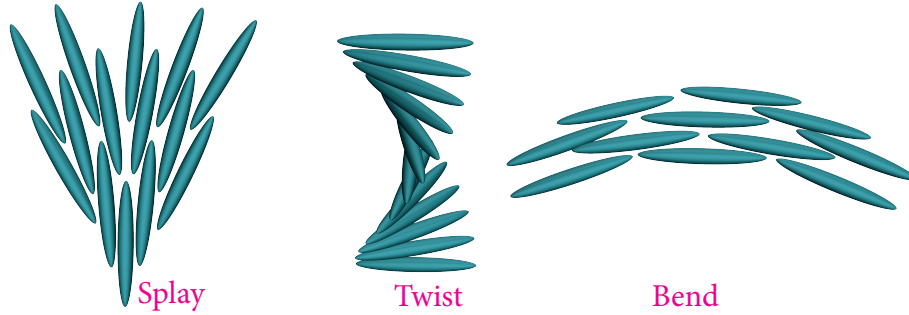
Splay   Twist   Bend

Figure 1.14: *Schematic representation of the splay, twist and bend deformations.*

1.3.3.2 Flow viscosity

Viscosity is a collective property resulting from the interaction of the molecules with one another, it is strongly dependent on the molecular environment. Three principal viscosities can be define for nematic liquid crystals depending on the relative orientation of the molecules with respect to the flow of the material. Depending on the orientation of director with respect to flow direction the following viscosities are defined.

(i) η_1:   director parallel to velocity gradient.

(ii) η_2:   director perpendicular to the velocity gradient (parallel to flow direction).
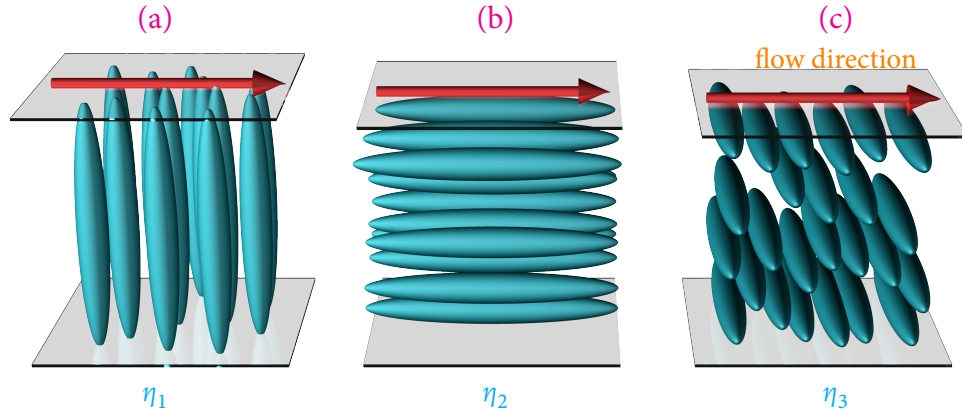
Figure 1.15: *The viscosity coefficients of a nematic liquid crystal. Arrows represent direction of flow.*

(iii) η_3:   director perpendicular to both velocity gradient and flow direction.

The three coefficients η_1, η_2 and η_3 are called Miesowicz coefficients.

1.3.3.3   Rotational viscosity

Rotational viscosity (γ_1) results when molecule rotates around an axis perpendicular to the director. Rotational viscosity (γ_1) is one of the most important parameter of liquid crystal devices because it determines the electro-optical switching speed. The magnitude of γ_1 depends on temperature, inter molecular interactions, and the molecular structure. For a liquid crystal slab of thickness d, γ_1 is given by [15, 16]

$$\gamma_1 = \frac{\tau_\circ K_{11} \pi^2}{d^2} \tag{1.16}$$

where K_{11} is the splay elastic coefficient and $\tau_\circ$ is the relaxation time. Thus γ_1 can be measured from the measurement of relaxation time ($\tau_\circ$).

1.3.4 Flexoelectricity

The nematic medium does not exhibit spontaneous polarization due to the apolar nature of the director. A macroscopic polarization can be induced in a nematic liquid crystal by splay and bend distortions of the director field. This was first proposed by Meyer (1969) and named as flexoelectric effect [17]. The flexoelectric polarization is given by,

$$\vec{P} = e_1(\nabla \cdot \hat{n})\hat{n} + e_3(\nabla \times \hat{n}) \times \hat{n} \qquad (1.17)$$
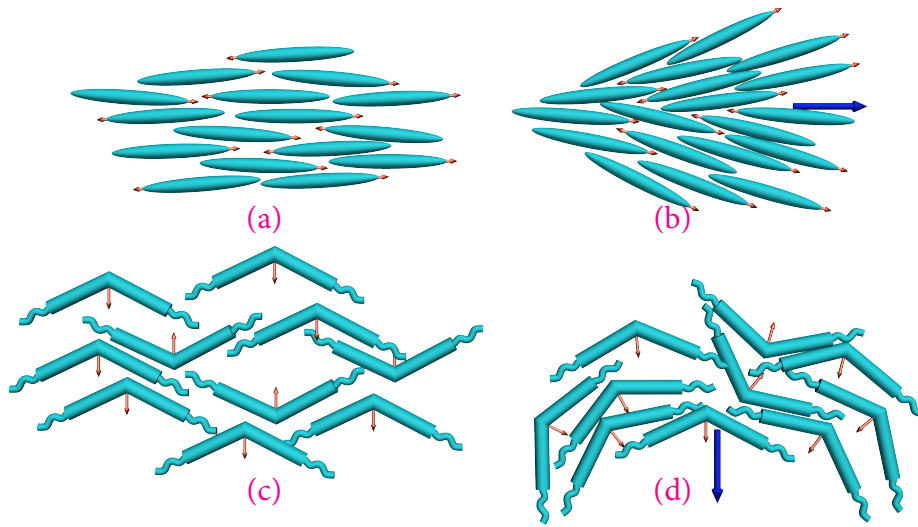
Figure 1.16: *The dipolar model of splay (a, b) and bend (c, d) deformation and corresponding polarization.*

where e_1 and e_3 are the two flexoelectric coefficients corresponding to splay and bend distortions respectively. According to Meyer's model only nematics made of polar molecules with shape anisotropy can be expected to exhibit flexoelectricity. For example, a nematic consisting of pear shaped molecules with longitudinal dipole moments become polarized under splay distortion and a nematic made of banana shaped molecules with transverse dipole moments becomes polarized under bend distortion. In the undistorted state, the dipole moments of the molecules are oriented with equal probability in opposite directions. They cancel each other and the net dipole density is zero.

Another microscopic model was developed by Prost and Marcerou [18] in which the flexoelectric effect arises due to quadrupolar moments of the molecules. The splay deformation develops a net dipole moment and the medium gets polarized. The quadrupolar contribution is independent of the shape of the molecules. The quadrupolar contribution to flexoelectric effect is of the same magnitude as due to dipolar contribution. Since all nematogenic molecules have finite quadrupole moments, flexoelectric effect is an universal property of nematics.

1.4 Types of alignments

Alignment of liquid crystals on substrate is very important from technological point of view [19, 20]. The uniform orientation of director also enables us to measure the several physical properties such as birefringence, dielectric and elastic constants. We discuss here three different alignments of liquid crystals that are relevant to the later chapters.

(a)   (b)   (c)
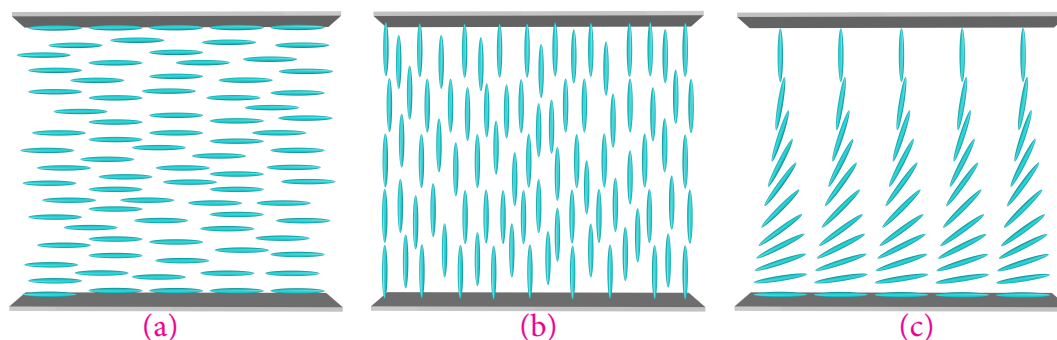
Figure 1.17: *Schematic diagrams of the (a) homogeneous, (b) homeotropic and (c) hybrid alignments of the molecules.*

1.4.1 Homogeneous alignment

The molecules can be aligned parallel to the plane of the glass plates by coating the glass plates with appropriate polyimide and rubbing. This geometry is called homogeneous

or planar geometry. The rubbing on polyimide generates micro-grooves along which the long axes of the molecules are aligned. In the case of uniaxial nematic liquid crystal the optic axis will be along the rubbing direction. A schematic representation of homogeneous alignment is shown in figure 1.17(a).

1.4.2 Homeotropic alignment

The molecules can be aligned perpendicular to the plane of the glass plate by coating suitable polyimide on to the glass plate. This geometry is called homeotropic geometry. In case of surfactant the head groups sit on the glass plate and the chains stay perpendicular to the plane of the glass plate and give rise to the perpendicular alignment of the long axes of the molecules. A schematic representation of homeotropic alignment is shown in figure 1.17(b).

1.4.3 Hybrid alignment

In this geometry one plate is coated with polyimide and rubbed in specified direction to achieve planar alignment whereas other plate is coated with homeotropic alignment layer to achieve perpendicular direction. This geometry is used to measure flexoelectric coefficient. A schematic representation of hybrid alignment is shown in figure 1.17(c).

1.4.4 Freedericksz transition

The dielectric displacement $\vec{D}$ in a nematic liquid crystal is given by [21, 22]

$$\vec{D} = \varepsilon_\circ \varepsilon_\perp \vec{E} + \varepsilon_\circ \Delta\varepsilon (\hat{n} \cdot \vec{E})\hat{n} \tag{1.18}$$

(a) $V < V_{th}$ (b) $V > V_{th}$
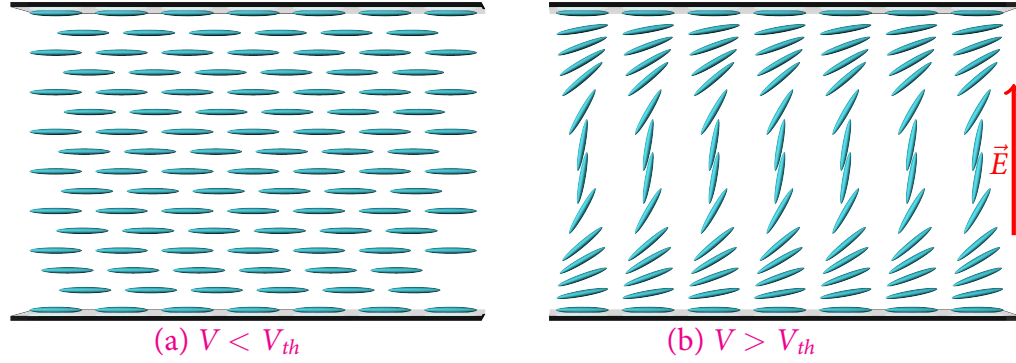
Figure 1.18: *Schematic representation of director configuration is shown (a) below and (b) above the threshold field respectively.*

and the dielectric energy density of a nematic is given by

$$W_{diel} = -\int_0^E \vec{D} \cdot d\vec{E} = -\frac{1}{2}\varepsilon_\circ\varepsilon_\perp\vec{E}^2 - \frac{1}{2}\varepsilon_\circ\Delta\varepsilon(\hat{n} \cdot \vec{E})^2 \qquad (1.19)$$

It is noted that the dielectric energy is lowered by an alignment of $\hat{n}$ with respect to $\vec{E}$, which depends on the sign of the $\Delta\varepsilon$. In a uniformly aligned sample when an electric field is applied perpendicular to the director ($\Delta\varepsilon > 0$) a distortion takes place only when the strength of applied field exceeds a certain well defined threshold value. This is called Freedericksz transition [12]. A schematic representation is shown in figure 1.18. The threshold voltage is given by

$$V_{th} = \pi\sqrt{\frac{K_{11}}{\varepsilon_\circ\Delta\varepsilon}} \qquad (1.20)$$

where K_{11} is the splay elastic constant.

References

[1] P. G. de Gennes and J. Prost, *The physics of liquid crystals.* 2nd Ed., Clarendon Press, Oxford, 1993.

[2] S. Chandrasekhar, *Liquid crystals.* Cambridge University Press, Cambridge, 1992.

[3] P. J. Collings and M. Hird, *Introduction to liquid crystals chemistry and physics.* Taylor & Francis, 1997.

[4] W. H. de Jeu, *Physical properties of liquid crystalline materials.* Liquid Crystal Monographs, Gordon and Breach, 1980.

[5] G. Friedel, "The mesomorphic states of matter," *Ann. Phys. Paris.*, vol. 18, pp. 273–474, 1922.

[6] M. J. Stephen and J. P. Straley, "Physics of liquid crystals," *Rev. Mod. Phys.*, vol. 46, pp. 617–704, Oct 1974.

[7] S. Chandrasekhar, B. K. Sadashiva, and K. A. Suresh, "Liquid crystals of disc-like molecules," *Pramana*, vol. 9, pp. 471–480, November 1977.

[8] D. Vorländer and A. Apel, "Die richtung der kohlenstoff-valenzen in benzo-labkömmlingen (ii.).," *Ber. dtsch. Chem. Ges. A/B*, vol. 65, pp. 1101–1109, July 1932.

[9] H. Takezoe and Y. Takanishi, "Bent-core liquid crystals: Their mysterious and attractive world," *Japanese Journal of Applied Physics*, vol. 45, no. 2A, pp. 597–625, 2006.

[10] G. Pelzl, S. Diele, and W. Weissflog, "Banana-shaped compounds—a new field of liquid crystals," *Advanced Materials*, vol. 11, no. 9, pp. 707–724, 1999.

[11] D. R. Link, G. Natale, R. Shao, J. E. Maclennan, N. A. Clark, E. Körblova, and D. M. Walba, "Spontaneous formation of macroscopic chiral domains in a fluid smectic phase of achiral molecules," *Science*, vol. 278, no. 5345, pp. 1924–1927, 1997.

[12] L. M. Blinov and V. G. Chigrinov, *Electrooptic effects in liquid crystals*. Springer-Verlag, New York, 1996.

[13] W. Maier and G. Meier. *Z. Naturforsch*, vol. 16a, 1961.

[14] F. C. Frank, "I. liquid crystals. on the theory of liquid crystals," *Discuss. Faraday Soc.*, vol. 25, pp. 19–28, 1958.

[15] S.-T. Wu and C.-S. Wu, "Experimental confirmation of the osipov-terentjev theory on the viscosity of nematic liquid crystals," *Phys. Rev. A*, vol. 42, pp. 2219–2227, Aug 1990.

[16] M. L. Dark, M. H. Moore, D. K. Shenoy, and R. Shashidhar, "Rotational viscosity and molecular structure of nematic liquid crystals," *Liquid Crystals*, vol. 33, no. 1, pp. 67–73, 2006.

[17] R. B. Meyer, "Piezoelectric effects in liquid crystals," *Phys. Rev. Lett.*, vol. 22, pp. 918–921, May 1969.

[18] Prost, J. and Marcerou, J.P., "On the microscopic interpretation of flexoelectricity," *J. Phys. France*, vol. 38, no. 3, pp. 315–324, 1977.

[19] A. A. Sonin, *The surface physics of liquid crystals*. Gordon and Breach Publishers, 1995.

[20] K. Takatoh, M. Sakamoto, R. Hasegawa, M. Koden, N. Itoh, and M. Hasegawa, *Alignment technology and applications of liquid crystal devices*. CRC Press, 2005.

[21] H. J. Deuling, "Deformation of nematic liquid crystals in an electric field," *Molecular Crystals and Liquid Crystals*, vol. 19, no. 2, pp. 123–131, 1972.

[22] H. Gruler and G. Meier, "Electric field-induced deformations in oriented liquid crystals of the nematic type," *Molecular Crystals and Liquid Crystals*, vol. 16, no. 4, pp. 299–310, 1972.

2

Experimental Setup

Iɴ this chapter we briefly discuss the procedure of liquid crystal cell preparation and the experimental techniques that are used for the measurement of birefringence (Δn), dielectric constants ($\varepsilon_{||}, \varepsilon_{\perp}$), splay ($K_{11}$) and bend ($K_{33}$) elastic constants, rotational viscosity (γ_1) and flexoelectric coefficients ($e_1 - e_3$). 5CB (pentylcyanobiphenyl) is used to calibrate experimental techniques.

2.1   Preparation of liquid crystal cell

Two glass plates (area 1.5 cm^2) coated with indium tin oxide (ITO) of thickness 1500 Å and resistivity 15-20 Ω/cm^2 are used to prepare cell. The ITO is a transparent conductor which is used as an electrode in liquid crystal cells. The required pattern of ITO on a glass plate is achieved by chemical etching. The patterned ITO glass plates are cleaned thoroughly several times with hexane and acetone. Then sonicated for 30 min

using an ultrasonicator water bath. After taken out from bath the water droplets on plates are removed by blowing N_2 gas. The patterned ITO glass plates are dried in an oven for 15 min. Appropriate polyimide spin coated on the patterned ITO glass plates at a speed of 3000 rpm. For our experiments we used two polimides namely AL-1254 and JALS-204. They are used for homogeneous and homeotropic alignments respectively. The coated glass plates are cured at 180 °C and 200 °C respectively in an oven for a duration of 1h. The cured glass (AL1254) plates are rubbed unidirectionally with a home made rubbing machine to align liquid crystal molecules in a particular direction. Two rubbed glass plates are kept one over the other with their active regions facing each other and the rubbing directions are antiparallel, and are attached using mixture of UV curable adhesive and silica beads. The thickness of cell is controlled by size of silica beads. The schematic representation of top view of a liquid crystal cell is shown in figure 2.1. The electrical connections to the cell are made by soldering copper wires using an ultrasonic soldering (Sunbonder USM-IV).
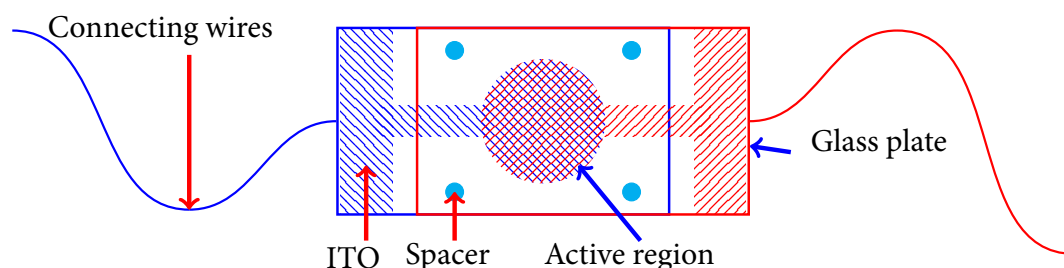
Figure 2.1: *Schematic diagram of liquid crystal sample cell (Top view). The central circular region is the overlapped electrode region.*

2.1.1 Measurement of cell thickness

The empty cell gap is measured using interferometric method with Ocean Optics (HR-4000) spectrometer. The experimental setup is shown in figure 2.2(a).

The empty cell is kept under spectrometer reflection probe which consists of optical fibres. It is illuminated by light through outer six fibres of probe and reflected light is collected by central fibre of the probe and fed to spectrometer as shown in figure 2.2(b).
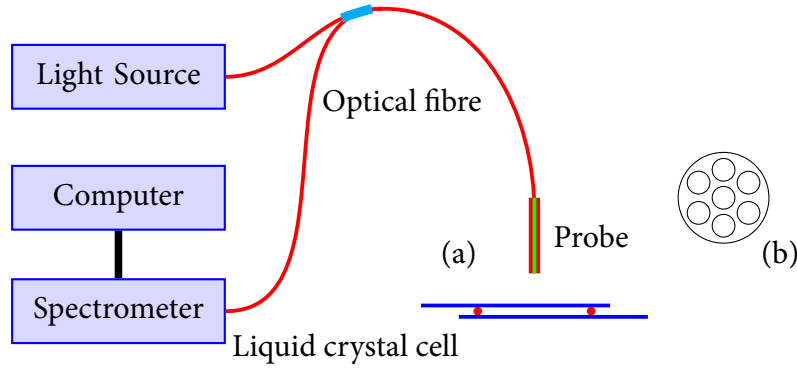
Figure 2.2: *(a) Schematic diagram for measurement of cell thickness. (b) Bottom view of probe.*

The corresponding spectrum is analized using SpectraSuite software. The spectrum consists alternative maxima and minima as shown in figure 2.3. The thickness of air gap between two glass plates (cell) is calculated by using the formula

$$d = \frac{\lambda_m \lambda_n}{\lambda_n - \lambda_m} \times \frac{n - m}{2} \qquad (2.1)$$

where λ_m and λ_n are wavelengths of mth and n^{th} maxima or minima.
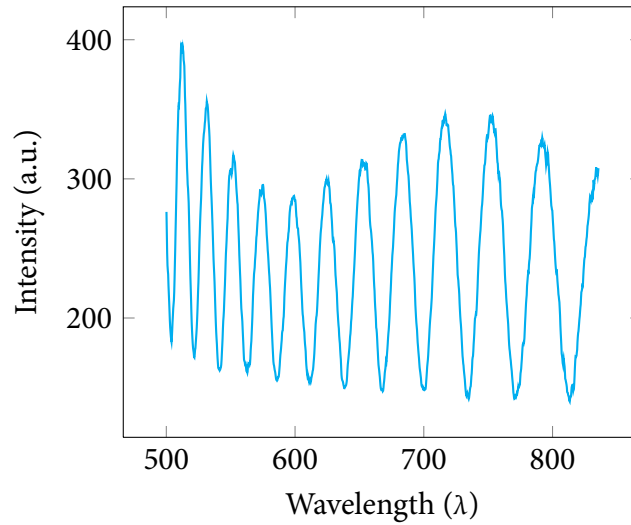
Figure 2.3: *The intensity variation from an empty cell.*

2.2   Measurement of dielectric constant

The cell forms a parallel plate capacitor with an effective area A separated by distance d. The empty cell capacitance is measured with the Agilent LCR Meter (E4980A). The capacitance measured is recorded as $C_\circ$. The cell is kept in heater and heated above T_{NI} of the liquid crystal sample. The sample is filled using capillary action in isotropic phase. Then it is cooled in the nematic phase and observed in a polarizing microscope to ensure desired alignment of liquid crystal director. The phase transition temperatures of the sample are noted and photographs are taken in various phases and at various temperatures. The ratio of capacitances with and without the sample gives the dielectric constant (ε). The dielectric constant measured in planar cell provides $\varepsilon_\perp$ as the applied field is perpendicular to the liquid crystal director. Similarly the dielectric constant measured in homeotropic cell provides $\varepsilon_{||}$ as the applied field is parallel to the director. The average dielectric constant and dielectric anisotropy can be easily estimated by using the relations $\langle \varepsilon \rangle = (\varepsilon_{||} + 2\varepsilon_\perp)/3$ and $\Delta\varepsilon = \varepsilon_{||} - \varepsilon_\perp$ respectively.

2.3   Measurement of birefringence

The birefringence ($\Delta n = n_e - n_o$) of a uniaxial liquid crystal sample can be measured with two techniques namely directly transmitted intensity measurement and phase modulation technique. Here we briefly discuss about the two techniques.

2.3.1   Intensity measurement technique

The birefringence of the sample is first measured using d.c. intensity measurement technique. The optical setup for measurement of birefringence using d.c. intensity measurement technique is shown in figure 2.4.
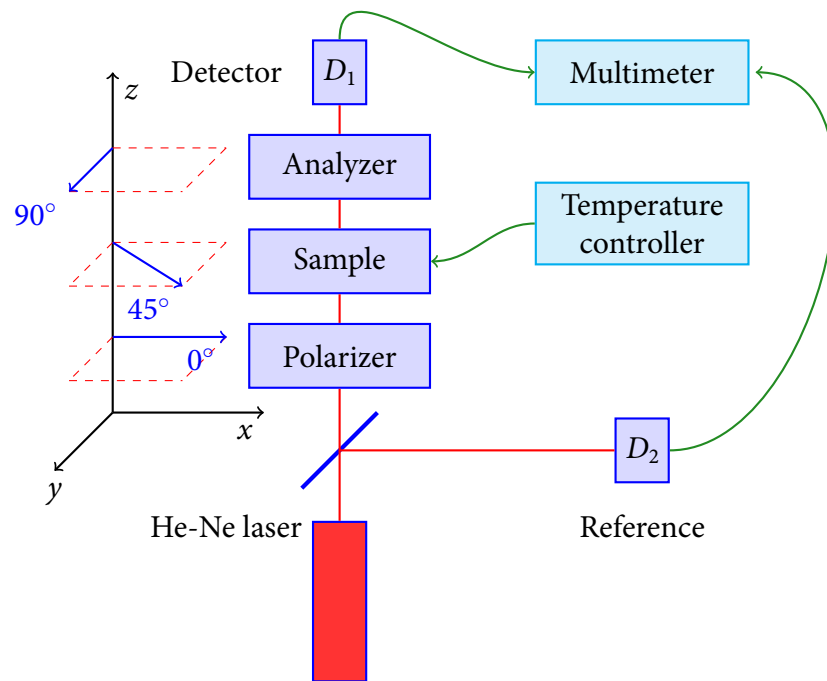
Figure 2.4: *Experimental diagram for measurement of birefringence using intensity measurement.*

The setup consists of two crossed Glan-Thompson polarizers, a He-Ne laser source and a detector. A vertical optical bench setup is used, where the sample is supported on a shelf with a hole for the light to pass through. The plane polarized light after first GT ploarizer passes through the sample in which the rubbing direction is kept at 45° with respect to first polarizer. The transmitted light passes through second GT polarizer and then goes to a detector. The detector output is connected to a Keithley DC voltmeter for measurement of output intensity. The temperature of sample is controlled by a temperature controller (Instec) with an accuracy of 10 mK. For measurement of temperature dependent birefringence, temperature is varied with finite steps and in every step the intensity at the detector is measured. All the measurements are controlled by a computer with the help of a software designed by us using LabVIEW.

Now consider liquid crystal sample of thickness *d* kept in between two crossed polarizers and the rubbing direction make an angle φ with polarizer. Assume polarizer and analyzer are in *x* and *y* direction and light propagates in *z* direction. The expression for the electric field of the transmitted light is given by [1]

$$E_{out} = P_{vertical}R(-\varphi)J_{lc}R(\varphi)P_{horizontal}E_{in} \tag{2.2}$$

where $R(\varphi)$ is rotation about an angle φ, is given by $R(\varphi) = \begin{pmatrix} \cos\varphi & \sin\varphi \\ -\sin\varphi & \cos\varphi \end{pmatrix}$,

J_{lc} is given by $J_{lc} = \begin{pmatrix} e^{-\frac{2\pi i}{\lambda}n_e d} & 0 \\ 0 & e^{-\frac{2\pi i}{\lambda}n_o d} \end{pmatrix}$, λ is the wavelength of the light and E_{in} is electric field of the incident light.

If the intensity of the light after the first polarizer is I_0 then intensity at the detector is given by

$$I = I_0 \sin^2(2\varphi)\sin^2\left(\frac{\pi\Delta n d}{\lambda}\right). \tag{2.3}$$

Setting φ=45°, the intensity at detector is given by

$$I_{meas} = I_0 \sin^2\left(\frac{\pi\Delta n d}{\lambda}\right) \tag{2.4}$$

and birefringence can be expressed as

$$\Delta n = \frac{\lambda}{\pi d}\arcsin\left(\sqrt{\frac{I_{meas}}{I_0}}\right). \tag{2.5}$$

2.3.2 Phase modulation technique

An optical setup for measurement of birefringence using phase modulation technique [2] is shown in figure 2.5. The setup consists of two crossed Glan-Thompson polarizers,

a photoelastic modulator, a He-Ne laser source and a detector. A photoelastic modulator (PEM) is used to modulate the polarization of the light source. The principle of PEM is that a transparent solid material becomes birefringent under compression or stretching. A fused silica bar is made to vibrate with a natural resonant frequency about 50 kHz and this vibration is sustained by a quartz piezoelectric transducer attached to the end of the bar. The transducer is controlled by an external controller. A vertical optical bench setup is used, where the sample is supported on a shelf. The plane polarized light after first GT ploarizer passes through PEM and sample where both are kept at 45° with respective to first polarizer. The light passes through second GT polarizer and then to a detector. The detector output is connected to a lock-in amplifier for detection of the first and second harmonics of AC signal.
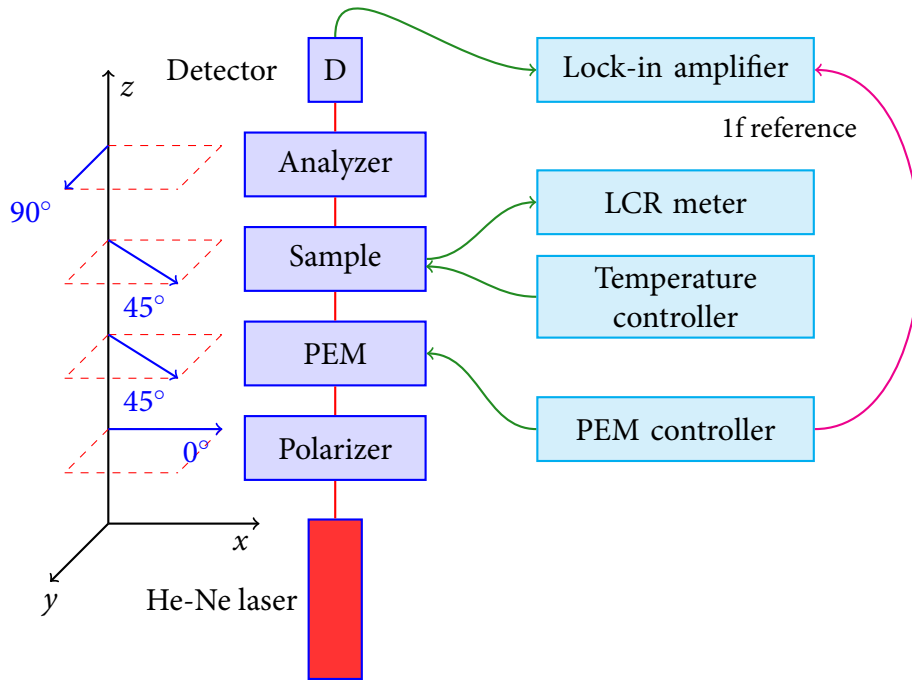
Figure 2.5: *Experimental diagram for the measurement of birefringence using PEM.*

The expression for transmitted electric field is given by

$$E_{out} = P_{vertical}R(-\varphi)J_{lc}J_{PEM}R(\varphi)P_{horizontal}E_{in}. \qquad (2.6)$$

Consider PEM making an oscillation with amplitude $A_\circ$ and an angular frequency ω. Then the retardation (A) due to the PEM can be expressed as $A = A_\circ \cos(\omega t)$, the Jones matrix for PEM is given by [3]

$$J_{PEM} = \begin{pmatrix} e^{\frac{2\pi i}{\lambda}\frac{A}{2}} & 0 \\ 0 & e^{\frac{-2\pi i}{\lambda}\frac{A}{2}} \end{pmatrix}. \tag{2.7}$$

The intensity at detector is given by

$$I = I_0 \sin^2(2\varphi) \sin^2\left(\frac{\pi(\Delta nd + A)}{\lambda}\right). \tag{2.8}$$

Setting $\varphi = 45°$, we get

$$I = I_0 \sin^2\left(\frac{\pi(\Delta nd + A)}{\lambda}\right). \tag{2.9}$$

Substituting $A = A_\circ \cos(\omega t)$ in above equation, we get

$$I = \frac{I_0}{2}\left(1 - \cos\left(\frac{2\pi}{\lambda}\Delta nd + \frac{2\pi}{\lambda}A_0\cos(\omega t)\right)\right) \tag{2.10}$$

by considering optical phase shift of the liquid crystal sample, $\Delta\Phi = \frac{2\pi d}{\lambda}\Delta n$ and expressing $A_\circ$ in units of phase angle, it reduces to

$$I = \frac{I_0}{2}\left[1 - \cos(\Delta\Phi)\cos(A_\circ\cos(\omega t)) + \sin(\Delta\Phi)\sin(A_\circ\cos(\omega t))\right]. \tag{2.11}$$

The above equation can be written as

$$\begin{aligned} I = {} & \frac{I_0}{2}\left[1 - \cos(\Delta\Phi) \times \{J_0(A_\circ) + 2(J_2(A_\circ)\cos(2\omega t)) + ...\}\right. \\ & \left. + \sin(\Delta\Phi) \times \{2(J_1(A_\circ)\cos(\omega t)) + ...\}\right] \end{aligned} \tag{2.12}$$

2.3 Measurement of birefringence

where J_0, J_1, J_2 are Bessel functions of various orders. Intensity can be written as

$$I = I_0 \left[\frac{1 - J_0(A_\circ)\cos(\Delta\Phi)}{2} + J_1(A_\circ)\sin(\Delta\Phi)\cos(\omega t) \right.$$
$$\left. + J_2(A_\circ)\cos(\Delta\Phi)\cos(2\omega t) + ... \right]. \tag{2.13}$$

Therefore the intensity measured by the lock-in amplifier with 1f and 2f signals are given by

$$I_{1f} = I_0 J_1(A_\circ)\sin(\Delta\Phi)$$
$$I_{2f} = I_0 J_2(A_\circ)\cos(\Delta\Phi). \tag{2.14}$$

In the present experiment $A_\circ = 2.405$ so that $J_0(A_\circ) = 0$, $J_1(A_\circ) = 0.519$ and $J_2(A_\circ) = 0.4318$.
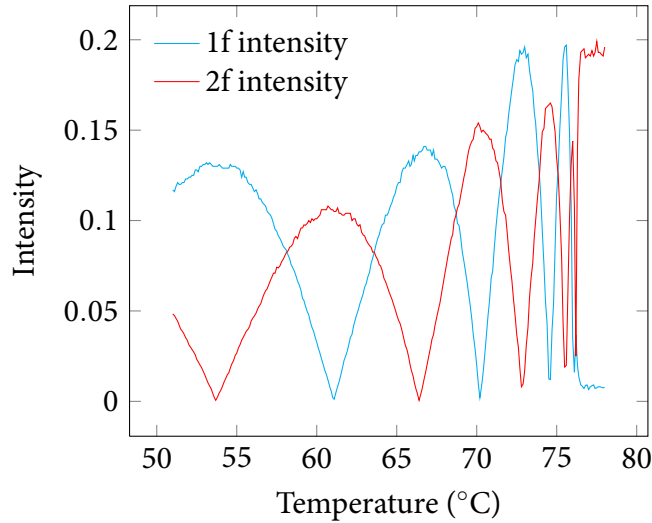
Figure 2.6: *Temperature dependent transmitted 1f and 2f signals of 6OCB.*

The birefringence of the sample is given by

$$\Delta n = \frac{\lambda}{2\pi d}\Delta\Phi = \frac{\lambda}{2\pi d}\arctan\left(\frac{I_{1f} \times J_2(A_\circ)}{I_{2f} \times J_1(A_\circ)}\right). \tag{2.15}$$
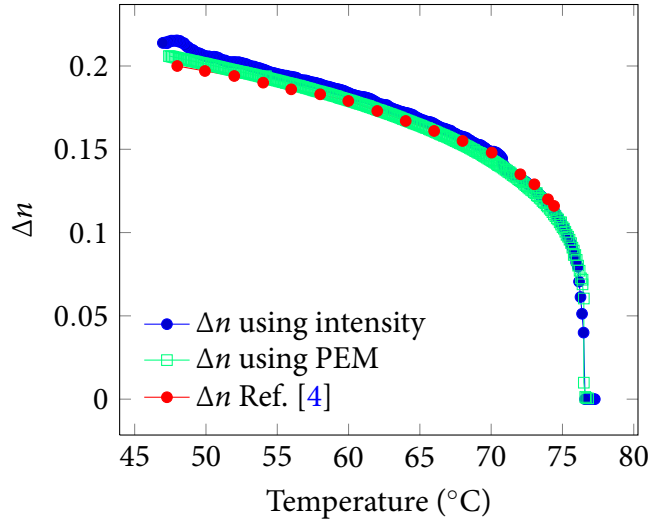
Figure 2.7: *Temperature dependent birefringence of 6OCB.*

The amplitude and frequency of PEM are regulated by its controller. The output frequency of PEM controller is given to lock-in amplifier as an external reference signal. The lock-in amplifier measures amplitude of first and second harmonics of the output signal with respect to reference frequency. The birefringence is calculated using equation 2.15.

The birefringence of 6OCB (*p*-hexyloxy-*p*'-cyanobiphenyl) measured by the above techniques are shown in figure 2.7. Our measurements are also compared with the data available in the literature [4] those are measured by direct intensity measurement technique. It is observed that the temperature variation of birefringence measured with phase modulation technique is smoother than the direct intensity measurement technique. In addition we can measure very small birefringence ($\sim 10^{-3}$) very accurately by phase modulation technique.

2.4 Measurement of elastic constants

The elastic constants are measured using electro-optic technique. The voltage dependent retardation of a planar aligned sample is used to measure splay and bend elastic

constants of liquid crystal with $\Delta\varepsilon > 0$.

(a) $V < V_{th}$ (b) $V > V_{th}$
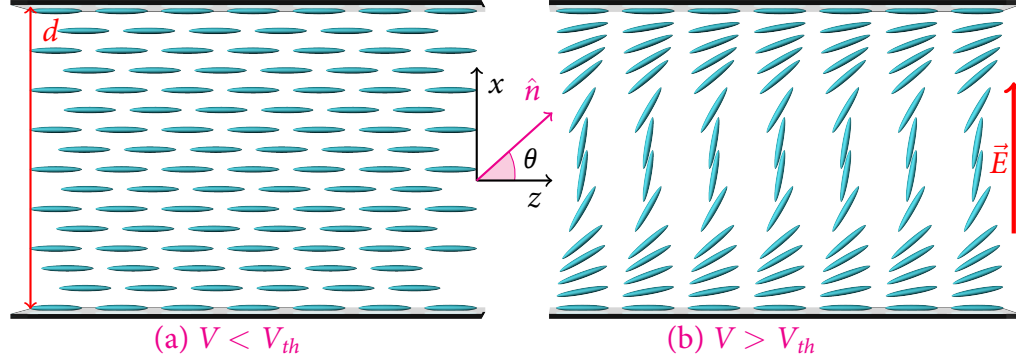
Figure 2.8: *Schematic representation of director configuration is shown (a) below and (b) above the threshold field respectively.*

Consider a liquid crystal with $\Delta\varepsilon > 0$ is enclosed between two conducting glass plates with a gap d as shown schematically in figure 2.8. If an electric field E is applied along the x-axis, the dielectric energy is lowered by tilting the director. Now consider director ($\hat{n}$) to be strongly anchored to the boundaries and parallel to the z-axis. The electric field is along the x direction and we write,

$$Director: \quad \hat{n} = (\sin\theta(x), 0, \cos\theta(x)) \tag{2.16}$$

$$Electric\ field: \quad \vec{E} = (E_x, 0, 0) \tag{2.17}$$

with $\theta(0) = \theta(d) = 0$. Now $\theta(x)$ is a function of x and has maximum θ_m at $x = d/2$. After applying electric field, the director deforms and free energy per unit area is given by [5–8]

$$F = \frac{1}{2}\int_0^d \left[(K_{11}\cos^2\theta + K_{33}\sin^2\theta)\left(\frac{d\theta}{dx}\right)^2 - \vec{D}\cdot\vec{E}\right]dx + 2f_s(\theta_0), \tag{2.18}$$

where $\vec{D}$ is displacement vector and f_s is surface free energy density. Considering there are no free ions in liquid crystal and $\vec{E}$ satisfies maxwell equations $\nabla\cdot\vec{D} = 0, \nabla\times\vec{E} = 0$. Since $\nabla\cdot\vec{D} = 0$, x-component of D is constant. D_x is independent of x but depends

on $\theta(x)$ and given by

$$D_x = \frac{\varepsilon_0 V}{\int_0^d (\varepsilon_{||} \sin^2 \theta + \varepsilon_\perp \cos^2 \theta) dx}. \tag{2.19}$$

Free energy density is given by

$$
F = \frac{1}{2} \int_0^d \left[(K_{11} \cos^2 \theta + K_{33} \sin^2 \theta) \left(\frac{d\theta}{dx} \right)^2 \right] dx
$$
$$
- \frac{\varepsilon_0 V^2}{2 \int_0^d (\varepsilon_{||} \sin^2 \theta + \varepsilon_\perp \cos^2 \theta)^{-1} dx} + 2 f_s(\theta_0). \tag{2.20}
$$

This free energy is minimised with appropriate Euler Lagrange equation [9]. The Euler-Lagrange equation yields

$$
\frac{d}{dx} \left[\frac{d\theta}{dx} (K_{11} \cos^2 \theta + K_{33} \sin^2 \theta) \right] = (K_{33} - K_{11}) \sin \theta \cos \theta \left(\frac{d\theta}{dx} \right)^2
$$
$$
- \frac{D_x^2}{\varepsilon_0} \frac{(\varepsilon_{||} - \varepsilon_\perp) \sin \theta \cos \theta}{(\varepsilon_{||} \sin^2 \theta + \varepsilon_\perp \cos^2 \theta)^2}. \tag{2.21}
$$

Multiplying by $2\frac{d\theta}{dx}$ and integrating once

$$
(K_{11} \cos^2 \theta + K_{33} \sin^2 \theta) \left(\frac{d\theta}{dx} \right)^2 = C + \frac{D_x^2}{\varepsilon_0} (\varepsilon_{||} \sin^2 \theta + \varepsilon_\perp \cos^2 \theta)^2 \tag{2.22}
$$

where C is integration constant and is calculated by putting condition $d\theta/dx = 0$ and $\theta(x) = \theta_m$ at $x = d/2$. Then

$$
C = -\frac{D_x^2}{\varepsilon_0} \frac{1}{\varepsilon_\perp \cos^2 \theta_m + \varepsilon_{||} \sin^2 \theta_m}
$$

putting $\gamma = (\varepsilon_{||} - \varepsilon_\perp)/\varepsilon_\perp$ and $\kappa = (K_{33} - K_{11})/K_{11}$ we get

$$
\frac{d\theta}{dx} = D_x \sqrt{\gamma/(\varepsilon_0 \varepsilon_\perp K_{11})} \left(\frac{\sin^2 \theta_m - \sin^2 \theta}{(1 + \kappa \sin^2 \theta)(1 + \gamma \sin^2 \theta_m)(1 + \gamma \sin^2 \theta)} \right)^{\frac{1}{2}}. \tag{2.23}
$$

Integrating inverse of equation 2.23 and for $x = d/2$ we have $\theta = \theta_m$

$$D_x = \frac{2}{d} \sqrt{\varepsilon_0 \varepsilon_\perp K_{11}/\gamma} \sqrt{1 + \gamma \sin^2 \theta_m} \int_0^{\theta_m} \left(\frac{(1 + \kappa \sin^2 \theta)(1 + \gamma \sin^2 \theta)}{\sin^2 \theta_m - \sin^2 \theta} \right)^{\frac{1}{2}} d\theta. \tag{2.24}$$

From equation 2.19 and equation 2.23 and substituting $\sin \theta = \sin \theta_m \sin \psi$ we get

$$\frac{V}{V_{th}} = \sqrt{1 + \gamma \sin^2 \theta_m} \int_\Theta^{\frac{\pi}{2}} \left[\frac{1 + \kappa \sin^2 \theta_m \sin^2 \psi}{(1 + \gamma \sin^2 \theta_m \sin^2 \psi)(1 - \sin^2 \theta_m \sin^2 \psi)} \right]^{\frac{1}{2}} d\psi \tag{2.25}$$

where $\Theta = \sin^{-1}(\sin \theta_0 / \sin \theta_m)$ and $V_{th} = \pi \sqrt{\frac{K_{11}}{\varepsilon_0 \varepsilon_\perp \gamma}}$ is the Freedericksz threshold voltage.

For any applied voltage, the optical phase difference is given by,

$$\delta \Phi = \frac{2\pi}{\lambda} \int_0^d [n_{eff}(x) - n_0] dx \tag{2.26}$$

where, $n_{eff}(x) = n_e n_0 / \sqrt{(n_e^2 \sin^2 \theta + n_0^2 \cos^2 \theta)}$ is the effective extraordinary index at x. Now inserting equation 2.23 in equation 2.26 we get

$$1 - \delta \Phi \cdot 2\pi \lambda / (n_e d) = (1/D_x) \sqrt{\varepsilon_0 \varepsilon_\perp K_{11}/\gamma} \sqrt{1 + \gamma \sin^2 \theta_m}$$

$$\times \frac{2}{d} \int_0^{\theta_m} \left[\frac{(1 + \kappa \sin^2 \theta)(1 + \gamma \sin^2 \theta)}{(1 + \nu \sin^2 \theta)(\sin^2 \theta_m - \sin^2 \theta)} \right]^{\frac{1}{2}} d\theta \tag{2.27}$$

where $\nu = (n_e^2 - n_0^2)/n_0^2$.

Inserting D_x from equation 2.24 we get

$$\left(1 - \delta \Phi \cdot \frac{2\pi \lambda}{n_e d} \right) \cdot \int_0^{\theta_m} \left[\frac{(1 + \kappa \sin^2 \theta)(1 + \gamma \sin^2 \theta)}{\sin^2 \theta_m - \sin^2 \theta} \right]^{\frac{1}{2}} d\theta =$$

$$\int_0^{\theta_m} \left[\frac{(1 + \kappa \sin^2 \theta)(1 + \gamma \sin^2 \theta)}{(1 + \nu \sin^2 \theta)(\sin^2 \theta_m - \sin^2 \theta)} \right]^{\frac{1}{2}} d\theta. \tag{2.28}$$

Substituting $\sin\theta = \sin\theta_m \sin\psi$ and rearranging, we get

$$\delta\Phi(V) = 2\pi\frac{n_e d}{\lambda}\left[\frac{\int_\Theta^{\pi/2}\sqrt{\frac{(1+\kappa\sin^2\theta_m\sin^2\psi)(1+\gamma\sin^2\theta_m\sin^2\psi)}{(1-\sin^2\theta_m\sin^2\psi)(1+\nu\sin^2\theta_m\sin^2\psi)}}d\psi}{\int_\Theta^{\pi/2}\sqrt{\frac{(1+\kappa\sin^2\theta_m\sin^2\psi)(1+\gamma\sin^2\theta_m\sin^2\psi)}{(1-\sin^2\theta_m\sin^2\psi)}}d\psi} - \frac{n_0}{n_e}\right]. \tag{2.29}$$

An electric field is applied orthogonal to the director in a well aligned sample and the optical phase difference is measured as a function of applied voltage using phase modulation technique. Above a certain voltage (called threshold voltage) the director orientation distorts and it is called Freedericksz transition. The threshold voltage is given by

$$V_{th} = \pi\sqrt{\frac{K_{11}}{\varepsilon_0\Delta\varepsilon}} \tag{2.30}$$

where K_{11} is splay elastic constant and $\Delta\varepsilon$ is dielectric anisotropy. For a fixed temperature the voltage dependent optical phase difference above threshold voltage is fitted iteratively using equations 2.25 and 2.29 using Θ, κ and θ_m as parameters. From Freedericksz transition splay (K_{11}) elastic constant is calculated and from κ ($= (K_{33} - K_{11})/K_{11}$) bend ($K_{33}$) elastic constant is calculated within $\pm 6\%$ error.

Algorithm for fitting to estimate K_{33}

    i. Read Δn, n_o, $\varepsilon_{||}$, $\varepsilon_\perp$ and K_{11}

    ii. Choose approximate values of κ, θ_0 and θ_m

    iii. Evaluate the V and $\delta\Phi$

    iv. Interpolate experimental data

    v. Measure χ^2

    vi. Adjust Θ and κ to get minimum χ^2

    vii. Calculate K_{33} using κ and K_{11}
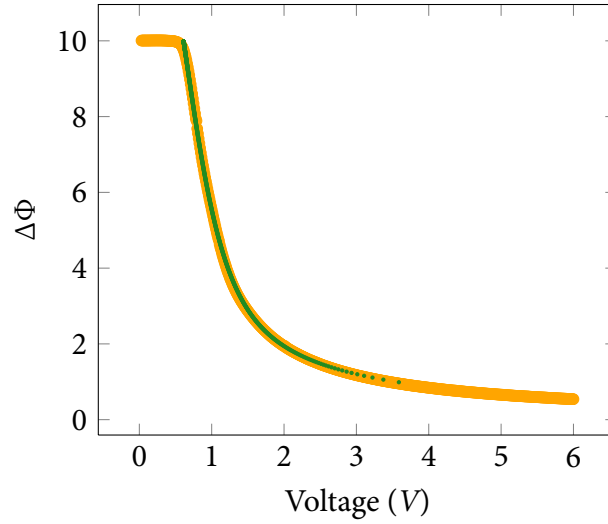
Figure 2.9: *The best fit to the theoretical retardation obtained by using equations 2.25 and 2.29 is given by a solid line.*

Bend elastic constant (K_{33}) is estimated using a nonlinear least square fitting of the experimental data using theoretical relations. A numerical program is written using Mathematica software (Wolfram). All the elliptic integrals are evaluated numerically by the inbuilt package available in Mathematica. Some of the parameters required to fit the experimental data above Freedericksz threshold are birefringence (Δn), ordinary refractive index (n_o), parallel ($\varepsilon_{||}$) and perpendicular ($\varepsilon_{\perp}$) dielectric constants and splay elastic constant (K_{11}). Initially one has to choose approximate values of κ, tilt angle of director at surface (θ_0) and maximum angle of director at the centre (θ_m) of the cell. These values are used to evaluate the voltage V (eqn. 2.25) and optical phase difference $\delta\Phi$ (eqn. 2.29). It is enough to generate voltage values up to 2.5 times of V_{th}. In general experimental values of applied voltage data points do not coincide with theoretically evaluated, hence the experimental data is interpolated to get experimental data points corresponding to the theoretically generated points. Mean square deviation (χ^2) is calculated by taking difference between theoretically calculated and experimentally obtained optical phase difference values. Θ and κ are varied as fit parameters to lower the value of χ^2. Best fit parameters Θ and κ are evaluated at minimum χ^2.

2.5 Measurement of viscosity

2.5.1 Measurement of passive viscosities

To measure the passive viscosity coefficients, i.e., the viscosities parallel and perpendicular to the director, we used a videomicroscopy technique where the Brownian motion of a tiny silica microsphere (diameter 0.98 μm) was tracked. Now consider colloidal particles (silica microspheres of radius r) irregularly dispersed in a liquid of viscosity η.

The probability that a particle will diffuse a distance δ in the plane in time τ obeys the Gaussian distribution [10]

$$P(\delta|\tau) = P_0(\tau) \exp\left(-\frac{\delta^2}{\Delta^2(\tau)}\right) \tag{2.31}$$

where $P_0(\tau)$ is a normalization constant and $\Delta(\tau)$ the width of the distribution. The self-diffusion coefficient of a random walker is given by the Stokes-Einstein relation

$$D = \frac{k_B T}{6\pi r \eta} \tag{2.32}$$

where k_B is the Boltzmann constant and T is the temperature [10].

We measure the passive viscosity coefficients ($\eta_{||}$ and $\eta_\perp$) parallel and perpendicular to the director $\hat{n}$. These can be compared to the Miesowicz viscosity coefficients η_1, η_2 (fig. 1.15) i.e., $\eta_{||} \simeq \eta_2$ and $\eta_\perp \simeq \eta_3$. The silica microspheres of diameter 0.98 μm (Bangs Laboratories) are dispersed in 0.5% water solution of octadecyldimethyl (3-trimethoxysilylpropyl) ammonium chloride (DMOAP) and mixed for several minutes. The microspheres are then rinsed with distilled water several times and dried for 30 min at 120 °C. The dried microspheres are dispersed in the liquid crystal mixtures with an approximate concentration of 0.1%. Uniform colloidal dispersion is obtained

by mechanical means like vortexing and sonication. The particles are observed under an inverted polarizing microscope (Nikon Eclipse, TE2000-U) with water immersion microscope objective (100X) and NA=1.1. The Brownian motion of an isolated microsphere is video recorded for at least 300 s and the position is determined with the help of a computer program. The obtained histogram of the microparticle displacements is Gaussian. The diffusion coefficient parallel and perpendicular to the director ($D_\parallel$ and $D_\perp$) of the thermal motion are obtained using the relation $D_{\parallel,\perp} = \Delta_{\parallel,\perp}^2/4\tau$. $\eta_\parallel$ and $\eta_\perp$ are calculated using $\eta_{\parallel/\perp} = \frac{k_B T}{6\pi r D_{\parallel,\perp}}$. We calibrated this technique using 5CB. It may be noted that this technique needs a very small amount of sample (a few micro litre) and hence very useful for studying unconventional liquid crystals.

2.5.2 Measurement of rotational viscosity
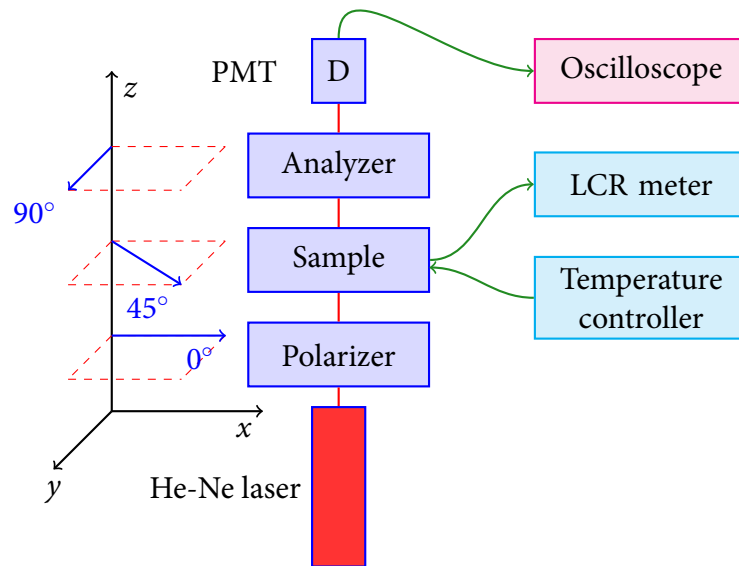
Figure 2.10: *Experimental diagram for measurement of rotational viscosity.*

Rotational viscosity (γ_1) is measured using phase-decay-time measurement [11] of a parallel aligned liquid crystal (LC) cell under small excitation voltage. The experimental setup for measurement of rotational viscosity (γ_1) is shown in figure 2.10. The measurement consists two steps; i) measurement of intensity with voltage at fixed

temperature, and ii) measurement of time dependent relaxation transmission intensity. The setup consists two Glan-Thompson polarizers, He-Ne laser and a photomultiplier tube (Hamamatsu). The rubbing direction of the sample is kept at 45° to both polarizer and analyzer and the intensity is measured using photomultiplier tube (PMT) with an oscilloscope. The equation of motion of planar aligned nematic liquid crystal under electric field is given by [12, 13]

$$(K_{11} \cos^2 \theta + K_{33} \sin^2 \theta)\frac{d^2\theta}{dx^2} + (K_{33} - K_{11}) \sin \theta \cos \theta \left(\frac{d\theta}{dx}\right)^2$$
$$+\varepsilon_0 \Delta\varepsilon E^2 \sin \theta \cos \theta = \gamma_1 \frac{d\theta}{dt} + \mathbb{I}\frac{d^2\theta}{dt^2} \qquad (2.33)$$

If the blackflow and inertial effects are ignored, and under small angle approximation $(\sin \theta \sim \theta$ & $K_{11} \sim K_{33})$

$$K_{11}\frac{d^2\theta}{dx^2} + \varepsilon_0 \Delta\varepsilon E^2 \theta = \gamma_1 \frac{d\theta}{dt} \qquad (2.34)$$

When electric field is switched off then

$$K_{11}\frac{d^2\theta}{dx^2} = \gamma_1 \frac{d\theta}{dt} \qquad (2.35)$$

and the solution is given by

$$\theta(x, t) = \theta_m \sin\left(\frac{\pi x}{d}\right) \exp\left(\frac{-t}{\tau_\circ}\right) \qquad (2.36)$$

where $\tau_\circ = \frac{\gamma_1 d^2}{K_{11}\pi^2}$ and θ_m is maximum tilt angle at the centre of the cell.

The phase decay time is expressed as [14]

$$\delta(t) = \delta_0 \exp\left(\frac{-2t}{\tau_\circ}\right) \qquad (2.37)$$

when δ_0 is equal or in the vicinity of $(N + 1/2)\pi$,

$$\delta(t) = \delta_0 \exp\left(\frac{-4t}{\tau_\circ}\right) \qquad (2.38)$$

when δ_0 is equal or in the vicinity of $N\pi$.

The time dependent transmitted intensity is

$$I(t) = I_0 \sin^2\left[(\Delta_{tot} - \delta(t))/2\right]. \qquad (2.39)$$
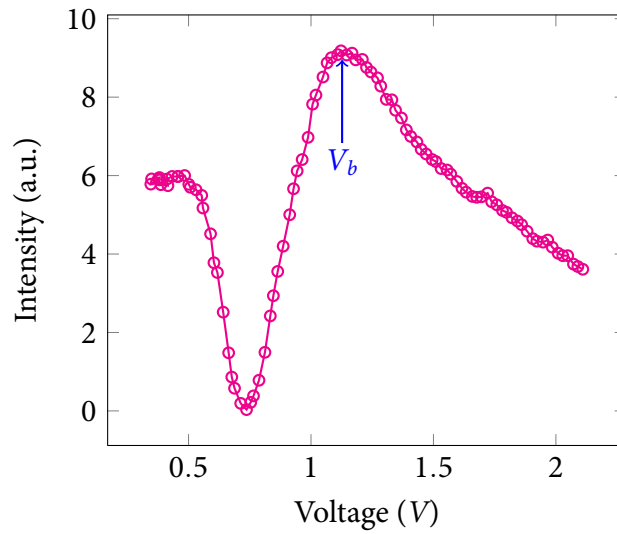
Figure 2.11: *Voltage dependent transmission intensity at $T = 33.2\,^\circ C$ in 5CB.*

The experimental procedure consists of two steps namely measurement of voltage dependent intensity at a fixed temperature and measurement of time dependent transmitted intensity after switching off the electric field. The voltage dependent transmitted intensity is measured to find the maxima and minima. A typical variation of voltage dependent intensity for 5CB is shown in figure 2.11. A small voltage (V_b) corresponding to the first maxima or minima was applied depending on the transmission intensity, such that the total phase retardation of the sample was $n\pi$. At time $t = 0$, the bias voltage (V_b) was removed and the relaxation transmission intensity change of
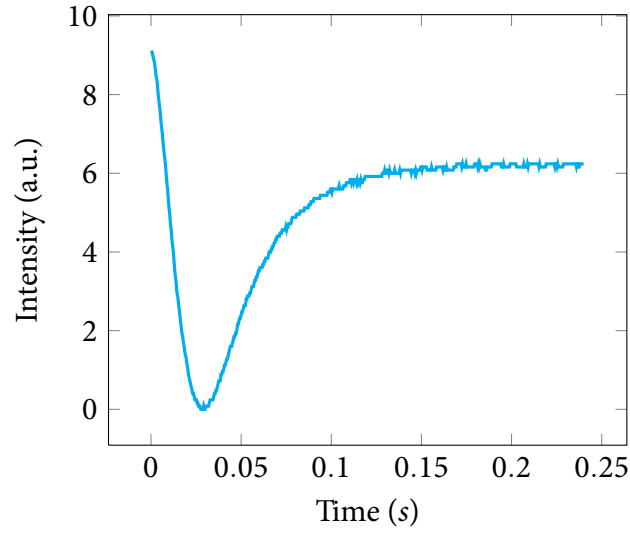
Figure 2.12: *Time dependent transmission intensity after the removal of the bias voltage V_b in 5CB ($T = 33.2\,^\circ C$).*
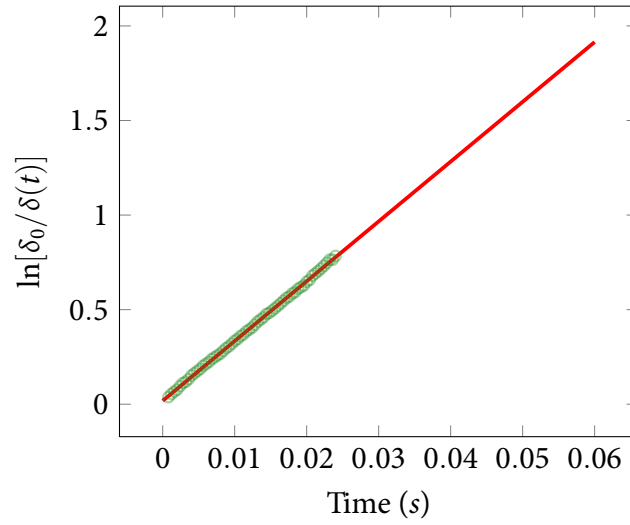
Figure 2.13: *Linear variation of $\ln[\delta_0/\delta(t)]$ with time (t) in 5CB ($T = 33.2\,^\circ C$).*

the liquid crystal cell was measured with an oscilloscope (fig. 2.12). The phase difference $\delta(t)$ for small director deformation (given by equation 2.37) is calculated from equation 2.39. The relaxation time $\tau_\circ$ is estimated from the plot of $ln[\delta_0/\delta(t)]$ with t (fig. 2.13). The rotational viscosity (γ_1) of the liquid crystal is calculated using

$$\gamma_1 = \frac{\tau_\circ K_{11} \pi^2}{d^2}. \tag{2.40}$$

The setup is calibrated using 5CB at a few temperatures. At T=28 °C the reported value is 63.1 mPa s and we obtained 62.7 mPa s. Our results are comparable to the values known in the literature [15].

2.6 Measurement of flexoelectric coefficients

We used a standard experimental technique for measuring flexoelectric coefficients ($e^* = e_1 - e_3$) of nematic liquid crystals [16, 17]. The experimental setup for measurement of flexoelectric coefficients is shown in figure 2.14.
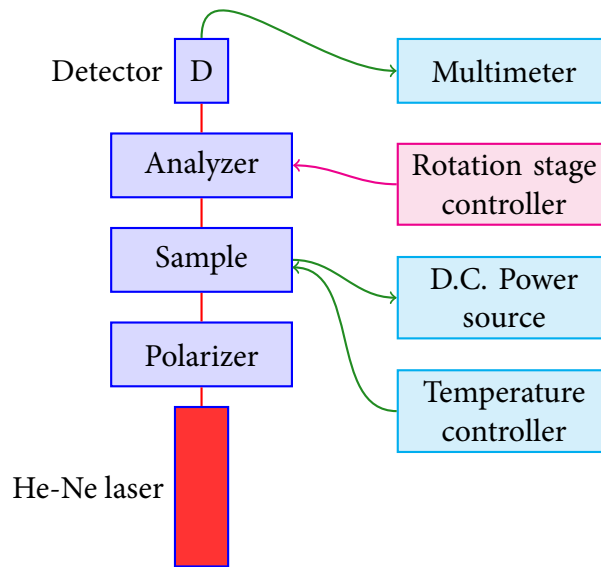
Figure 2.14: *Experimental diagram for the measurement of flexoelectric coefficients.*

The setup consists two GT polarizers, He-Ne laser and a detector. The Analyzer is mounted on rotating stage (Thor Labs) and its rotation can be controlled by a controller. We prepared a hybrid aligned cell in which the bottom plate is coated with AL-1254 to get homogeneous alignment and top plate is coated with JALS-204 to get homeotropic alignment. Two aluminium strip electrodes are placed 850 μm apart on the bottom plate such that electrodes are parallel to the rubbing direction which also acts as spacers. The thickness of the cell is about 20 μm. A schematic diagram is

shown in figure 2.15. A dc voltage is applied and intensity is measured with rotation of analyzer.
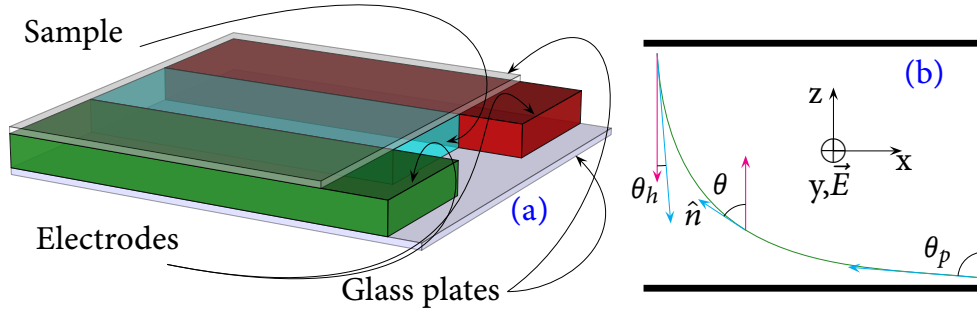
Figure 2.15: *(a) Geometry of the HAN cell used in the measurement of e^*/K. (b) Twist deformation produced by an inplane dc electric field along the y-axis. Top plate is coated with homeotropic alignment layer ($\theta_h \simeq 0°$) and bottom plate is coated with planar alignment layer ($\theta_p \simeq 90°$).*

The structure of cell causes splay-bend deformation in the director field, which give rise to flexoelectric polarization $\vec{P} = e_1(\nabla \cdot \hat{n})\hat{n} + e_3(\nabla \times \hat{n}) \times \hat{n}$. As we apply the field along y axis, an electric torque results which creates a twist in the director field.

The elastic energy density before the application of field is given by

$$f_{el} = \frac{K}{2}\left[\left(\frac{d\theta}{dz}\right)^2 + \sin^2\theta\left(\frac{d\varphi}{dz}\right)^2\right] \tag{2.41}$$

where θ is tilt angle, φ is twist angle and K is average Frank elastic constant. The splay-bend deformation is defined by $\varphi = 0$ and $d^2\theta/dz^2 = 0$. Now the coupling energy between $\vec{P}$ and $\vec{E}$ is $-\vec{P} \cdot \vec{E} = e^*E\sin^2\theta\sin\varphi\frac{d\theta}{dz}$, where φ is the twist caused by field $\vec{E}$. The equilibrium equations can be written as

$$K\left[\frac{d^2\theta}{dz^2} - \sin\theta\cos\theta\left(\frac{d\varphi}{dz}\right)^2\right] = -e^*E\sin^2\theta\cos\varphi\frac{d\varphi}{dz} \tag{2.42}$$

$$\frac{d}{dz}\left(K\sin^2\theta\frac{d\varphi}{dz}\right) = e^*E\sin^2\theta\cos\varphi\frac{d\theta}{dz}. \tag{2.43}$$

In the absence of electric field, $\varphi = 0$, and equation 2.42 reduces to

$$\frac{d\theta}{dz} = C_1 Z + C_2 \tag{2.44}$$

where C_1 and C_2 are two integration constants. In splay-bend distortion the boundary conditions are, $\theta(z = 0) = \pi/2$ and $\theta(z = d) = 0$. Tilt angle θ can be expressed as

$$\theta(z) = \frac{\pi}{2}\left(1 - \frac{z}{d}\right). \tag{2.45}$$

For low fields, φ is a linear function of $\vec{E}$. We can calculate φ by linearizing equation 2.43 in φ.

$$
\begin{aligned}
\frac{d}{dz}\left(K\sin^2\theta\frac{d\varphi}{dz}\right) &= e^*E\sin^2\theta\left(\frac{d\theta}{dz}\right) \\
or,\ \frac{d}{d\theta}\left(K\sin^2\theta\frac{d\varphi}{dz}\right) &= e^*E\sin^2\theta \\
or,\ K\sin^2\theta\left(\frac{d\varphi}{dz}\right) &= \frac{e^*E}{2}\left(\theta - \frac{\sin 2\theta}{2}\right) \\
or,\ K\sin^2\theta\left(\frac{d\varphi}{d\theta}\frac{d\theta}{dz}\right) &= \frac{e^*E}{2}\left(\theta - \frac{\sin 2\theta}{2}\right)
\end{aligned}
$$

Inserting the value of $d\theta/dz$ from equation 2.45 we get,

$$\frac{d\varphi}{d\theta} = \left(\frac{e^*Ed}{\pi K}\right)\left[\frac{1}{2}\sin 2\theta - \theta\right]\sin^{-2}\theta. \tag{2.46}$$

Integrating equation 2.46 we get $\varphi(z)$. Now the largest value $\varphi(d)$ at top plate is given by

$$\varphi(d) = \frac{e^*Ed}{\pi K}. \tag{2.47}$$

The cell is kept in between crossed polarizers such that the rubbing direction is parallel to polarizer. When there is no field, the polarized light emerges without intact and gives minimum intensity at $0°$ (crossed possition) and increases as we rotate analyzer
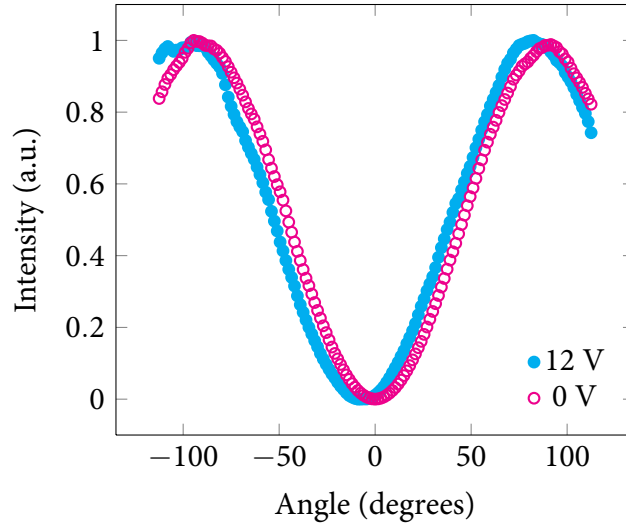
Figure 2.16: *Variation of intensity with the the rotation of analyzer.*
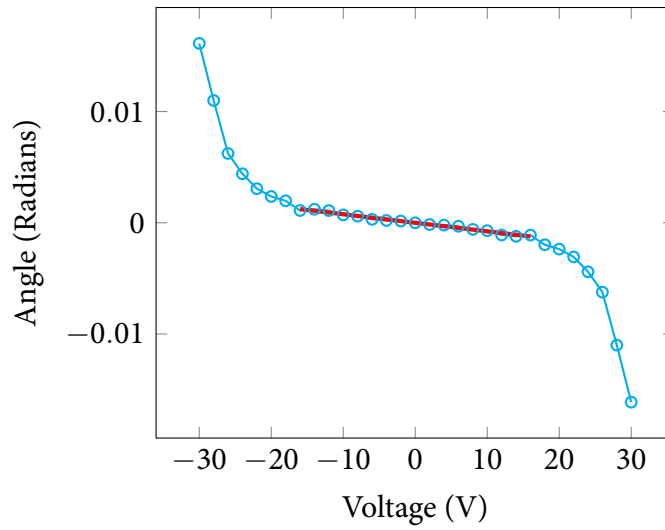
Figure 2.17: *Variation of field-induced azimuthal twist angle as a function of voltage. Solid line represent the best fit to the equation $\varphi = e^* E d / \pi K$.*

as shown in figure 2.16. When we apply dc field, twist deformation occurs in director field which causes a rotation of φ in the plane of polarization of transmitted light. The rotation φ is proportional to the magnitude of field $\vec{E}$ (eqn. 2.45). φ is measured as a function of applied electric field and e^*/K is estimated from the best fit in the linear region (fig. 2.17). The variation of intensity with rotation of analyzer at two different voltages are shown in the figure 2.16.

References

[1] T. Scharf, *Polarized light in liquid crystals and polymers.* Wiley-Interscience, 2007.

[2] T. C. Oakberg, "Measurement of low-level strain birefringence in optical elements using a photoelastic modulator," *Proc. SPIE*, vol. 2873, no. 3, pp. 17–20, 1996.

[3] J. C. Kemp, "Basic Laboratory setup for various measurements possible with the photoelastic modulator," *Application Note*, p. Hinds Instruments, 1975.

[4] V. Manjuladevi, *Experimental Studies on Phase Diagrams of Liquid Crystals.* PhD thesis, Jawaharlal Nehru University, New Delhi, 2004.

[5] F. C. Frank, "I. liquid crystals. on the theory of liquid crystals," *Discuss. Faraday Soc.*, vol. 25, pp. 19–28, 1958.

[6] H. Gruler and G. Meier, "Electric field-induced deformations in oriented liquid crystals of the nematic type," *Molecular Crystals and Liquid Crystals*, vol. 16, no. 4, pp. 299–310, 1972.

[7] H. J. Deuling, "Deformation of nematic liquid crystals in an electric field," *Molecular Crystals and Liquid Crystals*, vol. 19, no. 2, pp. 123–131, 1972.

[8] H. Gruler, T. Sheffer, and G. Meier, "Elastic constants of nematic liquid crystals. I. theory of the normal deformation," *Z. Naturforsch*, vol. 27a, pp. 966–976, 1972.

[9] Y. A. Nastishin, R. D. Polak, S. V. Shiyanovskii, V. H. Bodnar, and O. D. Lavrentovich, "Nematic polar anchoring strength measured by electric field techniques," *Journal of Applied Physics*, vol. 86, no. 8, pp. 4199–4213, 1999.

[10] P. M. Chaikin and T. C. Lubensky, *Principles of Condensed Matter Physics.* Cambridge University Press, 1998.

[11] S.-T. Wu, "Phase retardation dependent optical response time of parallel-aligned liquid crystals," *Journal of Applied Physics*, vol. 60, no. 5, pp. 1836–1838, 1986.

[12] J. L. Ericksen, "Conservation laws for liquid crystals," *Transactions of the Society of Rheology*, vol. 5, no. 1, pp. 23–34, 1961.

[13] F. M. Leslie, "Some constitutive equations for liquid crystals," *Archive for Rational Mechanics and Analysis*, vol. 28, pp. 265–283, 1968.

[14] S.-T. Wu and C.-S. Wu, "Experimental confirmation of the osipov-terentjev theory on the viscosity of nematic liquid crystals," *Phys. Rev. A*, vol. 42, pp. 2219–2227, Aug 1990.

[15] A. V. Zakharov, A. V. Komolkin, and A. Maliniak, "Rotational viscosity in a nematic liquid crystal: A theoretical treatment and molecular dynamics simulation," *Phys. Rev. E*, vol. 59, pp. 6802–6807, Jun 1999.

[16] Dozov, I., Martinot-Lagarde, Ph., and Durand, G., "Flexoelectrically controlled twist of texture in a nematic liquid crystal," *J. Physique Lett.*, vol. 43, no. 10, pp. 365–369, 1982.

[17] P. R. M. Murthy, V. A. Raghunathan, and N. V. Madhusudana, "Experimental determination of the flexoelectric coefficients of some nematic liquid crystals," *Liquid Crystals*, vol. 14, no. 2, pp. 483–496, 1993.

3

Optical, dielectric and viscoelastic properties of liquid crystal mixtures of rod-like and bent-core molecules

3.1 Introduction

Most of the liquid crystal displays (LCDs) use liquid crystalline mixture because all the desired physical and electroptical properties can not be achieved in a single compound. Efforts are made to obtain the desired properties by synthesizing new kinds of liquid crystal molecules. This led to the discovery of new liquid crystals such as discotic and bent-core liquid crystals. Recently the liquid crystals made of bent-core molecules created interest in the liquid crystal community. The bent molecules exhibit several phases such as B_1, B_2, ... and B_8 (B-phases) etc as mentioned in the introduction. In the beginning there were some experimental studies on binary mixtures of bent-core and rod-like molecules. Here

we summarise a few of them. A new orientational transition in binary mixtures of rod and bent-core molecules was reported by Pratibha *et al.* [1, 2]. Dodge *et al.* [3, 4] measured the bend elastic (K_{33}) constant in mixtures of 8OCB with different kinds of bent-core molecules and showed that the addition of a small concentration of bent-core liquid crystal in calamitic compound system reduces K_{33} by a factor of two or more. Later Kundu *et al.* [5] studied mixture of BC12 and 8OCB at various concentrations and reported anomalous trend in the temperature dependence of K_{11} and K_{33} in the nematic phase and explained the results on the basis of their mutual orientation [5] in the presence of short-range smectic fluctuations. They [6] also reported the evidence of polar clusters of bent-core molecules in the nematic phase of a binary mixture of rod-like and bent-core molecules. In this chapter, we present the measurements of Δn, K_{11}, K_{33} and γ_1 as a function of temperature and we show that these physical properties of the mixture are significantly different than the previously reported in other binary systems. We emphasize that the difference is owing to the structural similarity i.e., the molecular structure of the rod is matched with one half of the bow in the present system.

3.2 Results and Discussion

3.2.1 Chemical structures and phase diagram

We prepared various mixtures of compounds 4-biphenylyl-4″-*n*-undecycloxybenzoate and 1,3-phenylene-bis[4-(3-methylbenzoyloxy)]-4′-*n*-dodecylbiphenyl-4′-carboxylate. The chemical structures of the compounds and their individual phase transition temperatures are shown in figure 3.1.

Cr 114 °C B$_2$ 128.5 °C I

Cr 98.5 °C SmA$_2$ 109.5 °C N 125.0 °C I
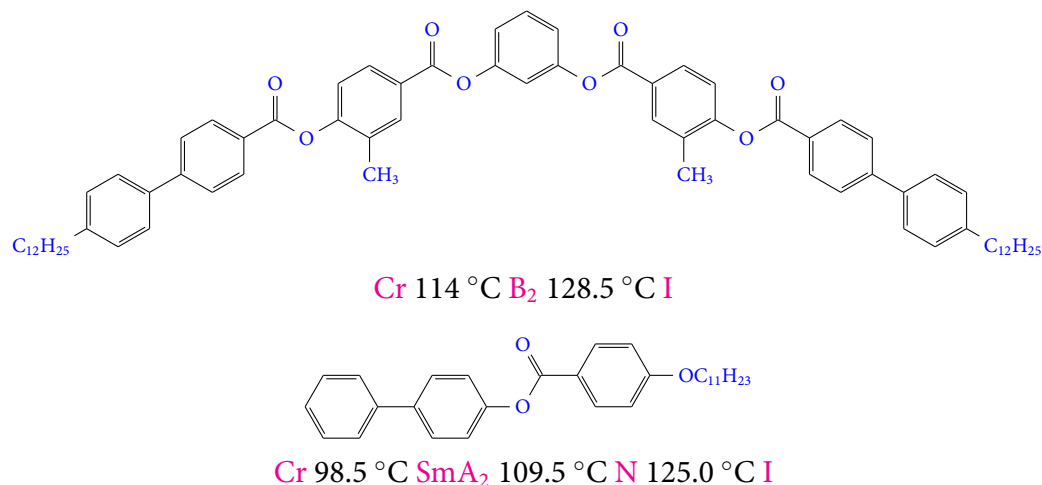
Figure 3.1: *Chemical structures of the compounds and their phase transition temperatures.*
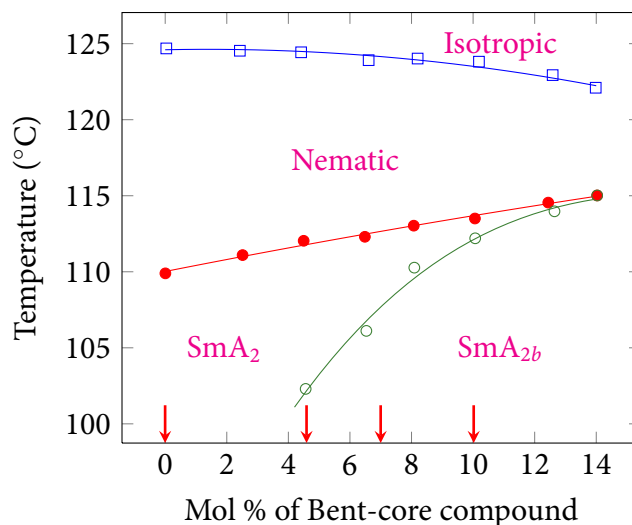
Figure 3.2: *Phase diagram of the mixtures of the above two compounds. Vertically down arrows indicate the concentrations chosen for the experiments. (Adopted from ref. [1])*

The mixture exhibits some new phase transitions and the detailed phase diagram is reported by Pratibha *et al.* [1, 7]. Part of the phase diagram showing nematic-isotropic (NI) phase transition is reproduced (fig. 3.2) and is the interest of the present study. The isotropic-nematic transition temperature decreases (fig. 3.2) and nematic-SmA$_2$ transition temperature increases with increasing concentration of bent-core compound and SmA$_{2b}$ appears beyond $\simeq$ 4 mol %. Recently Sasaki *et al.* [8] made detail calorimetric measurements and showed that the critical heat anomaly associated

with the SmA_2 to SmA_{2b} transition is described with Fisher-renormalization form of the usual scaling expression.

3.2.2 Optical and static dielectric constant measurements
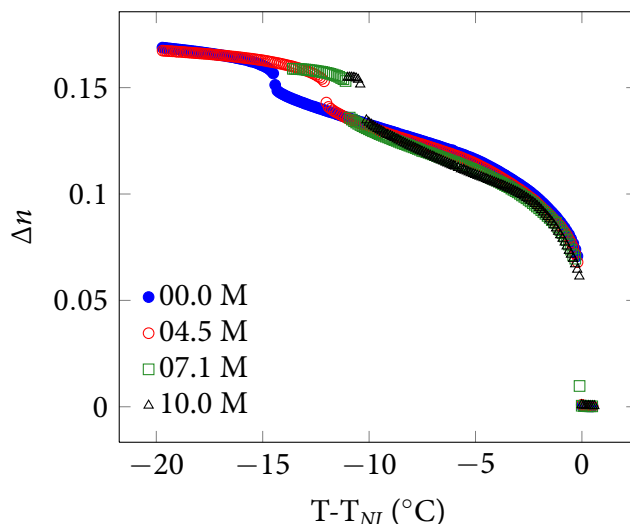
Figure 3.3: *Variation of birefringence (Δn) of the mixtures as a function of temperature.*

First we discuss the optical and dielectric properties. The optical anisotropy (birefringence) was measured using phase modulation technique as discussed earlier in chapter-2. The temperature dependent variation of birefringence (Δn) of the pure compound and various mixtures are shown in figure 3.3. Δn jumps to 0.06 from 0 at nematic-isotropic transition in the pure as well as in all the mixtures and increases with decreasing temperature in the nematic phase. Δn is almost constant in all the mixtures at a fixed temperature which suggests that the orientational order, S ($\propto \Delta n$) is not affected by the inclusion of the bent-core molecules. A significant jump in Δn is also observed at nematic-smectic-A (NS) transition in all the mixtures including the pure compound indicating that the nematic-smectic-A transition is first order and consistent with the calorimetric measurements [8]. Further, the relative jump in Δn across nematic-smectic-A transition appears to increase with increasing concentration of the bent-core compound suggesting the increase in coupling of smectic order

parameter ψ and fluctuation in the nematic order parameter S as the McMillan parameter ($\alpha = T_{SN}/T_{NI}$) increases from 0.96 to 0.97 in the present mixtures. It may be mentioned that observations of such enhancement in the optical anisotropy is rare. Measurement of Δn, K_{11} and K_{33} of mixture of the present bent-core compound with 8OCB were reported by Kundu *et al.* [5]. They reported inverse effect i.e., Δn decreases significantly with increasing concentration of bent-core compound.
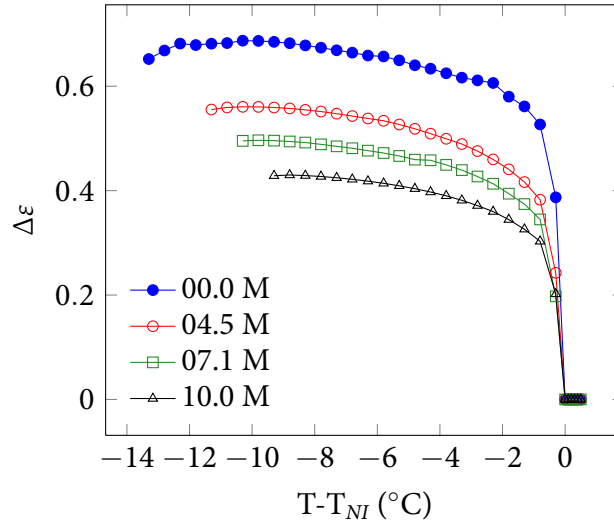
Figure 3.4: *Variation of dielectric anisotropy ($\Delta \varepsilon$) of the mixtures as a function of temperature at f=4.11 kHz.*

The temperature dependent variation of dielectric anisotropy for the various mixtures ($\Delta \varepsilon = \varepsilon_{||} - \varepsilon_{\perp}$) is shown in figure 3.4. The dielectric anisotropy is positive and relatively small and decreases with increasing concentration of bent-core compound at a fixed temperature. The resultant dipole moment of the rod-like molecules is along the long axis whereas the bent-core molecules have transverse dipole moments (see figure 3.1). We have discussed that the low frequency dielectric constants are mostly contributed by orientational order S and molecular dipole moment. The reduction in dielectric anisotropy with increasing concentration of the bent-core compound in the nematic phase keeping the orientational order almost the same suggests that the long axes of the bent-core molecules on an average are parallel to the long axes of the rod-like molecules as shown schematically in figure 3.5(a).
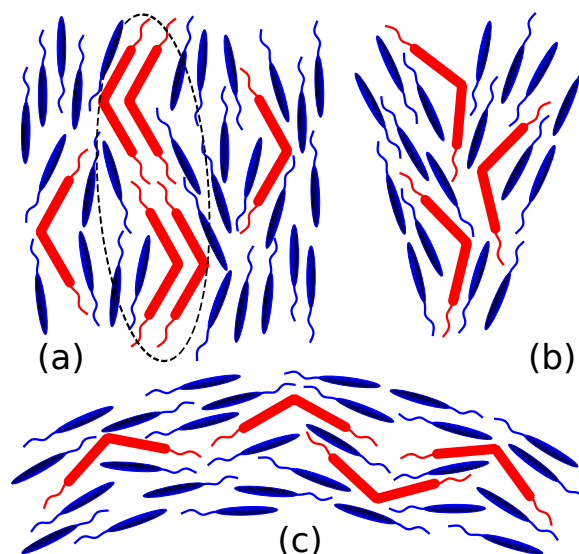
Figure 3.5: *(a) Mutual alignment of rod and bent-core molecules in nematic phase. Dotted region shows a temporary cluster in the nematic phase. Schematic representation of (b) splay and (c) bent distortion of the director in the mixtures.*

3.2.3 Splay, bend elastic constant and rotational viscosity measurements
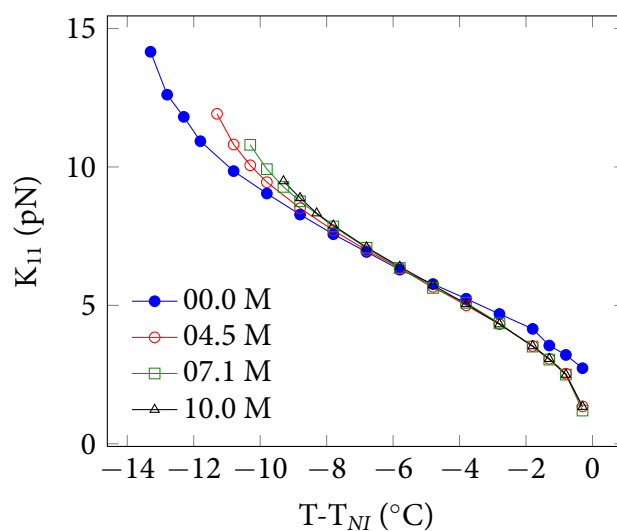
Figure 3.6: *Variation of splay elastic constant (K_{11}) of various mixtures as a function of temperature.*

In this section we discuss the viscoelastic properties. The optical phase difference ($\Delta\Phi$) of the sample was measured as a function of applied voltage to measure splay (K_{11}) and bend (K_{33}) elastic constants at various temperatures. The variation of experimental
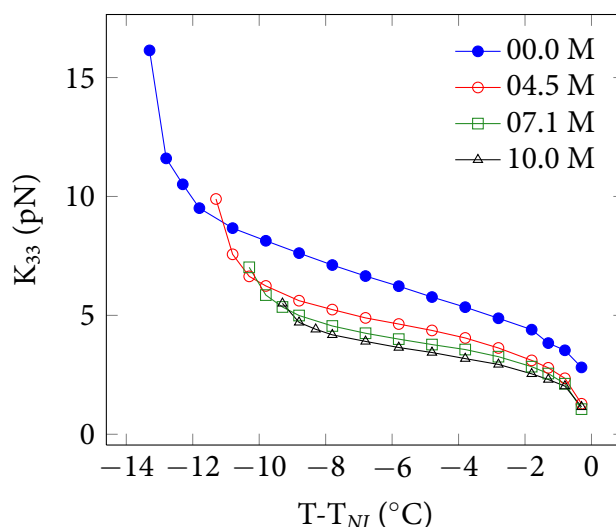
Figure 3.7: *Variation of bend elastic constant (K_{33}) of various mixtures as a function of temperature.*

data ($\Delta\Phi$) is fitted with equations 2.25 and 2.29 and the details of the fitting procedure is discussed in chapter-2. The temperature-dependent variation of splay (K_{11}) and bend (K_{33}) elastic constants are shown in figure 3.6 and figure 3.7 respectively. We notice that K_{11} increases with decreasing temperature in the nematic phase and shows a little change of curvature as the smectic phase is approached. Interestingly at a fixed temperature there is no significant change in K_{11} with increasing concentration of bent-core compound. Since Δn ($\propto S$) do not change with the concentration, K_{11} ($\propto S^2 \propto \Delta n^2$) is also not affected by the increasing concentration of bent-core molecules. On the other hand K_{33} decreases significantly (fig. 3.7) with increasing concentration of bent-core compound. Variation of K_{11} and K_{33} at two temperatures namely $T - T_{NI} = -3.8\,°C$ and $-7.8\,°C$ is shown in figure 3.8. It is observed that K_{11} remain constant and K_{33} is reduced by a factor of ~ 1.7 as the concentration is increased from 0 to 10 mol % and tends to saturate beyond this concentration.

Measurement of K_{11} and K_{33} in the mixture of present bent-core compound with 8OCB were reported by Kundu *et al.* [5] and they found that both decreases with increasing concentration of bent-core compound in the mixtures. There were no structural similarities between the two molecules in their study. The strikingly different
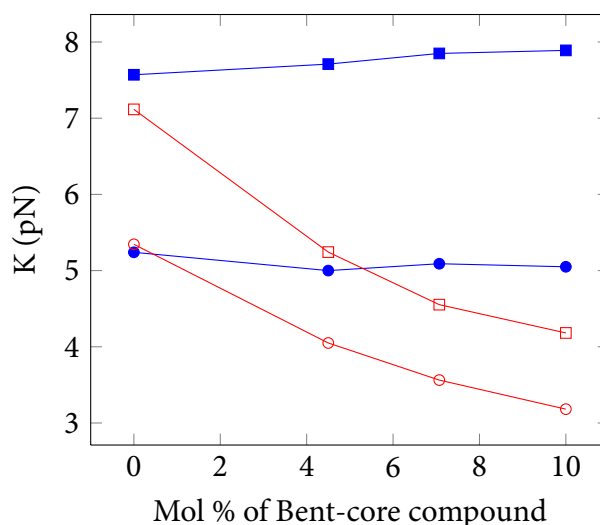
Figure 3.8: *Variation of both K_{11} and K_{33} with the concentration of bent-core compound. Closed symbols represent K_{11} and open symbols represent K_{33}. Circles and squares represent measurements at 3.8 and 7.8 °C below T_{NI} respectively. Continuous lines are drawn as guides to the eye.*

results i.e., both Δn and K_{11} remaining constant in the present mixtures can arise due to the structural similarity of the aromatic and aliphatic parts of the rod to the one half of the bow of bent-core molecule. Further, as mentioned earlier the bow axes of bent-core molecules are parallel to the long axes of rod-like molecules (fig. 3.5(a)), and the bent molecules do not facilitate splay fluctuations hence K_{11} remain almost the same in all mixtures. The decrease of bend elastic constant (K_{33}) is due to the coupling of bent shape of the molecules with bent distortion. In this case the strain in the bent distortion is partly relieved due to the coupling and as a result K_{33} can be significantly lower than K_{11}. A schematic representation of the splay and bend distortions in the mixture is shown in figure 3.5(b) and 3.5(c) respectively. The pretransitional divergence of K_{33} in pure calamitic (rod) compound as the nematic-SmA$_2$ transition is approached is due to smectic short-range fluctuations in the sense that the bent fluctuations are suppressed at the onset of smectic short-range order. Such pretransitional divergence of K_{33} in the mixture is also observed in other calamitic liquid crystals [4, 9]. Furthermore, it is noticed that the relative divergence in K_{33} compared to the pure compound is reduced with increasing concentration of bent-core compound as the nematic-SmA transition is approached. This is a consequence of reduced K_{33} in the sense that bent

fluctuations are relatively larger in the mixtures compared to the pure compound.
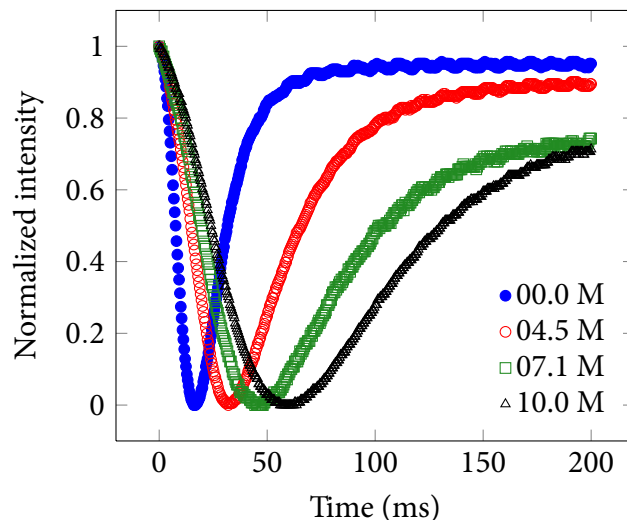
Figure 3.9: *Time dependent normalised transmitted intensity after the removal of the bias voltage V_b at $T - T_{NI} = -2\,°C$ for various mixtures.*

Here we discuss the rotational viscosity (γ_1) of the mixtures in the nematic phase. The details of the experimental techniques are discussed in chapter-2. The normalized intensity of the transient response in various mixtures is shown in figure 3.9. The time dependence of the retardation was estimated from the normalized intensity by using equation 2.39. γ_1 was estimated from equation 2.40 by measuring the relaxation time $\tau_\circ$ as discussed in chapter-2. The temperature-dependent variation of γ_1 is shown in figure 3.10. γ_1 of the pure calamitic compound is relatively low and comparable to many known calamitic compounds [10]. It increases with decreasing temperature in the nematic phase as expected due to the increase in the orientational order parameter (S) [11]. In the mixture, γ_1 increases significantly compared to the pure compound with increasing concentration of bent-core compound. For example, at two shifted temperatures namely $T - T_{NI} = -1.8\ °C$ and $-6.8\ °C$, it increases by a factor of four when the concentration of bent-core compound is increased from 0 to 10 mol % (fig. 3.11).
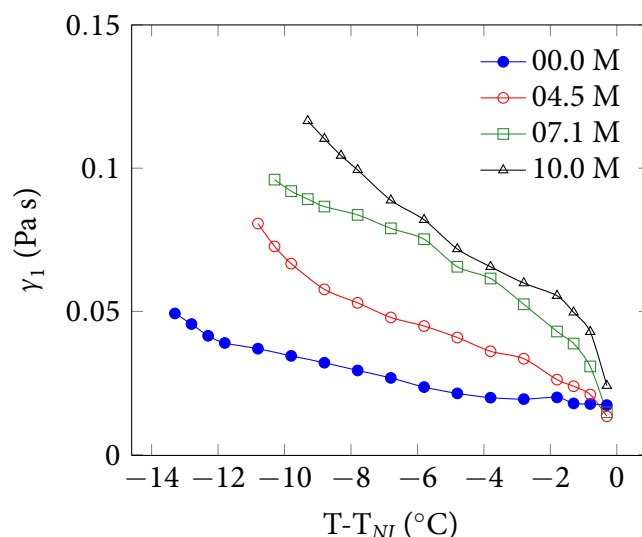
Figure 3.10: *Variation of rotational viscosity (γ_1) of mixtures as a function of shifted temperature.*
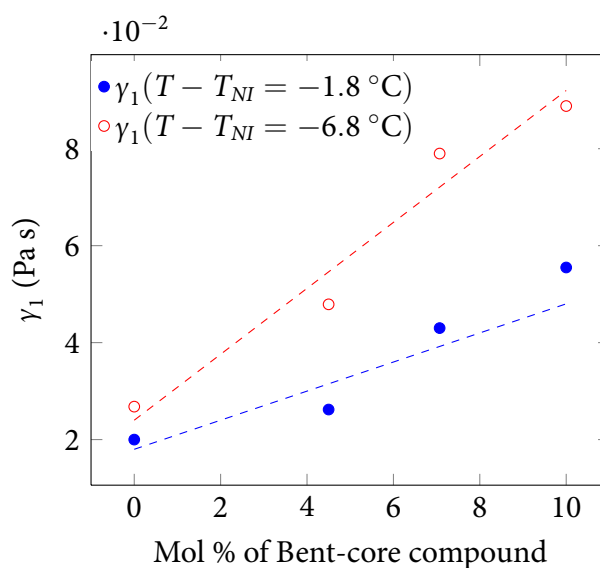
Figure 3.11: *Variation of γ_1 with the concentration of bent-core molecules at two different shifted temperatures. Continuous lines are drawn as guides to the eye.*

It may be mentioned that in the mixture the increase in γ_1 can be solely attributed to the increase in $\tau_\circ$ since K_{11} almost remains constant. The temperature dependent variation of γ_1 measured by magnetic field was also reported to be higher in pure bent-core compounds than conventional calamitic compounds [12, 13]. In some cases it was reported to be 10 times higher and explained due to the formation of temporary

smectic clusters that originate from the bent-shape of the molecules [12, 14]. Existence of such clusters in the nematic phase is revealed in dynamic light scattering [15] and rheological studies [16]. In the present mixture γ_1 is almost 4 times larger even at relatively small concentration (10 mol %) of bent-core compound and is expected to be contributed by such temporary clusters of bent-core molecules. A schematic representation of such temporary clusters in the nematic phase is depicted in figure 3.5(a). The size and the number of clusters can increase with increasing concentration of bent-core molecules and γ_1 of the mixture can increase.

3.3 Conclusions

We measured birefringence, splay and bend elasticity and rotational viscosity of several mixtures of a rod-like molecule, whose aromatic and aliphatic parts matched with one half of the bent-core molecule, at various concentrations. We observed that the birefringence and hence the orientational order (S) remain the same in all mixtures. The dielectric anisotropy decreases with increase in concentration of bent-core molecules indicating that bow axes of bent-core molecules align parallel to the long axes of rod-like molecules. The splay elastic constant ($\propto S^2$) remains constant whereas, bend elastic constant decreases significantly with increasing concentration of bent-core molecules, suggesting the coupling of bent-shape with the bend distortion. The increase in rotational viscosity with concentration suggests the presence of temporary smectic clusters of bent-core molecules in the mixtures.

References

[1] R. Pratibha, N. V. Madhusudana, and B. K. Sadashiva, "An orientational transition of bent-core molecules in an anisotropic matrix," *Science*, vol. 288, no. 5474,

pp. 2184–2187, 2000.

[2] R. Pratibha, N. V. Madhusudana, and B. K. Sadashiva, "Two-dimensionally periodic phases in mixtures of compounds made of rodlike and bent-core molecules," *Phys. Rev. E*, vol. 71, p. 011701, Jan 2005.

[3] M. R. Dodge, C. Rosenblatt, R. G. Petschek, M. E. Neubert, and M. E. Walsh, "Bend elasticity of mixtures of v-shaped molecules in ordinary nematogens," *Phys. Rev. E*, vol. 62, pp. 5056–5063, Oct 2000.

[4] M. R. Dodge, R. G. Petschek, C. Rosenblatt, M. E. Neubert, and M. E. Walsh, "Light scattering investigation above the nematic smectic-*a* phase transition in binary mixtures of calamitic and bent-core mesogens," *Phys. Rev. E*, vol. 68, p. 031703, Sep 2003.

[5] B. Kundu, R. Pratibha, and N. V. Madhusudana, "Anomalous temperature dependence of elastic constants in the nematic phase of binary mixtures made of rodlike and bent-core molecules," *Phys. Rev. Lett.*, vol. 99, p. 247802, Dec 2007.

[6] B. Kundu, R. Pratibha, and N. Madhusudana, "Orientational order in liquid crystals exhibited by some binary mixtures of rod-like and bent-core molecules," *The European Physical Journal E: Soft Matter and Biological Physics*, vol. 31, pp. 145–152, 2010.

[7] N. V. Madhusudana, "On some liquid crystals made of banana-shaped molecules and their mixtures with rod-like molecules," *Liquid Crystals*, vol. 36, no. 10-11, pp. 1173–1184, 2009.

[8] Y. Sasaki, K. Ema, K. V. Le, H. Takezoe, S. Dhara, and B. K. Sadashiva, "Critical behavior at transitions from uniaxial to biaxial phases in a smectic liquid-crystal mixture," *Phys. Rev. E*, vol. 82, p. 011709, Jul 2010.

[9] S. W. Morris, P. Palffy-Muhoray, and D. A. Balzarini, "Measurements of the bend and splay elastic constants of octyl-cyanobiphenyl," *Molecular Crystals and Liquid Crystals*, vol. 139, no. 3-4, pp. 263–280, 1986.

[10] M. L. Dark, M. H. Moore, D. K. Shenoy, and R. Shashidhar, "Rotational viscosity and molecular structure of nematic liquid crystals," *Liquid Crystals*, vol. 33, no. 1, pp. 67–73, 2006.

[11] W. H. de Jeu, *Physical Properties of Liquid Crystalline Materials*. Liquid Crystal Monographs, Gordon and Breach, 1980.

[12] E. Dorjgotov, K. Fodor-Csorba, J. T. Gleeson, S. Sprunt, and A. Jákli, "Viscosities of a bent-core nematic liquid crystal," *Liquid Crystals*, vol. 35, no. 2, pp. 149–155, 2008.

[13] P. Tadapatri, U. S. Hiremath, C. V. Yelamaggad, and K. S. Krishnamurthy, "Permittivity, conductivity, elasticity, and viscosity measurements in the nematic phase of a bent-core liquid crystal," *The Journal of Physical Chemistry B*, vol. 114, no. 5, pp. 1745–1750, 2010.

[14] M. Majumdar, P. Salamon, A. Jákli, J. T. Gleeson, and S. Sprunt, "Elastic constants and orientational viscosities of a bent-core nematic liquid crystal," *Phys. Rev. E*, vol. 83, p. 031701, Mar 2011.

[15] S. Stojadinovic, A. Adorjan, S. Sprunt, H. Sawade, and A. Jakli, "Dynamics of the nematic phase of a bent-core liquid crystal," *Phys. Rev. E*, vol. 66, p. 060701, Dec 2002.

[16] C. Bailey, K. Fodor-Csorba, J. T. Gleeson, S. N. Sprunt, and A. Jakli, "Rheological properties of bent-core liquid crystals," *Soft Matter*, vol. 5, pp. 3618–3622, 2009.

4

Optical, dielectric and viscoelastic properties of ambient-temperature nematic binary mixtures of bent-core and rod-like molecules

4.1 Introduction

I**N** the previous chapter we studied the binary mixture of a rod and bent-core compounds that exhibits nematic phase much above the ambient temperature. In this chapter we discuss the measurements of the temperature variation of several physical properties in ambient-temperature nematic liquid crystal mixtures of a rod (5CB) and a bent-core molecules. Both the compounds have low nematic-isotropic phase transition temperatures and exhibit only nematic phase.

In the literature all the experiments reported so far on the binary mixtures exhibit nematic phase much above the ambient temperature. For practical applications room temperature nematic phase is desired. Thus, studies on ambient-temperature mixtures could be rewarding from both the fundamental and application points of view. In this chapter for the first time we report measurement of birefringence (Δn), static dielectric constants ($\varepsilon_{||}$ and $\varepsilon_{\perp}$) splay, bend elastic constants (K_{11}, K_{33}), rotational viscosity (γ_1), diffusion coefficients ($D_{||}$, $D_{\perp}$) of a microsphere and corresponding viscosities ($\eta_{||}$, $\eta_{\perp}$) of ambient-temperature liquid crystal mixtures of bent-core and rod-like molecules. We show that the results are distinctly different than previously studied mixtures.

4.2 Results and Discussion

4.2.1 Samples and phase behaviour

We studied various mixtures of a bent-core nematic compound 3-[4-(4-dodecyloxybe nzylideneamino)benzoyloxy]-4-hexylphenyl4-(4-dodecyloxybenzylideneamino)- ben- zoate and a calamitic nematic compound pentylcyanobiphenyl (5CB). The chemical structures and the phase transition temperatures of the compounds are shown in figure 4.1. The synthesis and some preliminary characterization of the bent-core compound has already been reported [1]. Both the compounds exhibit nematic phase at ambient temperature and they have antagonistically oriented resultant dipoles with respect to their long axes.

The phase diagram of the binary mixtures is shown in figure 4.2. It is noted that initially nematic-isotropic transition temperature (T_{NI}) increases with increasing mol % of bent-core compound and reaches to a maximum at $\sim$ 30 mol % of bent-core compound before it decreases at much higher mol %. Thus, the nematic range in the intermediate region of concentrations is enhanced in the mixture.
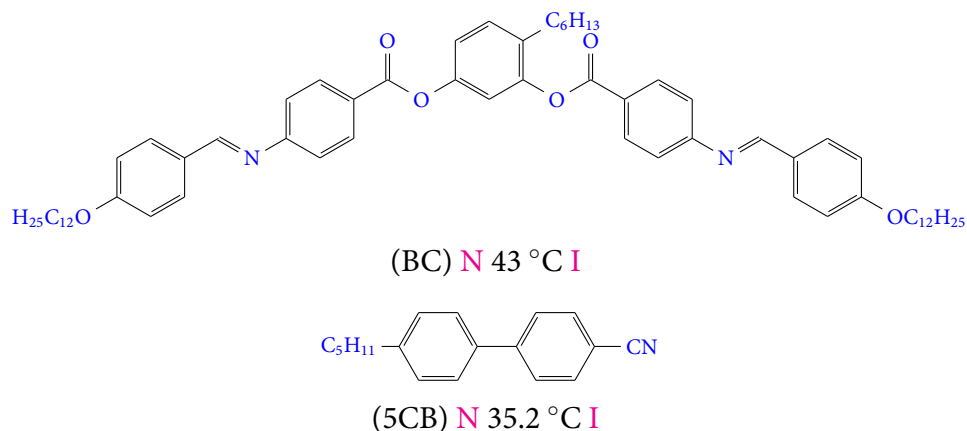
Figure 4.1: *Chemical structures of the compounds and the phase transition temperatures.*
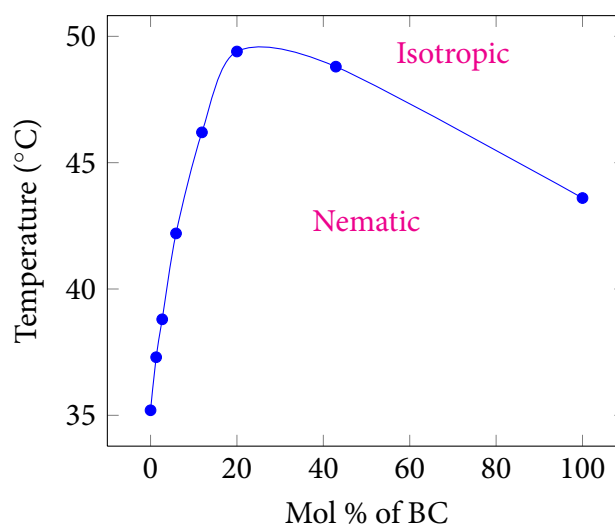
Figure 4.2: *Phase diagram of the binary mixture. Continuous line is drawn as guide to eyes.*

4.2.2 Optical and static dielectric constant measurements

In our physical measurements we restricted the mixing ratio of bent-core up to ~ 43 mol % beyond which the dielectric anisotropy tends to change the sign and the passive viscosity is so high that the Brownian motion of the microparticle appears to be seized. All the mixtures were observed carefully under optical polarizing microscope and found that all of them exhibit uniaxial nematic phase. The temperature variation of Δn of the mixtures is shown in figure 4.3. In all samples, Δn increases with decreasing temperature. At a fixed shifted temperature (i.e., $T - T_{NI}$), Δn is decreasing

and tends to saturate at much higher mol % of bent-core compound. The temperature variation of Δn can be approximated by the Haller extrapolation formula [2], $\Delta n = \Delta n_0 (1 - T/T^{**})^{\beta}$, where β, T^{**}, are the fit parameters and Δn_0 is the birefringence of the perfectly aligned sample. The fit parameters are listed in table 4.1. T^{**} is slightly higher than T_{NI} and β is of the order of $\simeq 0.2$ instead of 0.5 as predicted in the mean field theory [3]. Similar values of β were also reported in many other calamitics [4] and in binary mixtures of calamitic and bent-core liquid crystals [5]. The order parameter (S) of the long molecular axis was estimated using the relation $S = \Delta n / \Delta n_0$. The temperature variation of order parameter S of the mixtures are shown in figure 4.4. S increases in the nematic phase as the temperature is reduced. S decreases slightly from ~ 0.54 to ~ 0.5 when the mol % is increased to 5.9 and finally tends to saturate beyond it.
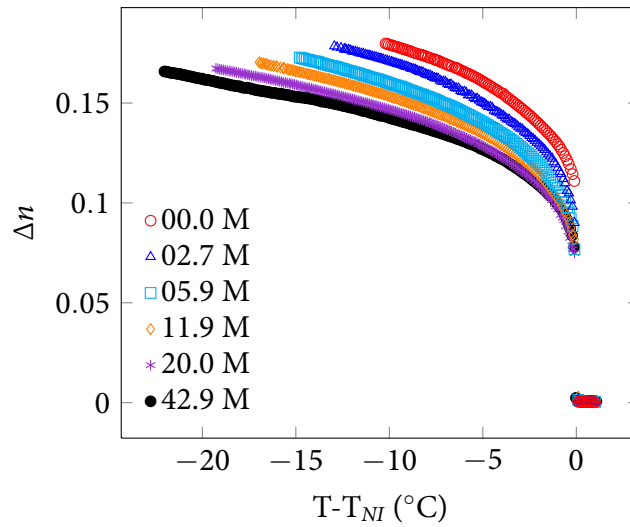
Figure 4.3: *Temperature variation of birefringence (Δn) of the mixtures.*

The variation of static dielectric constant as a function of shifted temperature is shown in figure 4.5. It is observed that the parallel component of dielectric constant ($\varepsilon_{||}$) decreases rapidly with increasing mol % of bent-core compound whereas the perpendicular component ($\varepsilon_{\perp}$) remains almost constant. The dielectric anisotropy is positive ($\Delta \varepsilon > 0$) and reduces significantly with increasing mol % of bent-core compound. Since both the molecules have large dipole moments which are presumably oriented
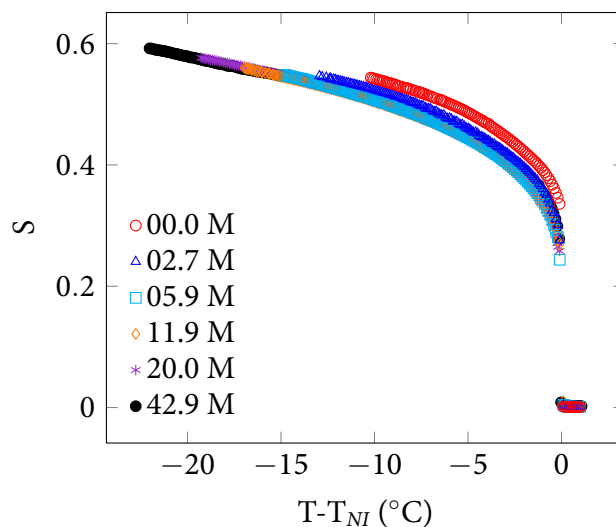
Figure 4.4: *Temperature variation of estimated orientational order parameter (S) of the mixtures.*

Mol %	T_{NI} (K)	T^{**} (K)	Δn_0	β
0	308.2	308.9	0.33	0.18
2.7	311.8	312.2	0.33	0.19
5.9	315.2	315.6	0.31	0.20
11.9	319.2	319.5	0.30	0.20
20	322.4	322.6	0.29	0.20
42.9	321.8	322.1	0.27	0.18

Table 4.1: *Fit parameters Δn_0, T^{**} and β obtained from Haller's extrapolation formula.*
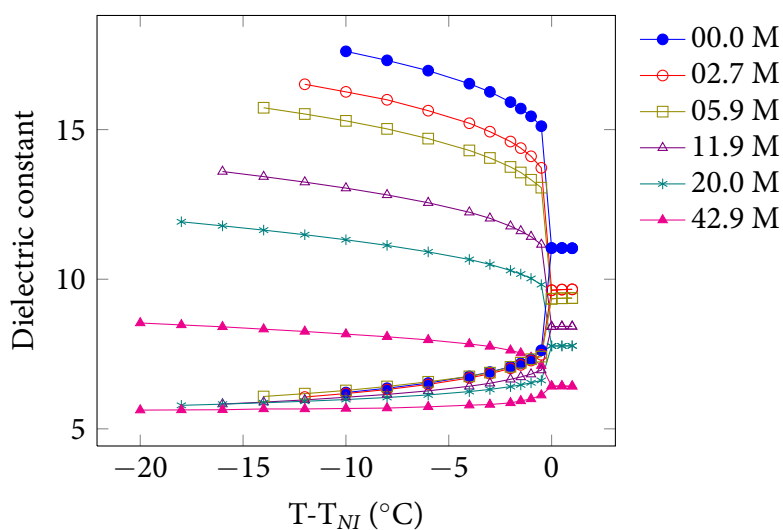
Figure 4.5: *Temperature variation of dielectric constant. Continuous lines are drawn as a guide to the eye.*

antagonistically in the nematic phase i.e., in case of 5CB the dipole moment is parallel to the long axis and in case of bent-core molecule it is almost perpendicular to the bow axis. In the isotropic phase of the mixtures it is fair to assume that the isotropic dielectric constant $\varepsilon_{iso} \propto \mu^2$, where μ is the mean-square effective molecular dipole moment [6]. The reduction in ε_{iso} with increasing mol % of bent-core as observed indicates that the effective dipole moments in the isotropic phase is reduced. In the nematic phase the bow axis is assumed to be parallel to the director and the molecules rotate freely about their long axis, so that the effect of transverse dipole moment is suppressed and as a result $\varepsilon_\perp$ remains constant. The longitudinal component of dipole moment of the bent-core molecule is much lesser than 5CB molecule and hence the effective longitudinal dipole moment per unit volume in the mixture decreases with increasing mol % of bent-core molecules and as a result $\varepsilon_{||}$ can decrease.
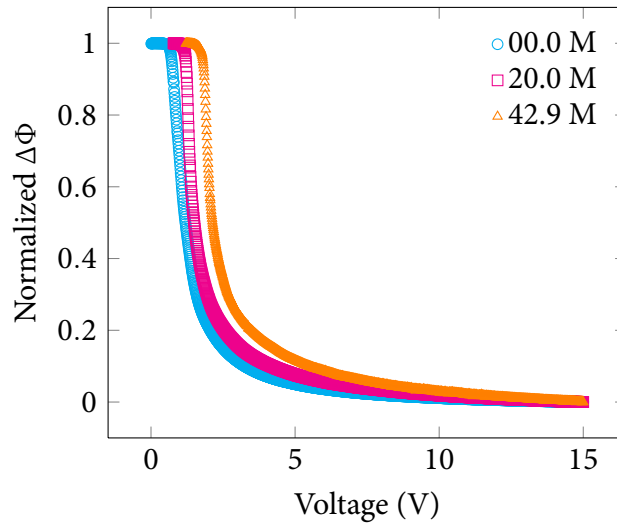
Figure 4.6: *Voltage dependent normalized optical retardation ($\Delta\Phi$) for various mol % of bent-core compound.*

4.2.3 Splay, bend elastic constant measurements

The splay and bend elastic constants (K_{11}, K_{33}) were measured from the voltage dependent retardation in planar cell as described in chapter-2. Variation of normalized retardation as a function of applied voltage for a few mixtures are shown in figure 4.6.
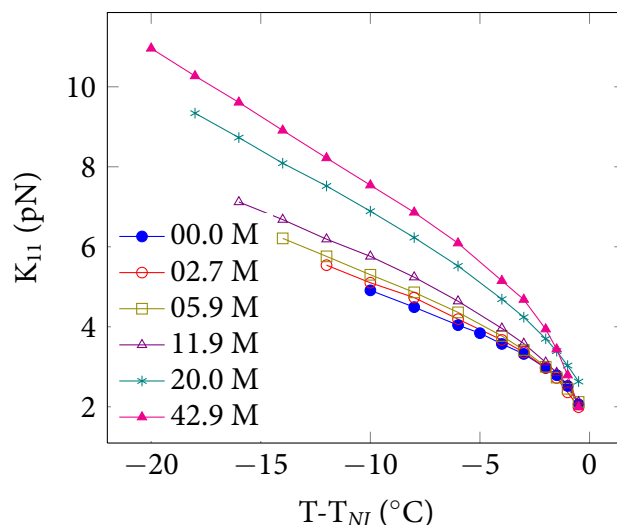
Figure 4.7: *Temperature variation of splay (K_{11}) elastic constant at various mol % of bent-core compound.*
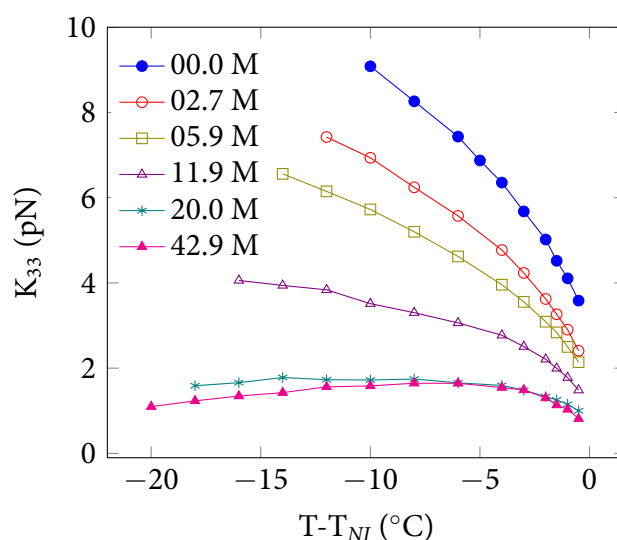
Figure 4.8: *Temperature variation of bend (K_{33}) elastic constant at various mol % of bent-core compound.*

It is noticed that the Freedericksz threshold voltage increases with increasing mol % of bent-core compound. The temperature variation of both K_{11} and K_{33} are shown in figure 4.7 and figure 4.8. In all the samples K_{11} increases as the temperature is reduced (fig. 4.7) and at a fixed shifted temperature, K_{11} increases with increasing mol % of bent-core compound. In case of K_{33} it is noticed that at a fixed shifted temperature K_{33} decreases rapidly (fig. 4.8) with increasing mol % of bent-core compound. At 20

mol % of bent-core compound, K_{33} is almost independent of temperature except very close to T_{NI}. Further, at 42.9 mol % of bent-core compound K_{33} increases initially and then decreases slightly as the temperature is reduced showing a broad maximum approximately at $T - T_{NI} \simeq -6\,°C$. In figure 4.9 the variation of K_{11} and K_{33} at some shifted temperatures are presented with mol % of bent-core compound. It is observed that at $T - T_{NI} = -10\,°C$, K_{11} increases by 50% with respect to pure 5CB, whereas K_{33} decreases almost exponentially before it reaches to a minimum value when the mol % of bent-core compound is increased to $\simeq 43\%$. At a shifted temperature e.g., $T - T_{NI} = -10\,°C$, the reduction is about 80% compared to pure 5CB. The ratio of K_{33}/K_{11} as a function of mol % of bent-core at a few temperatures is also shown in figure 4.10. The ratio reduces below 1 at 7 mol % of bent-core compound and reaches to 0.2 at $\simeq 43$ mol %. Similar cross over was also reported in polymeric nematic liquid crystals and it was shown that the ratio reduces to $\simeq 0.83$ when the effective chain-length to diameter ratio increases by a factor of three [7]. In the present binary system the ratio K_{33}/K_{11} is significantly small (0.2 at 43 mol %) mainly due to the decrement of K_{33}.
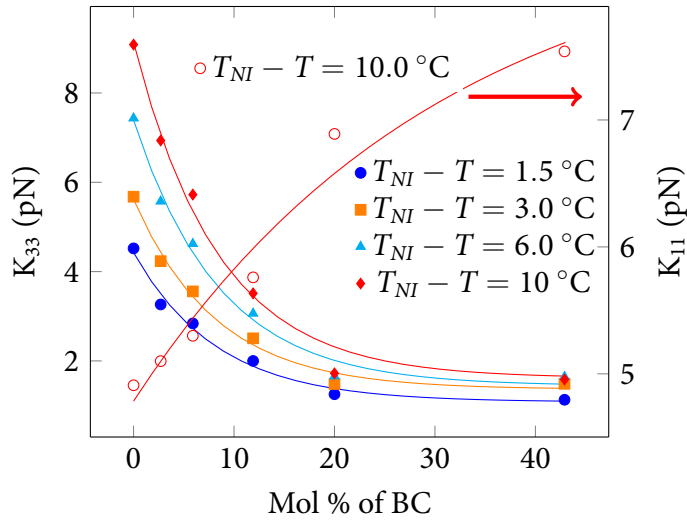
Figure 4.9: *Variation of K_{11} and K_{33} with mol % of bent-core compound at various shifted temperatures.*

There have been a few reports on the measurements of K_{11} and K_{33} in binary mixtures of rod-like and bent-core molecules as mentioned earlier. In these studies it was
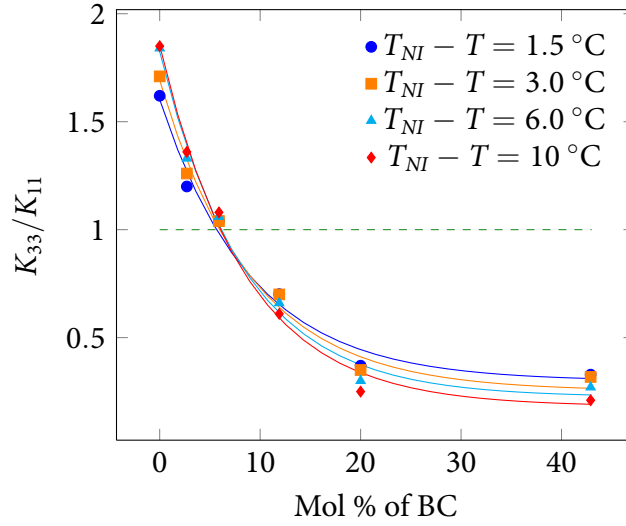
Figure 4.10: *Variation of K_{33}/K_{11} with mol % of bent-core compound.*

found that both K_{11} and K_{33} decreases with increasing mol % of bent-core compound and the rate of decrement of K_{33} with mol % of bent-core is several times faster than K_{11}. In the previous chapter we showed that K_{33} decreases significantly whereas K_{11} remains almost constant in the binary mixture due to the structural similarity of the rod molecule with one half of the bent-core molecule. The increase of K_{11} with increasing mol % of bent-core was also reported recently [8]. The reduction in K_{33} is due to the coupling of the bent-shape of the molecules with the bend distortion as explained in the previous chapter. The anomalous temperature dependence of K_{33} at ~ 43 mol % (i.e., it decreases with decreasing temperature) is due to the enhanced orientational order (S) of the bent-core molecules. Similar observation at higher mol % of bent-core was also reported by Kundu *et al.* [9]. It suggests that the coupling of the *bent shape* of the molecule with the bent-distortion is stronger at higher *S*.

In the mean field theory, $K_{ii} \propto S^2$. $S \propto \Delta n$ and can be measured from the temperature dependent variation as discussed earlier. To gain more insight on the relationship between the order parameter and elastic constants we plotted the variation of K_{11} and K_{33} as a function of Δn in figure 4.11 and figure 4.12. The experimental data are fitted with $K_{ii} \propto \Delta n^x$, where x is a fit parameter. The fit parameter x is listed in table 4.2. It is observed that the exponent x for K_{11} is 2 up to 11.9 mol % and consistent with the

Mol %	$\simeq x$ for K_{11}	$\simeq x$ for K_{33}
0	2.0	2.2
2.7	2.0	2.2
5.9	2.0	2.1
11.9	2.0	1.7
20	2.2	-
42.9	2.8	-

Table 4.2: *Fit parameters obtained from $K_{ii} \propto \Delta n^x$ in the samples.*

prediction of the mean field theory. It increases to 2.8 at $\simeq$ 43 mol %. On the other hand the exponent x for K_{33} is about 2 up to 5.9 mol % and starts decreasing beyond this concentration (table. 4.2). It clearly indicates that the coupling of bent-shape with the bent distortion is significant beyond 5.9 mol % of bent-core compound. At higher concentration (particularly at 20 and $\simeq$ 43 mol %) K_{33} initially increases and finally decreases with increasing Δn showing a maxima at $\Delta n = 0.14$. The initial increase is due to the increasing orientational order (S) as expected. However with increasing S the coupling with bend distortion also gets stronger as a result K_{33} starts to decrease.
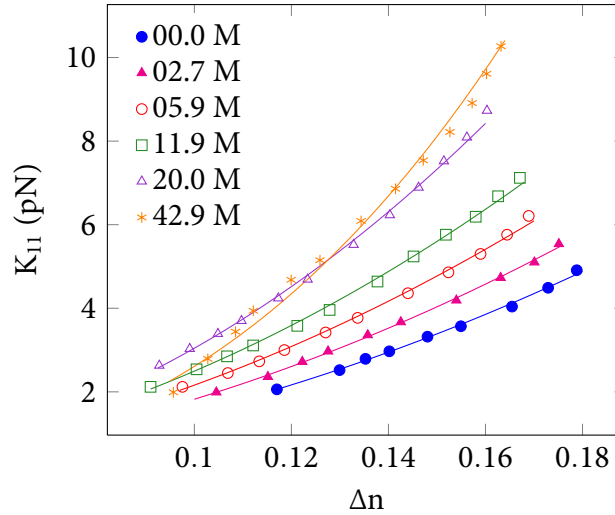
Figure 4.11: *Variation of K_{11} with Δn at various mol % of bent-core compound. Continuous lines are fit to the equation $K_{11} \propto \Delta n^x$.*

For the enhancement of K_{11}, at least two considerations can be made. K_{11} can increase in the mixture due to increase in S as predicted in the mean field theory ($K_{11} \propto S^2$). On the contrary, we observe (fig. 4.4) that S decreases slightly with increasing mol %
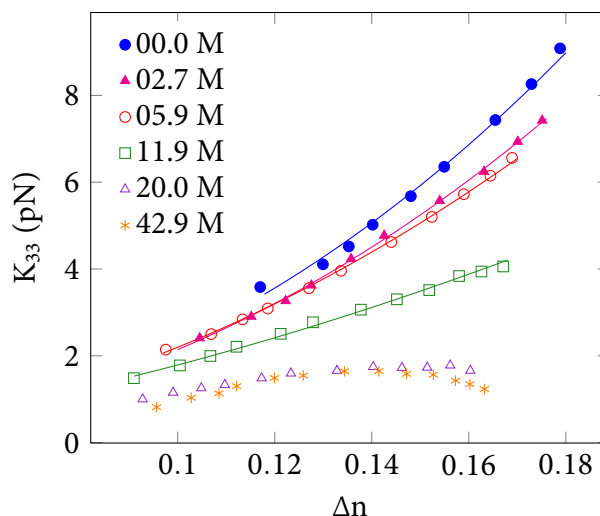
Figure 4.12: *Variation of K_{33} with Δn at various mol % of bent-core compound. Continuous lines are fit to the equation $K_{33} \propto \Delta n^x$.*

of bent-core compound. Thus the stiffening of K_{11} can not be attributed to the enhancement of *S*. Another possible explanation is based on the evolution of transverse correlation (i.e., along the short axis) of two or more bent-core molecules that is developed due to the restricted free-rotation along the long axis. This can lead to the formation of smectic clusters of a few bent-core molecules. The larger exponent (i.e., $x > 2$) for K_{11} at higher mol % of bent-core could be a pointer to the existence of short axis correlation. There are several reports suggesting formation of smectic clusters in bent-core nematic liquid crystalss or in binary mixtures of rod and bent-core molecules [5, 10, 11]. It is possible that the enhancement of K_{11} is due to the presence of such clusters whose corresponding elastic constants are expected to be larger. The number density and size of these clusters can increase with increasing concentration of bent-core molecules.

4.2.4   Viscosity measurements

Nematic liquid crystals have anisotropic shear viscosity which depends on the orientation of director $\hat{n}$ and shear. There could be three viscosity coefficients (fig. 1.15). These parameters are measured for several nematic liquid crystals. However, there

are no reports of these viscosities in the bent-core nematic liquid crystals. The practical difficulty in measuring is the lack of a large quantity of sample. So here we use a videomicroscopy technique in which a few micro litre (μl) sample is enough for the experiment. The details of the experimental technique is explained in chapter-2.
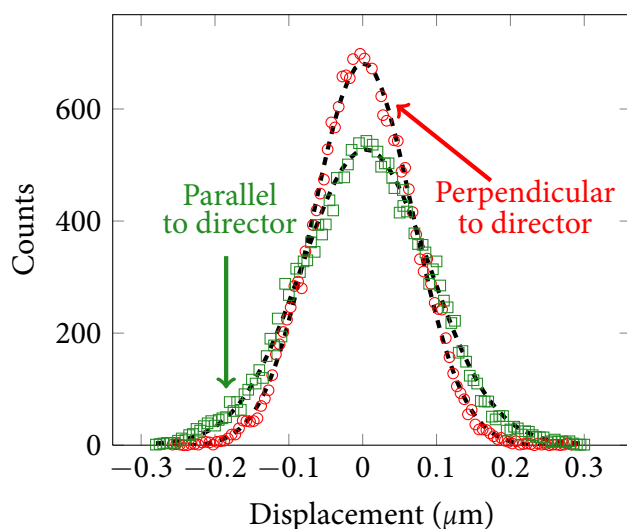
Figure 4.13: *Typical histograms of the displacements of a microsphere of diameter 0.98 μm in direction parallel and perpendicular to the nematic director at room temperature for the mixture with 10 mol % of bent-core compound. Dotted lines are fit (eqn. $P = P_0 \exp(-s^2/\Delta^2(\tau))$) to the corresponding data.*
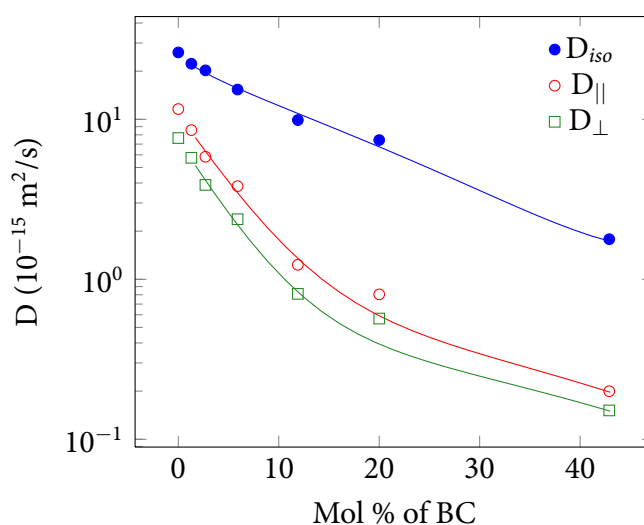
Figure 4.14: *Variation of diffusion coefficients parallel ($D_{||}$) and perpendicular ($D_{\perp}$) to the director with mol % of bent-core compound at 25 $^\circ$C (open symbols) and $T_{NI} + 5\,^\circ$C (closed symbol)*
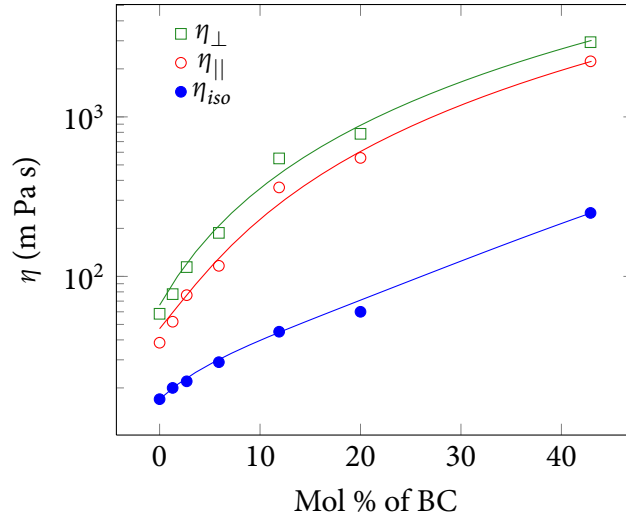
Figure 4.15: *Estimated viscosities using the Stokes-Einstein relation. Continuous lines are drawn as a guide to the eye.*

The microparticle undergoes Brownian motion and the histogram of the displacement has a Gaussian shape. Typical histograms i.e., the variation of the displacement of a colloid in particular interval over a specified time (counts) along and perpendicular to the director in a planar aligned cell is shown in figure 4.13. The variation of self-diffusion coefficients $D_{||}$ and $D_{\perp}$ of the microsphere with mol % of bent-core compound is shown in figure 4.14. The isotropic diffusion coefficient, D_{iso} is significantly higher than $D_{||}$ and $D_{\perp}$ of nematic phase and all of them decrease as the mol % of the bent-core compound is increased. The corresponding viscosities can be obtained from the Stokes-Einstein equation $\eta_{||,\perp} = k_B T/(6\pi r D_{||,\perp})$, where r is the radius of the microparticle. From the experimental arrangement we can expect that $\eta_{||} \simeq \eta_2$ and $\eta_{\perp} \simeq \eta_3$, where η_2, η_3 are the Miesowicz viscosities with flow direction parallel and perpendicular to the director respectively.

It may be pointed out that a dipole defect is associated with each microparticle. Hence the effective hydrodynamic radius of the microparticle could be slightly larger than the actual size. However, it appears not to affect the measurements significantly, since the estimated values of $\eta_{||}$ and $\eta_{\perp}$ for pure 5CB at room temperature in a planar cell are

comparable to the Miesowicz viscosities η_2 and η_3, respectively. The estimated viscosities against mol % of bent-core are shown in figure 4.15. It is noticed that the isotropic viscosity (η_{iso}) increases only slightly with the mol % of bent-core compound. This is perhaps due to the molecular size effect of bent-core molecules in the mixture. In all the samples $\eta_{||} < \eta_{\perp}$ as expected and both of them increase relatively more rapidly than η_{iso} with the mol % of bent-core compound (fig. 4.15). For example, $\eta_{||}/\eta_{iso} \simeq 12$ and $\eta_{\perp}/\eta_{iso} \simeq 9$ at $\simeq 43$ mol % of bent-core compound at ambient temperature. Such a large enhancement in the passive viscosities with increasing mol % of bent-core compound indicates the existence of clusters as mentioned earlier. Experimental evidence on the existence of such clusters has been revealed in various other experiments [5, 10–15].
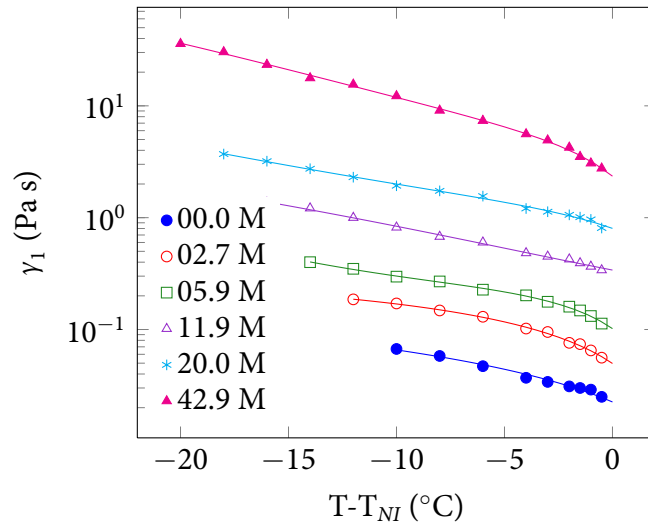
Figure 4.16: *Variation of rotational viscosity (γ_1) of various mixtures as a function of shifted temperature.*

We also measured the rotational viscosity (γ_1) of the samples at various temperatures which is also expected to be influenced by the presence of such clusters. The experimental technique is discussed in chapter-2. The temperature variation of γ_1 for the mixtures are shown in figure 4.16 and concentration dependence of γ_1 at a few shifted temperatures for a few mixtures of different mol % of bent-core compound is shown in figure 4.17. It is found that γ_1 increases rapidly with the mol % of bent-core compound. For example, at $T - T_{NI} = -10\,°\text{C}$, it increases almost by a factor of 180 when
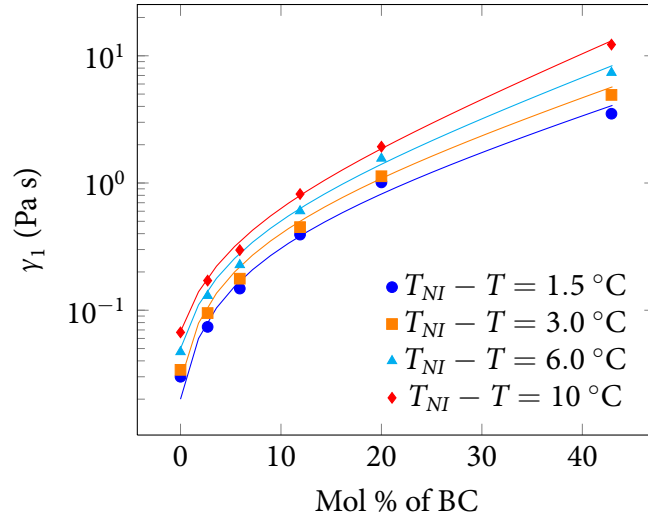
Figure 4.17: *Variation of γ_1 with the mol % of bent-core compound at a few shifted temperatures.*
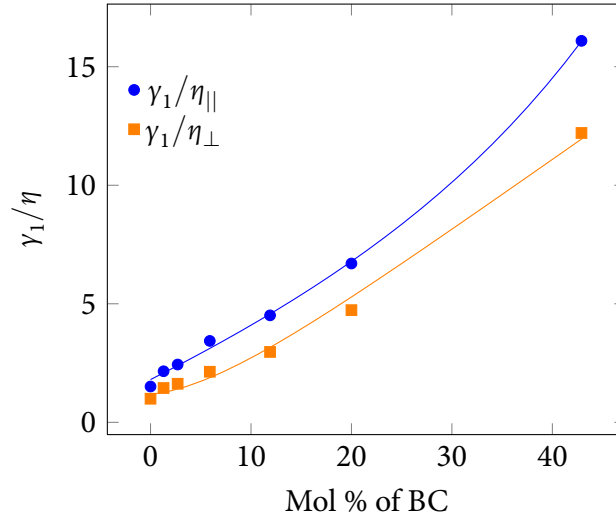
Figure 4.18: *Ratio of $\gamma_1/\eta_{||,\perp}$ with mol % of bent-core compound.*

the mol % of bent-core compound is increased to $\simeq 43$ in the mixtures. Measurement of γ_1 with the phase-decay-technique and flow viscosities using pulsed magnetic field of a few pure bent-core nematic liquid crystals have been reported recently [16, 17]. It was reported that the ratio $\Gamma = \gamma_1/\eta$ is significantly less for bent-core compound ($\Gamma \sim 0.02$) than the calamitic liquid crystals mainly due to the large value of flow viscosity [17]. On the contrary, in the present study we observe that Γ increases remarkably with mol % of bent-core compound compared to pure 5CB. For example, in pure 5CB, $\Gamma_\perp = \gamma_1/\eta_\perp \sim 1$, $\Gamma_{||} = \gamma_1/\eta_{||} \sim 1.5$ and increases to 12, 16 respectively

(fig. 4.18) when the mol % of bent-core compound is increased to $\simeq 43$ mol %. It may be noted that all viscosities γ_1, η_2 and η_3 increases with the mol % of bent-core compound but the rate of increment of γ_1 is much faster than the other two. Such exor-
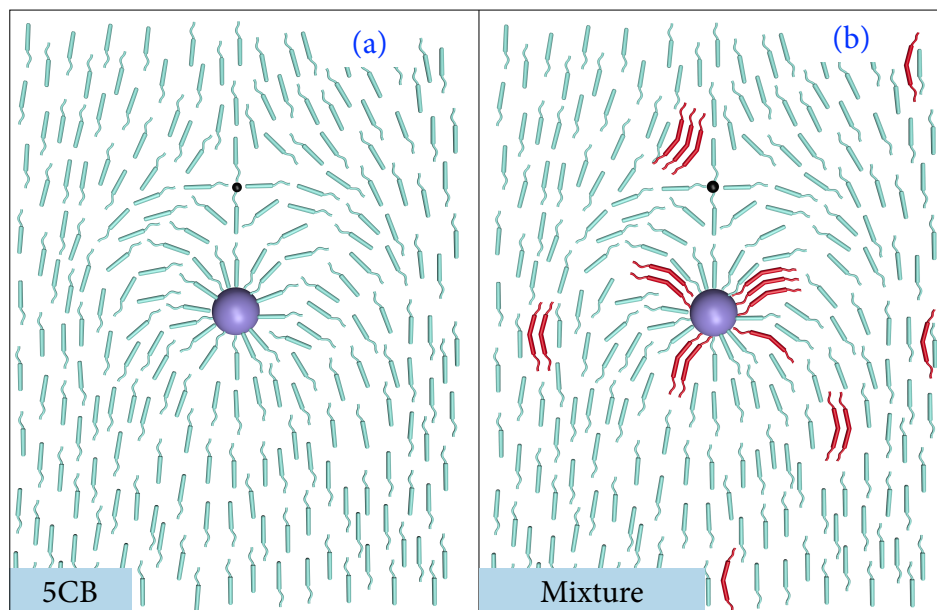
Figure 4.19: *Schematic representation of director orientation around a microparticle with dipole defect. (a) in rod-like molecules (b) in the mixture. The small dot above the microparticle is the center of the dipole defect. Note the attachment of a few clusters of bent-core molecules surrounding the microparticle.*

bitantly large increase in γ_1 can not be accounted by the increase of mol % of bent-core molecules (with large molecular weight) alone. The relatively faster enhancement of γ_1 with respect to the passive viscosities can be attributed to the presence of smectic clusters of bent-core molecules. In the present mixtures both the compounds do not have any smectic phases. Nevertheless the smectic clusters are formed inherently due to the highly restricted free rotation of the bent-core molecules along the bow axis. Further, the bent-core molecules presumably align perpendicularly on the surface of the microparticle due to the DMOAP coating. In that case the steric barrier and partial pinning of the molecules on the microsphere's surface prevent free rotation of the bent-core molecules along the bow axis and a few bent-core molecules can form smectic clusters or permanent layers at the surface which in principal can reduce the Brownian motion of the microparticle and can increase the passive viscosities. A schematic

representation of such clusters surrounding the microparticle with dipole defects are shown in figure 4.19. It may be mentioned that no Brownian motion was observed in pure bent-core compound at room temperature. This is perhaps due to the very large viscosities and presence of a few smectic layers surrounding the microparticle.

4.3 Conclusions

In conclusion, measurements of optical, dielectric and viscoelastic properties of room temperature nematic liquid crystals with rod-like and bent-core molecules have shown following interesting results: (1) mutual alignment of bow axis in 5CB is such that the effective dipole moment in the isotropic and in the nematic phase parallel to the director is reduced; (2) significant stiffening of splay and large softening of bend elastic constants; (3) large reduction in both the diffusion coefficients in the nematic phase compared to the isotropic phase and hence unprecedented increase in the passive viscosities; (4) two order of magnitude enhancement in rotational viscosity with increasing mol % of bent-core compound. The stiffening of K_{11} and extraordinarily large viscosities are attributed to the presence of smectic clusters of bent-core molecules in the mixtures. Present studies suggest that ambient-temperature bent-core nematic could be advantageous as a dopant for optimizing the birefringence, dielectric constants and elastic properties of low molecular weight liquid crystals but the enhanced viscosities in the mixtures are highly disadvantageous as well as a matter of concern and has to be reduced for practical application.

References

[1] J. Matraszek, J. Mieczkowski, J. Szydlowska, and E. Gorecka, "Nematic phase formed by banana-shaped molecules," *Liquid Crystals*, vol. 27, no. 3, pp. 429–436, 2000.

[2] I. Haller, "Thermodynamic and static properties of liquid crystals," *Progress in Solid State Chemistry*, vol. 10, Part 2, no. 0, pp. 103 – 118, 1975.

[3] P. G. de Gennes, *The Physics of Liquid Crystals*. Oxford University, Oxford, 1974.

[4] S. Dhara and N. Madhusudana, "Enhancement of the orientational order parameter of nematic liquid crystals in thin cells," *The European Physical Journal E: Soft Matter and Biological Physics*, vol. 13, pp. 401–408, 2004.

[5] B. Kundu, R. Pratibha, and N. Madhusudana, "Orientational order in liquid crystals exhibited by some binary mixtures of rod-like and bent-core molecules," *The European Physical Journal E: Soft Matter and Biological Physics*, vol. 31, pp. 145–152, 2010.

[6] H. Fröhlich, *Theory of Dielectrics*. Oxford: Clarendon Press, second ed., 1958.

[7] S. D. Lee and R. B. Meyer, "Crossover behavior of the elastic coefficients and viscosities of a polymer nematic liquid crystal," *Phys. Rev. Lett.*, vol. 61, pp. 2217–2220, Nov 1988.

[8] S. T. Hur, M. J. Gim, H. J. Yoo, S. W. Choi, and H. Takezoe, "Investigation for correlation between elastic constant and thermal stability of liquid crystalline blue phase i," *Soft Matter*, vol. 7, pp. 8800–8803, 2011.

[9] B. Kundu, R. Pratibha, and N. V. Madhusudana, "Anomalous temperature dependence of elastic constants in the nematic phase of binary mixtures made of rodlike and bent-core molecules," *Phys. Rev. Lett.*, vol. 99, p. 247802, Dec 2007.

[10] C. Bailey, K. Fodor-Csorba, J. T. Gleeson, S. N. Sprunt, and A. Jakli, "Rheological properties of bent-core liquid crystals," *Soft Matter*, vol. 5, pp. 3618–3622, 2009.

[11] S. Stojadinovic, A. Adorjan, S. Sprunt, H. Sawade, and A. Jakli, "Dynamics of the nematic phase of a bent-core liquid crystal," *Phys. Rev. E*, vol. 66, p. 060701, Dec 2002.

[12] O. Francescangeli and E. T. Samulski, "Insights into the cybotactic nematic phase of bent-core molecules," *Soft Matter*, vol. 6, pp. 2413–2420, 2010.

[13] S. H. Hong, R. Verduzco, J. C. Williams, R. J. Twieg, E. DiMasi, R. Pindak, A. Jakli, J. T. Gleeson, and S. Sprunt, "Short-range smectic order in bent-core nematic liquid crystals," *Soft Matter*, vol. 6, pp. 4819–4827, 2010.

[14] O. Francescangeli, F. Vita, C. Ferrero, T. Dingemans, and E. T. Samulski, "Cybotaxis dominates the nematic phase of bent-core mesogens: a small-angle diffuse x-ray diffraction study," *Soft Matter*, vol. 7, pp. 895–901, 2011.

[15] M. Cifelli and V. Domenici, "Nmr investigation of the dynamics of banana shaped molecules in the isotropic phase: a comparison with calamitic mesogens behaviour," *Phys. Chem. Chem. Phys.*, vol. 9, pp. 1202–1209, 2007.

[16] P. Tadapatri, U. S. Hiremath, C. V. Yelamaggad, and K. S. Krishnamurthy, "Permittivity, conductivity, elasticity, and viscosity measurements in the nematic phase of a bent-core liquid crystal," *The Journal of Physical Chemistry B*, vol. 114, no. 5, pp. 1745–1750, 2010.

[17] E. Dorjgotov, K. Fodor-Csorba, J. T. Gleeson, S. Sprunt, and A. Jákli, "Viscosities of a bent-core nematic liquid crystal," *Liquid Crystals*, vol. 35, no. 2, pp. 149–155, 2008.

5

Optical, dielectric and viscoelastic properties of a pure bent-core nematic liquid crystal

5.1 Introduction

I N the previous chapters we studied binary mixtures of rod and bent-core compounds. We found that the physical properties are significantly different in the mixtures. In this chapter we present various physical properties of a pure bent-core nematic liquid crystal. Recently some interesting experimental results are reported in the nematic phase of bent-core (BC) liquid crystals, *i.e.*, large flexoelectric coefficient [1, 2], unusual electroconvection [3–5] and Kerr effect [6]. Olivares *et al.* [7] conducted a dynamic light scattering measurement in a pure bent-core compound with oxazole heterocyclic ring in the central core, and suggested that the temperature dependence of elastic constants is weak with no signature of pretransitional

behavior towards the transition temperature of the smectic (SmC) phase. Recently Dozov *et al.* [8] theoretically showed that a spontaneous symmetry breaking phase transition inside the nematic phase is possible because of mutual tendency of banana-shaped molecules to induce a local bend director with negative bend elastic constant. However, there is report on the measurement on the temperature dependent elastic constants in pure bent-core nematic liquid crystals. In this chapter for the first time we carry out the temperature dependent measurement of various physical parameters of bent-core nematic liquid crystals. We emphasise that the temperature dependence of K_{11} and K_{33} is significantly different from that in rod-like molecules; i.e., K_{33} is much lower compared to K_{11} except very near the SmC phase transition.

5.2 Results and Discussion

5.2.1 Sample and phase behaviour
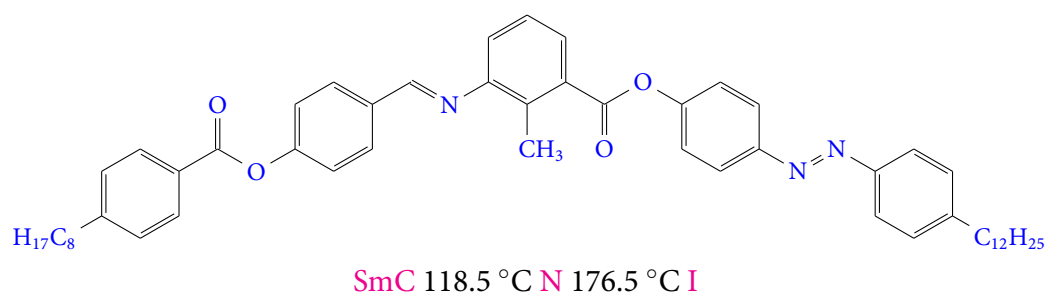
SmC 118.5 °C N 176.5 °C I

Figure 5.1: *Chemical structure of the bent-core molecule used in the experiment.*

The chemical structure of the compound is shown in figure 5.1. It has the following phase transitions: SmC 118.5 °C N 176.5 °C I. The compound exhibits a large temperature range of nematic phase and it is also stable as there was no significant change in the transition temperatures after several cycles of heating and cooling.

5.2.2 Optical and static dielectric constant measurements
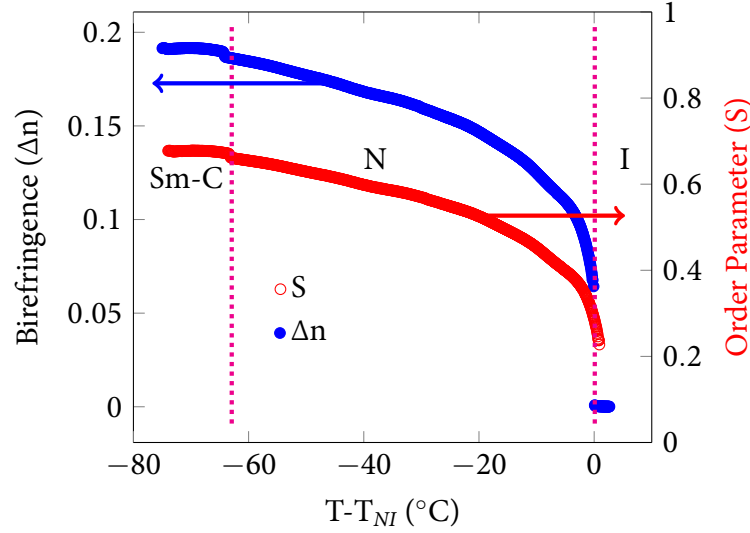
Figure 5.2: *Variation of birefringence (Δn) and order parameter (S) as a function of temperature.*

The main aim of this chapter is to measure elastic constants of bent-core nematic liquid crystal. However we first systematically measure and discuss the optical and dielectric properties as they are needed to understand the elastic properties. The variation of birefringence (Δn) as a function of temperature is shown in the figure 5.2. It is noticed that birefringence appears abruptly at the nematic-isotropic (NI) phase transition and gradually increases as the temperature decreases in the nematic phase. A small jump in the birefringence data is also observed near nematic-SmC phase transition at $T - T_{NI} = -64\,°\text{C}$. The temperature dependent birefringence in the nematic liquid crystals can be approximated by the formula $\Delta n = \Delta n_o (1 - T/T^{**})^\beta$, where T^{**} and β are the adjustable fit parameters and $\Delta n_\circ$ is the birefringence of the perfectly aligned sample. The equation fits well in the entire nematic range with fit parameters $\Delta n_\circ = 0.28$ and $\beta = 0.21$. The order parameter S was estimated using the relation $S = \Delta n / \Delta n_\circ$. The temperature variation of the calculated order parameter is also shown in figure 5.2. The order parameter in the nematic phase just below the nematic-isotropic phase transition was approximately 0.2 and reached to 0.7 with a small jump at nematic-SmC phase transition. The temperature dependent S was also measured by

Weissflog *et al.* [9] and Dong *et al.* [10] in the nematic phase of bent-core nematic liquid crystals using nuclear magnetic resonance spectroscopy, and similar temperature dependence with slightly smaller values of *S* was reported.
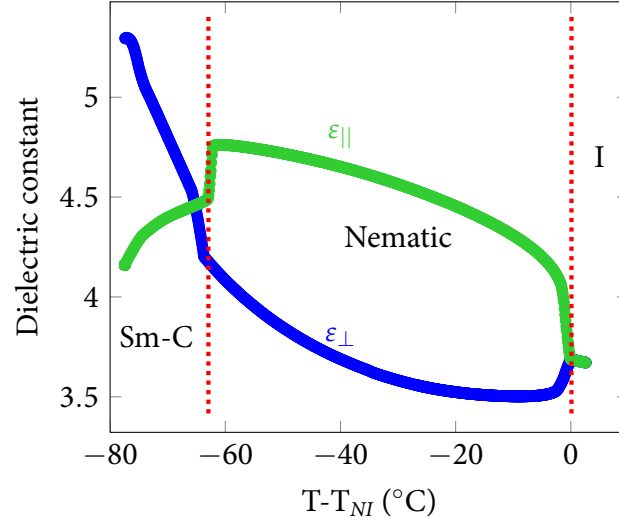
Figure 5.3: *Variation of parallel ($\varepsilon_{||}$) and perpendicular ($\varepsilon_\perp$) components of the dielectric constant as a function of temperature.*

The variation of parallel ($\varepsilon_{||}$) and perpendicular ($\varepsilon_\perp$) components of dielectric constant as a function of temperature is shown is figure 5.3. In the nematic phase, the dielectric anisotropy is small and positive and changes sign in the SmC phase. The temperature dependent dielectric constant can be understood as follows: The molecules have both longitudinal and transverse dipole components mainly due to the ester linkages. In the nematic phase, molecules freely rotate about their long axes, so that the effect of transverse dipoles is suppressed. But the longitudinal dipoles respond to an electric field dielectrically. Hence positive dielectric anisotropy results in the nematic phase. The change of sign of dielectric anisotropy from the nematic phase to the SmA phase of rod like molecules was reported by de Jeu *et al.* [11] and it was explained by an increased dipolar correlation between the molecules in the same layer. In addition to such effect, we consider the bent-shape of the molecules, i.e., local packing of the bent-shaped molecules in the SmC layers hindering the free rotation about their molecular long axis, leading to quasi-macroscopic transverse dipoles, which respond to the electric field, contributing the increase of $\varepsilon_\perp$. The increasing $\varepsilon_\perp$ with decreasing temperature

is caused by larger rotational hindrance. As discussed by de Jeu *et al.* [11], the decrease of $\varepsilon_{||}$ is explained by increased antiparallel correlation between the dipoles along the molecular long axis. This could be possible even in the local packing condition. In addition, the layer formation suppresses the dielectric response about the molecular short axis, contributing the decrease of $\varepsilon_{||}$ in the SmC phase. The sharp variation of dielectric constants across the nematic to SmC transition (fig. 5.3) in the present bent core liquid crystal compared to the slow variation in rod-like molecules [11] is due to the contribution of rotational hindrance.

5.2.3 Splay, bend elastic constant measurements
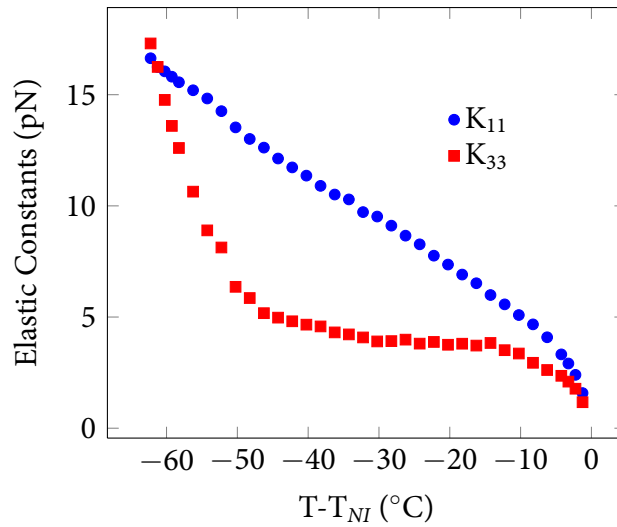
Figure 5.4: *Variation of K_{11} and K_{33} as a function of shifted temperature.*

The temperature dependence of K_{33} and K_{11} is shown in figure 5.4. The value of K_{11} increases monotonically as the temperature is lowered and no pretransitional divergence is observed. The value of K_{33} at a given temperature is always lower than K_{11} except very to close the nematic-SmC transition and shows pretransitional divergence below $T - T_{NI} \approx -50\,°\text{C}$. For example at $T - T_{NI} \approx -1\,°\text{C}$. i.e., just below the nematic-isotropic transition $K_{33}/K_{11} \sim 0.7$ and reduces to ~ 0.4 at about $T - T_{NI} \approx -45\,°\text{C}$.

Then because of pretransitional increase of K_{33} below $T - T_{NI} \approx -50\ °C$, the ratio K_{33}/K_{11} increases to 1 with approaching nematic-SmC transition.
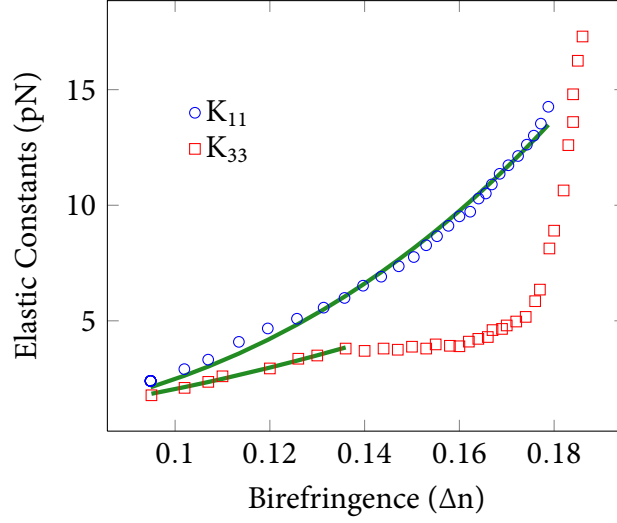
Figure 5.5: *Temperature dependent K_{11} and K_{33} against Δn. Solid lines are best fit to K_{11} and K_{33} vs Δn^x. x=2.9 and 2 in cases of K_{11} and K_{33}, respectively.*

K_{11} and K_{33} are plotted as a function of birefringence (fig. 5.5). It is observed that K_{33} is proportional to Δn^2 ($\propto S^2$) in the vicinity of the nematic-isotropic transition as predicted by the simple mean field theory. K_{11} is also fitted with $K_{11} \propto \Delta n^x$ and the value of $x = 2.9$. Slightly lower value of x ($= 2.5$) was reported in the rod and bent-core mixtures [12]. In the case of rod like molecules (e.g.; 8OCB, octyl cyano biphenyl) it is known that K_{33} is always higher and the ratio $K_{33}/K_{11} \simeq 2$, very close to the nematic-isotropic transition and increases to $\simeq 6$ as the SmA phase is approached [12, 13]. The values of K_{11} in both 8OCB and the present compound are comparable, although the temperature dependence of K_{11} is stronger ($x = 2.9$) in the pure bent-core nematic liquid crystal than 8OCB.

The unusual ratio of K_{33}/K_{11} and the temperature dependence of these two elastic constants are expected to originate from the bent structure of the molecules. A schematic representation of splay and bend distortion of bent-core molecules are shown in figure 5.6(a) and 5.6(b). The almost linear increase in K_{11} can be attributed to the increase in the order parameter as seen in the birefringence measurement (fig. 5.2). Here the
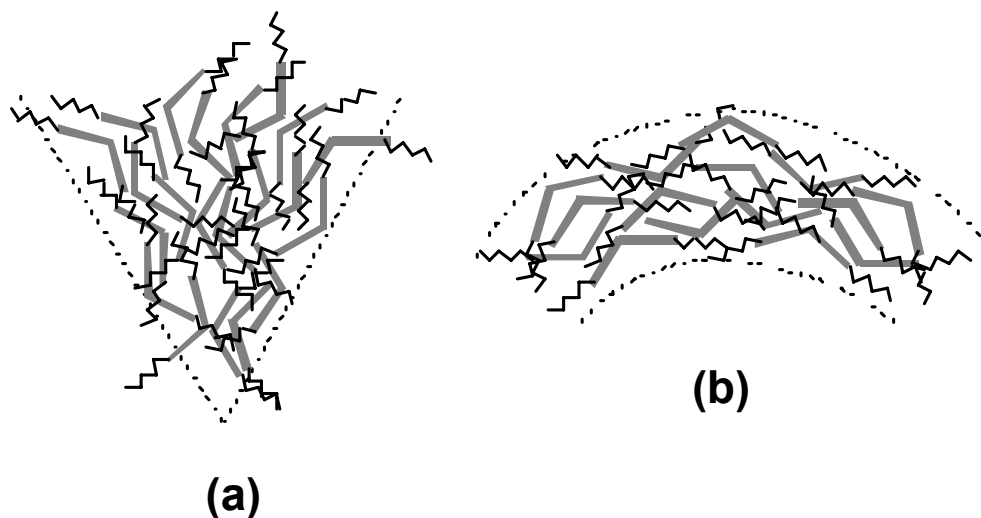
Figure 5.6: *Schematic representation of (a) splay and (b) bend distortion in bent-core nematic liquid crystals.*

bent shape does not facilitate the splay distortion in the medium (fig. 5.6(a)). However, as the temperature is lowered the bent shape coupled to the bend distortion easily facilitates the bent distortion. As a result K_{33} becomes lower in the nematic phase. In this case the strain in the bend distortion is partly relieved by changing the equilibrium distribution of the molecules with one side "up" or "down" as shown in figure 5.6(b). As the temperature is lowered towards the SmC phase, because of smectic short-range fluctuations, K_{33} starts to change the temperature dependence at $T - T_{NI} \approx -30\,^{\circ}\mathrm{C}$. The divergence of elastic constants near the SmC phase has been theoretically studied by de Gennes [14] and Chen and Lubensky [15]. According to both the theories all three elastic constants show pretransitional divergence. In the present compound we find no pretransitional divergence in K_{11} and the exponent of divergence of K_{33} is ≈ 0.43 which is much lower than the predicted value (0.7) indicating that the existing theoretical models are insufficient to explain the pretransitional behaviour near SmC of bent-core liquid crystals. It may be pointed out that there are also some experimental reports on the measurement of elastic constants in some binary mixtures by using a light scattering technique above the nematic to SmC transition [16, 17]. They reported that K_{33} obtains a maximum value just above the nematic to SmC transition

point and such behaviour can not be explained by any of the existing models. It may be mentioned that previously this compound was reported to show the uniaxial to biaxial nematic transition ($N_u - N_b$) [18] at $T - T_{NI} \approx -30\,^\circ$C, though recently Le *et al.* [19] have shown that the medium is uniaxial. Interestingly the temperature at which K_{33} starts changing the temperature-dependence ($T - T_{NI} \approx -30\,^\circ$C) coincides with the transition temperature reported [18], suggesting the onset smectic short-range fluctuation at that temperature. Thus the biaxial-like order seen in the X-ray as reported in reference [18] could be due to the presence of smectic short-range fluctuations, as suggested [20, 21].

5.2.4   Rotational viscosity measurement

In this section we discuss the rotational viscosity of bent-core nematic liquid crystal. To measure the rotational viscosity we measure relaxation time $\tau_\circ$ using phase-decay-time measurement in the entire nematic phase at various temperatures. The details of the technique is already discussed in chapter-2. The variation of relaxation time $\tau_\circ$ as a function of temperature is shown in figure 5.7.
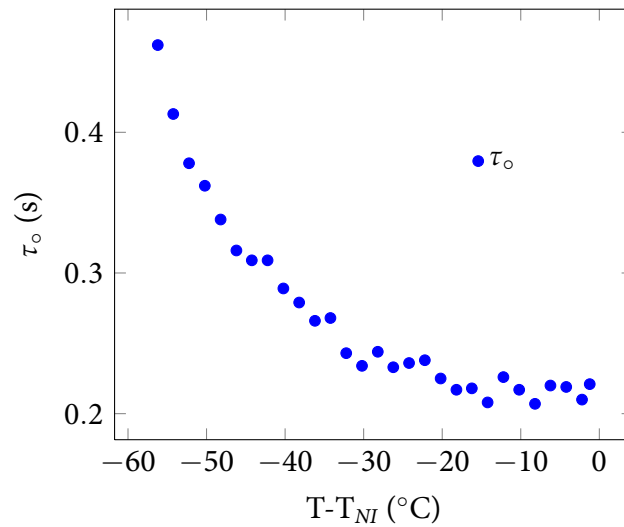
Figure 5.7: *Variation of $\tau_\circ$ as a function of shifted temperature.*

It is observed that near the nematic-isotropic transition the relaxation time $\tau_\circ$ is $\simeq$ 0.22 s and gradually increases with decreasing temperature, and tend to diverge as the smectic-C (SmC) phase is approached. The temperature dependent variation of $\gamma_1 = \tau_0 K_{11} \pi^2 / d^2$ calculated from the measurement of relaxation time is shown in figure 5.8. It is noted that the value of γ_1 is about 0.1 Pa s or less near the nematic-isotropic transition and increases superlinearly to 0.35 Pa s with decreasing temperature until the shifted temperature $T - T_{NI} \sim -45$ °C, and then tends to diverge before the nematic to Sm-C transition occurs. The measurement of γ_1 of a bent-core nematic liquid crystal with negative dielectric anisotropy was reported by Dorjgotov [22] by pulsed magnetic field. According to their report, the rotational viscosity is almost 10 times larger than the calamitic liquid crystals. Such larger rotational viscosity was attributed to the formation of temporary clusters owing to the bent-shape of the molecules in the sense that the bent-shape and the transverse dipole moment of the molecules together facilitates the formation of clusters. On the other hand the present compound exhibits a positive dielectric anisotropy and the value of γ_1 is slightly larger by a factor of two or three (far from the nematic-isotropic transition) compared to that in many calamitic liquid crystals, suggesting the size of temporary clusters to be very small.
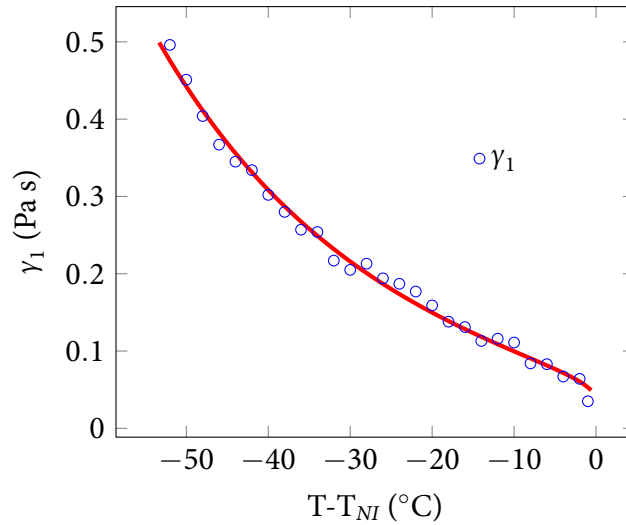
Figure 5.8: *Variation of γ_1 as a function of temperature. Solid line is a theoretical fit to Osipov-Terentjev [23] theory.*

Further the close proximity in the values and the temperature dependencies of γ_1 of the present bent-core compound with the calamitic materials urge us to consider and compare the experimental results with the known theories. Osipov and Terentjev developed a microscopic theory (OT theory) [23] for describing the rotational viscosity of liquid crystals. They derived general expression for the microscopic stress tensor of the nematic which was presented in terms of molecular moments of inertia and the intermolecular interaction potential and showed that rotational viscosity (γ_1)

$$\gamma_1 = g_0 \left(\frac{T}{T_c} \right)^4 \left(\frac{E_1}{K_B T_c} \right)^{-3} \left(\frac{J_0 S}{k_B T_c} \right)^{0.5} \exp \left(\frac{E_1 + J_0 S}{k_B T} \right) \tag{5.1}$$

where g_0 is a constant, $J_0 = B k_B T_c$, E_1 is the activation energy, S is the order parameter. The temperature dependent γ_1 can be well fitted to the above equation up to $T - T_{NI} = -54\,^\circ$C with the fit parameters $g_0 = 1.9 \times 10^{-4}$ Pa s, $J_0 = 48.5$ meV and $E_1 = 0.525$ eV. The fitting of the experimental data with the above equation is shown in figure 5.8, showing very good fit. The fit parameters are comparable to the values known in many calamitic liquid crystals [24].

Finally we want to make a brief comment on the temperature dependence of γ_1. As we mentioned earlier that Prasad *et al.* [18] had reported a uniaxial to biaxial nematic transition at $T - T_{NI} \sim -30\,^\circ$C though later Le *et al.* [19] showed that the medium is uniaxial and subsequentially Lavrentovich *et al.* [25] showed by detailed experiments that such transition is absent. From our study it is also clear that there is no indication of the aforesaid transition. Moreover, the temperature dependence of the rotational viscosity is well fitted to the Osipov-Terentjev [23] theory over a wide temperature range including the suggested transition temperature $T - T_{NI} \sim -30\,^\circ$C. Upward deviation from the Osipov-Terentjev theory at lower temperature was also observed in calamitic liquid crystals [24], and was explained by the pretransitional effect when approaching to the crystal phase. Here we attribute the deviation below ($T - T_{NI} \sim -45\,^\circ$C) to the effect of short-range smectic fluctuations. Thus rapid increase in $\tau_\circ$ and

hence the γ_1 is due to the onset of the smectic short-range fluctuations in the nematic phase.

5.3   Conclusions

In conclusion, we for the first time measured K_{11} and K_{33} elastic constants and rotational viscosity (γ_1) as a function of temperature in a pure bent-core liquid crystal. Our measurement shows that K_{33} is much lower than K_{11} except for the temperature region close to the nematic to SmC transition. The temperature dependence clearly shows a strong coupling of bent-shape with the bend distortions in pure compound. Thus, various physical properties and their temperature dependence related to K_{33} are strongly influenced and further the bent-shape has to be taken into account in understanding the physical properties of bent-core molecules. Temperature dependence of rotational viscosity shows the effect of smectic short-range order fluctuations. The temperature dependent viscosity data prior to the onset of smectic fluctuations can be fitted well with the Osipov-Terentjev theory.

References

[1] J. Harden, B. Mbanga, N. Éber, K. Fodor-Csorba, S. Sprunt, J. T. Gleeson, and A. Jákli, "Giant flexoelectricity of bent-core nematic liquid crystals," *Phys. Rev. Lett.*, vol. 97, p. 157802, Oct 2006.

[2] K. V. Le, F. Araoka, K. Fodor-Csorba, K. Ishikawa, and H. Takezoe, "Flexoelectric effect in a bent-core mesogen," *Liquid Crystals*, vol. 36, no. 10-11, pp. 1119–1124, 2009.

[3] D. Wiant, J. T. Gleeson, N. Éber, K. Fodor-Csorba, A. Jákli, and T. Tóth-Katona, "Nonstandard electroconvection in a bent-core nematic liquid crystal," *Phys. Rev. E*, vol. 72, p. 041712, Oct 2005.

[4] S. Tanaka, S. Dhara, B. K. Sadashiva, Y. Shimbo, Y. Takanishi, F. Araoka, K. Ishikawa, and H. Takezoe, "Alternating twist structures formed by electroconvection in the nematic phase of an achiral bent-core molecule," *Phys. Rev. E*, vol. 77, p. 041708, Apr 2008.

[5] S. Tanaka, H. Takezoe, N. Éber, K. Fodor-Csorba, A. Vajda, and A. Buka, "Electroconvection in nematic mixtures of bent-core and calamitic molecules," *Phys. Rev. E*, vol. 80, p. 021702, Aug 2009.

[6] S. Dhara, F. Araoka, M. Lee, K. V. Le, L. Guo, B. K. Sadashiva, K. Song, K. Ishikawa, and H. Takezoe, "Kerr constant and third-order nonlinear optic susceptibility measurements in a liquid crystal composed of bent-shaped molecules," *Phys. Rev. E*, vol. 78, p. 050701, Nov 2008.

[7] J. A. Olivares, S. Stojadinovic, T. Dingemans, S. Sprunt, and A. Jákli, "Optical studies of the nematic phase of an oxazole-derived bent-core liquid crystal," *Phys. Rev. E*, vol. 68, p. 041704, Oct 2003.

[8] I. Dozov, "On the spontaneous symmetry breaking in the mesophases of achiral banana-shaped molecules," *EPL (Europhysics Letters)*, vol. 56, no. 2, p. 247, 2001.

[9] W. Weissflog, S. Sokolowski, H. Dehne, B. Das, S. Grande, M. W. Schröder, A. Eremin, S. Diele, G. Pelzl, and H. Kresse, "Chiral ordering in the nematic and an optically isotropic mesophase of bent-core mesogens with a halogen substituent at the central core," *Liquid Crystals*, vol. 31, no. 7, pp. 923–933, 2004.

[10] R. Y. Dong, K. Fodor-Csorba, J. Xu, V. Domenici, G. Prampolini, and C. A. Veracini, "Deuterium and carbon-13 nmr study of a banana mesogen: Molecular structure and order," *The Journal of Physical Chemistry B*, vol. 108, no. 23, pp. 7694–7701, 2004.

[11] W. H. de Jeu, T. W. Lathouwers, and P. Bordewijk, "Dielectric properties of di-*n*-heptyl azoxybenzene in the nematic and in the smectic-*a* phases," *Phys. Rev. Lett.*, vol. 32, pp. 40–43, Jan 1974.

[12] B. Kundu, R. Pratibha, and N. V. Madhusudana, "Anomalous temperature dependence of elastic constants in the nematic phase of binary mixtures made of rodlike and bent-core molecules," *Phys. Rev. Lett.*, vol. 99, p. 247802, Dec 2007.

[13] M. R. Dodge, C. Rosenblatt, R. G. Petschek, M. E. Neubert, and M. E. Walsh, "Bend elasticity of mixtures of v-shaped molecules in ordinary nematogens," *Phys. Rev. E*, vol. 62, pp. 5056–5063, Oct 2000.

[14] P. G. De Gennes, "Some remarks on the polymorphism of smectics," *Molecular Crystals and Liquid Crystals*, vol. 21, no. 1-2, pp. 49–76, 1973.

[15] J. H. Chen and T. C. Lubensky, "Landau-ginzburg mean-field theory for the nematic to smectic-*c* and nematic to smectic-*a* phase transitions," *Phys. Rev. A*, vol. 14, pp. 1202–1207, Sep 1976.

[16] L. Solomon and J. D. Litster, "Light-scattering measurements in the ⁻7s5-8ocb nematic-smectic-*a*-smectic-*c* liquid-crystal system," *Phys. Rev. Lett.*, vol. 56, pp. 2268–2271, May 1986.

[17] J. Huang and J. T. Ho, "Light-scattering study in nematic smectic-*A* smectic-*C* multicritical mixtures," *Phys. Rev. A*, vol. 38, pp. 400–406, Jul 1988.

[18] V. Prasad, S.-W. Kang, K. A. Suresh, L. Joshi, Q. Wang, and S. Kumar, "Thermotropic uniaxial and biaxial nematic and smectic phases in bent-core mesogens," *Journal of the American Chemical Society*, vol. 127, no. 49, pp. 17224–17227, 2005.

[19] K. V. Le, M. Mathews, M. Chambers, J. Harden, Q. Li, H. Takezoe, and A. Jákli, "Electro-optic technique to study biaxiality of liquid crystals with positive dielectric anisotropy: The case of a bent-core material," *Phys. Rev. E*, vol. 79, p. 030701, Mar 2009.

[20] A. G. Vanakaras and D. J. Photinos, "Thermotropic biaxial nematic liquid crystals: Spontaneous or field stabilized?," *The Journal of Chemical Physics*, vol. 128, no. 15, p. 154512, 2008.

[21] N. Vaupotič, J. Szydlowska, M. Salamonczyk, A. Kovarova, J. Svoboda, M. Osipov, D. Pociecha, and E. Gorecka, "Structure studies of the nematic phase formed by bent-core molecules," *Phys. Rev. E*, vol. 80, p. 030701, Sep 2009.

[22] E. Dorjgotov, K. Fodor-Csorba, J. T. Gleeson, S. Sprunt, and A. Jákli, "Viscosities of a bent-core nematic liquid crystal," *Liquid Crystals*, vol. 35, no. 2, pp. 149–155, 2008.

[23] M. A. Osipov and E. M. Terentjev, "Rotational diffusion and rheological properties of liquid crystals," *Z. Naturforsch*, vol. A44, p. 785, 1989.

[24] M. L. Dark, M. H. Moore, D. K. Shenoy, and R. Shashidhar, "Rotational viscosity and molecular structure of nematic liquid crystals," *Liquid Crystals*, vol. 33, no. 1, pp. 67–73, 2006.

[25] B. Senyuk, H. Wonderly, M. Mathews, Q. Li, S. V. Shiyanovskii, and O. D. Lavrentovich, "Surface alignment, anchoring transitions, optical properties, and topological defects in the nematic phase of thermotropic bent-core liquid crystal a131," *Phys. Rev. E*, vol. 82, p. 041711, Oct 2010.

6

Optical, dielectric and viscoelastic properties of a liquid crystal with asymmetric bent-core (hockey stick-shaped) molecules

6.1 Introduction

In chapter-3 and chapter-4 we studied various physical properties of binary mixtures of rod and bent-core compounds. In the last chapter (chapter-5) we also studied various properties of a pure bent-core nematic liquid crystal. In this chapter we discuss the measurement of various physical properties of a liquid crystal with hockey stick-shaped molecules. It exhibits nematic, SmA and anticlinic smectic-C (SmC$_a$) phase transitions.

6.2 Results and Discussion

6.2.1 Sample and phase behaviour

The chemical name of the hockey stick-shaped compound is 4-n-butyloxyphenyl [4-(4-n-heptyloxybenzoyloxy4-benzoyloxy)]biphenyl-3-carboxylate. It exhibits metastable liquid crystalline phase transitions. The chemical structure and the phase transition temperatures of the compound is shown in figure 6.1. The synthesis and some preliminary characterisation was reported previously [1].

SmX 97.0 °C SmC$_a$ 110.5 °C SmA 114.5 °C N 123.5 °C I
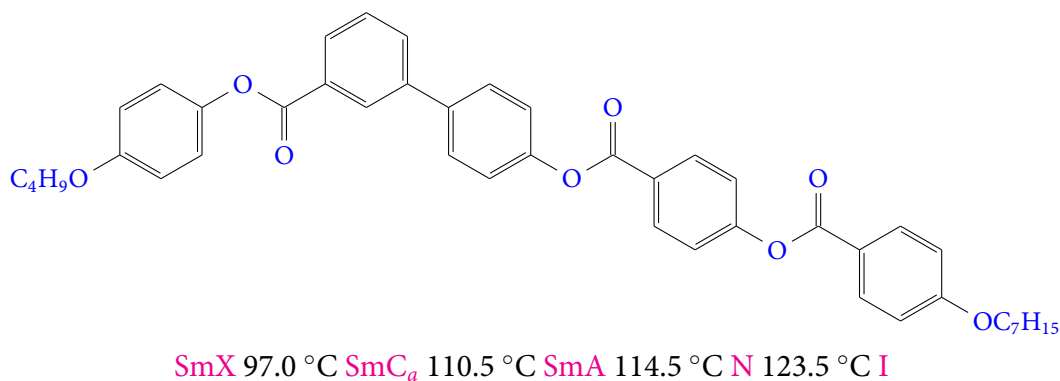
Figure 6.1: *Chemical structure of the compound and the phase transition temperatures.*

The molecule is achiral, asymmetric, hockey stick-shaped and has several strong dipolar groups. The texture obtained in between two glass plates without any surface treatment is shown in figure 6.2. In the nematic phase a typical schlieren texture with four brush defects are observed (fig. 6.2 (i)). SmA is spontaneously aligned homeotropically below the nematic-SmA transition temperature (fig. 6.2(iii)) and again the dark region of the texture is transformed into schlieren texture as the temperature is reduced to SmC$_a$ (fig. 6.2(iv)) phase. SmC$_a$ exhibits two and four brush defects with dynamic fluctuations (fig. 6.2(iv)), suggesting it to be an anticlinic SmC (SmC$_a$) phase. The anticlinic structure in case of rod-like molecule is schematically shown in chapter-1 (fig. 1.6). The textures obtained in planar and homeotropic cells under optical polarizing microscope is shown in figure 6.3. It is noticed that all the phases can be
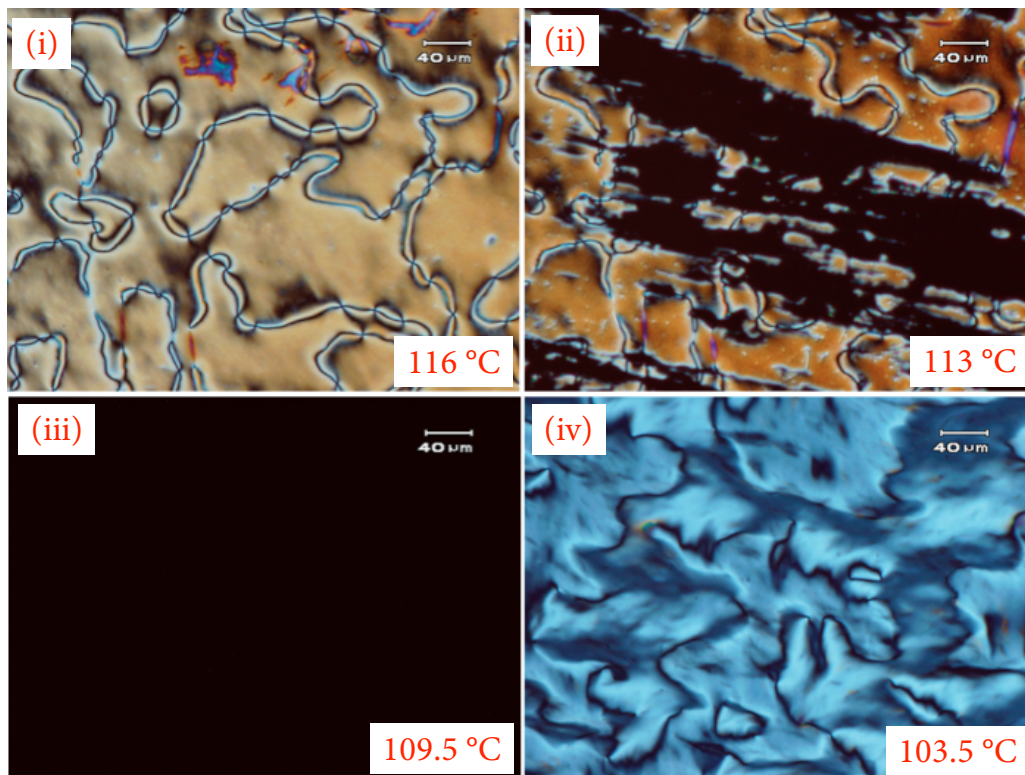
Figure 6.2: *Photomicrographs obtained in untreated cell under cooling at different temperatures (i) nematic phase (ii) at nematic-SmA transition (iii) SmA and (iv) SmC$_a$.*

aligned well in planar cells. In homeotropic cell both nematic and SmA phases are well aligned. In case of SmC$_a$ phase the overall texture is dark in homeotropic cell except some comparatively brighter and smaller regions are seen due to the tilting of the molecules with respect to the layer normal.

6.2.2 Optical and static dielectric measurements

The temperature dependent variation of Δn and a differential scanning calorimetric (DSC) thermogram are shown in figure 6.4. The enthalpies of isotropic to nematic, nematic to SmA and SmA to SmC$_a$ transitions are 0.38, 0.98 and 0.23 kJ/mol respectively. Δn jumps to 0.06 from 0 at nematic-isotropic (NI) transition and gradually increases as the temperature is lowered. At nematic-SmA transition it shows significant increase (0.02) and tends to saturate in the SmA phase. A similar jump (0.02)
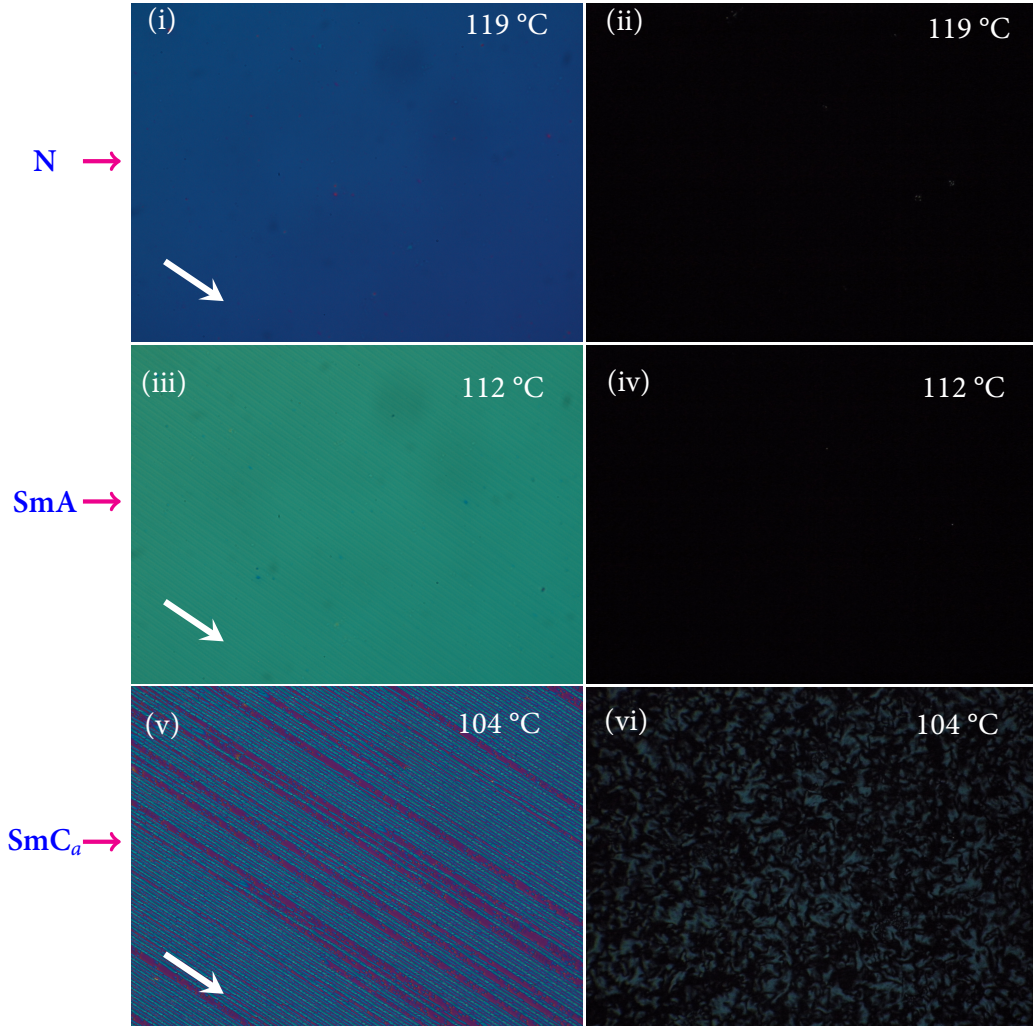
Figure 6.3: *Photomicrographs obtained in planar cell (i, iii, v) and in homeotropic cell (ii, iv, vi) at various temperatures under polarizing optical microscope. White arrows indicate the rubbing directions.*

in Δn is also seen at SmA- SmC$_a$ transition and further Δn increases as the temperature is decreased. Since $\Delta n \propto S$, where S is the orientational order parameter, it is anticipated that orientational order parameter increases with decreasing temperature showing finite jumps across the transitions. Hence, these are first order phase transitions. Further, nematic-SmA transition (fig. 6.4) is comparatively less sharp than SmA-SmC$_a$ transition due to the presence of smectic short-range fluctuations in the nematic phase. Finite enthalpies of these transitions also suggest that the transitions are first order. It may be pointed out that usually the measurement of Δn in lower

symmetric smectic phases are difficult and rare due to poor alignment of the liquid crystal director. Moreover SmC_a is biaxial because of tilting of the molecules from the layer normal. The narrow lines along the rubbing direction in figure 6.3(v) could be due to the local biaxial order of SmC_a phase. Nevertheless in the present system it was possible to measure Δn because the director in the SmA phase is well aligned (fig. 6.3(iii)) and the effective principal axis in the SmC_a phase still remains parallel to the rubbing direction because of opposite tilt of the molecules in successive layers.
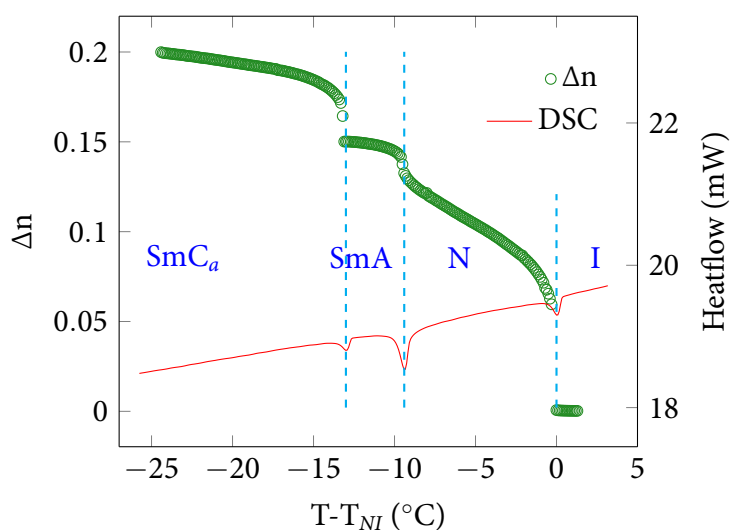
Figure 6.4: *A DSC thermogram in cooling cycle (rate $5°$/min) and variation of birefringence (Δn).*

Temperature dependent variation of dielectric constants $\varepsilon_{||}$, $\varepsilon_{\perp}$ and average value, $\bar{\varepsilon}$ ($= (\varepsilon_{||} + 2\varepsilon_{\perp})/3$) are shown in figure 6.5. $\bar{\varepsilon}$ in the nematic phase is less and further reduces in smectic phases from the extrapolated value of the isotropic dielectric constant. Usually $\bar{\varepsilon}$ is expected to increase as the temperature is reduced due to the increase in density and contribution from orientational polarization [2]. In the present compound the opposite behaviour especially in the smectic phases are due to the strong antiparallel correlation of the longitudinal components of dipole moments. The dielectric anisotropy $\Delta\varepsilon$ ($= \varepsilon_{||} - \varepsilon_{\perp}$) is positive in all the phases. $\varepsilon_{||}$ increases as the temperature is lowered in the nematic phase and starts to decrease sharply at the nematic-SmA transition and decreases rather slowly in the SmC_a phase. The decrease
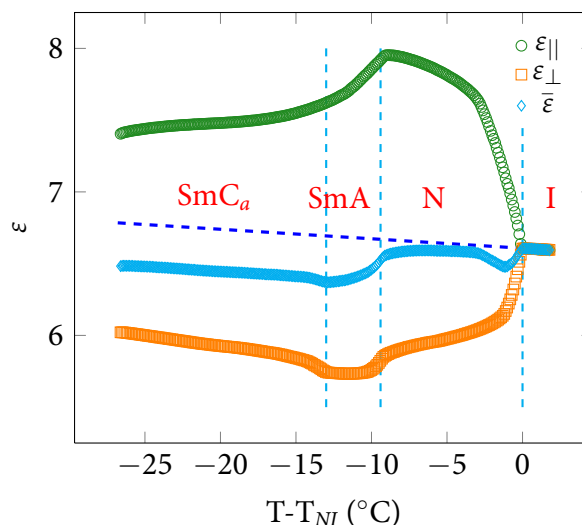
Figure 6.5: *Variation of dielectric constant ($\varepsilon_{||}$, $\varepsilon_{\perp}$ and $\bar{\varepsilon}$) as a function of temperature. Dotted vertical lines are drawn to indicate the transitions. Dashed line denotes the extrapolated value of isotropic dielectric constant.*

in $\varepsilon_{||}$ in conventional and in unconventional compounds with similar molecular structure is due to the increase in antiparallel correlation between the long axis components of dipoles in the SmA layer [3]. The slow decrease of $\varepsilon_{||}$ as the temperature is reduced in the SmC$_a$ phase is due to the tilting of the molecules in addition to the antiparallel correlation. $\varepsilon_{\perp}$ decreases in the nematic phase as the temperature is decreased from the isotropic phase. It is further lower in the SmA phase than both nematic and SmC$_a$ with slope change at the transitions. The lower value of $\varepsilon_{\perp}$ in the SmA phase suggests that there is also an antiparallel correlation between the short axis components of the dipoles in the SmA layer. This result is opposite to the behaviour seen in pure bent-core nematic liquid crystal (chapter-5). It may be mentioned that since the molecules have anticlinic tilt in successive layers of SmC$_a$ phase, $\varepsilon_{||}$ in this phase refers to the dielectric constant when the electric field is parallel to the layer normal rather than the director. Further both the planar and homeotropic alignment of the SmC$_a$ phase is relatively poor than the SmA phase due to the reason mentioned above and the absolute accuracy in the measurements of Δn, $\varepsilon_{||}$ and $\varepsilon_{\perp}$ in this phase is expected to be somewhat less than both in nematic and SmA phases.

6.2.3 Splay, bend elastic constant measurements

To measure K_{11} and K_{33} we measured voltage dependent optical retardation ($\Delta\Phi$) at various temperatures in the nematic phase. The temperature variation of K_{11} and K_{33} are shown in figure 6.6. K_{11} is significantly higher than K_{33} in the entire nematic phase. K_{33} increases much slower than K_{11} with decreasing temperature and shows strong pretransitional divergence as the SmA phase is approached. Similar behaviour were also seen in the previous studies in the pure bent-core compound. It has been shown that the bent shape of the molecules facilitate bend distortion as a result K_{33} is lower than K_{11}. The hockey stick-shaped molecule also has asymmetric bent-shape and the present result is the manifestation of the same effect as described in the previous chapters.
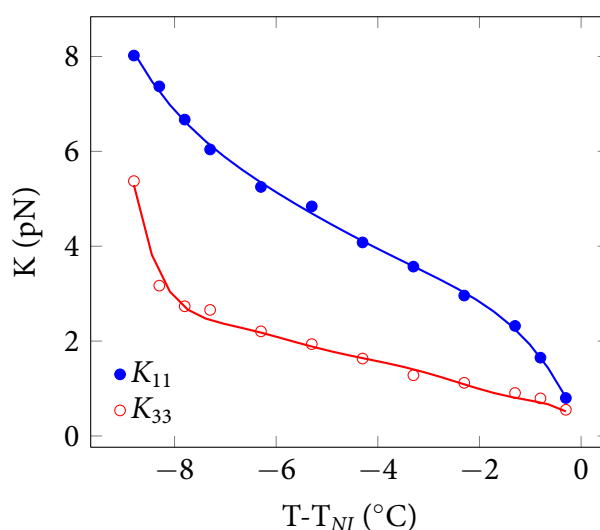
Figure 6.6: *Variation of splay (K_{11}) and bend (K_{33}) elastic constants in the nematic phase as a function of shifted temperature. Continuous lines are drawn as a guide to the eye.*

6.2.4 Rotational viscosity measurement

We also measured rotational viscosity (γ_1) in the nematic phase as a function of temperature by using the time dependent phase-decay method. Representative variation of $\ln[\delta_o/\delta(t)]$ with time (t) at two different temperatures together with the best fits
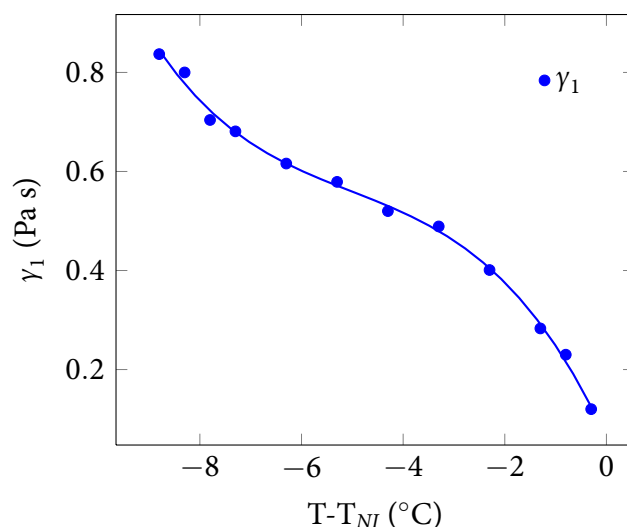
Figure 6.7: *Variation of rotational viscosity (γ_1) as a function of shifted temperature. Continuous line is drawn as a guide to the eye*

are shown in the figure 6.8. γ_1 increases as the temperature is lowered in the nematic phase and a change in curvature is observed at $T - T_{NI} \simeq -5\,°C$ suggesting a pretransitional effect of smectic short-range order in the nematic phase. γ_1 in this compound is slightly larger than in pure bent-core nematic liquid crystals (chapter-5) and significantly higher than that of many known calamitic nematic liquid crystals [4]. The larger rotational viscosity in this hockey stick-shaped compound partially may arise due to the effect of molecular weight compared to the calamitics. However in case of bent-core compounds we attributed it to the existence of temporarily fluctuating smectic clusters of a few molecules in the nematic phase that are expected to originate from the restricted free rotation of the bent-core molecules along the long axis. Existence of such temporary clusters in the nematic phase is also revealed in rheological [5] and dynamic light scattering studies [6] and more recently in small angle X-ray studies [7–10]. The hockey-stick shaped molecule can be considered as highly asymmetric bent-core molecule and hence the enhanced rotational viscosity is believed to originate from the temporarily fluctuating clusters.
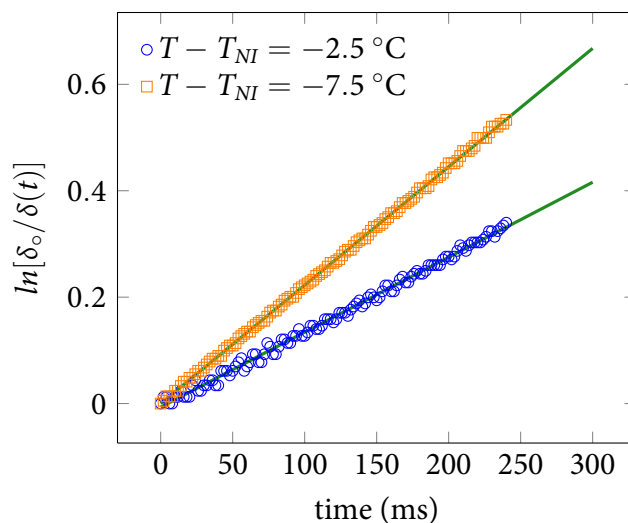
Figure 6.8: *Variation of $ln[\delta_o/\delta(t)]$ at two shifted temperatures namely T-T_{NI}=-7.5°C and -2.5°C with best fits.*

6.2.5 Dielectric relaxation

The hockey stick-shaped molecule has several dipolar groups which are oriented in different directions. Since $\Delta\varepsilon > 0$, it is anticipated that the molecule has relatively strong longitudinal dipole moment along the long axis as a result $\varepsilon_{||}$ can relax at relatively low frequency. In case of $\varepsilon_\perp$ no dipolar relaxation was found up to 10 MHz.

Variation of $\varepsilon_{||}$ as a function of frequency in the three phases at three different temperatures are shown in figure 6.9. It is observed that there are two relaxations, one is temperature dependent (below $\sim$1 MHz) and the relaxation frequency decreases with decreasing temperature. The other one is above $\sim$1 MHz frequency and is independent of temperature. The high frequency relaxation is temperature independent and is attributed to the relaxation due to the finite resistance of ITO which is even present in empty cell. The low frequency relaxation is due to the longitudinal component of the molecular dipole moment of the long axis. Cole-Cole plots of the dielectric constant are shown in figure 6.10. They are semicircular with the centers on the x-axis suggesting that the relaxation is Debye type. Similar low frequency relaxations are also seen in other bent-core compounds [11]. Since the relaxation region due to ITO
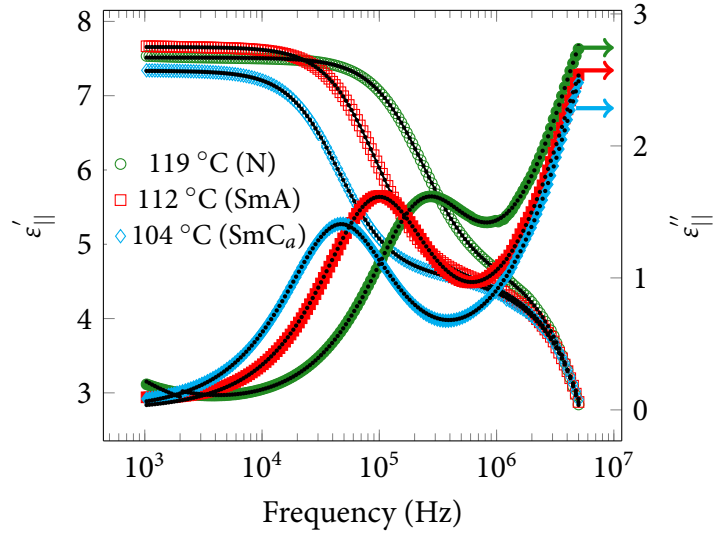
Figure 6.9: *Frequency dispersion of real ($\varepsilon'_{||}$)(open symbols) and imaginary ($\varepsilon''_{||}$) (filled symbols) parts of the dielectric constant at three different temperatures namely 119 °C (N), 112 °C (SmA) and 104 °C (SmC$_a$). Dotted lines are theoretical fit to the equation (6.1).*
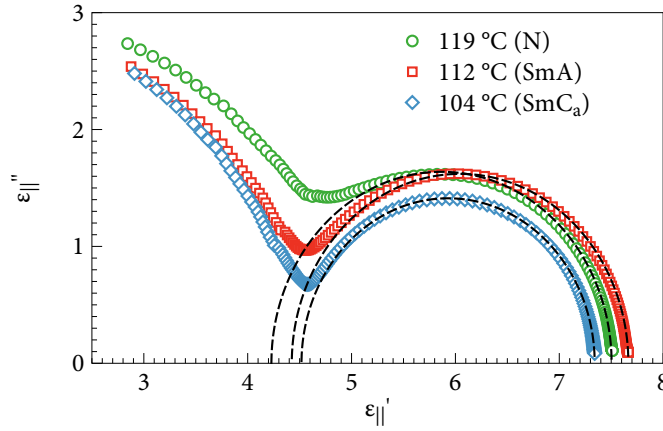
Figure 6.10: *Cole-Cole plot for $\varepsilon_{||}$ relaxation at the same temperatures. The centers of the semicircles lies on the $\varepsilon'_{||}$ axis suggesting that the relaxation is Debye type. Dashed lines are theoretical fit to the Cole-Cole equation. The high frequency portion of the semicircles are due to the ITO cell relaxations.*

is partially overlapped with dipolar relaxation we fitted complex dielectric constant ($\varepsilon^*(\omega) = \varepsilon'(\omega) - i\varepsilon''(\omega)$) as a function of frequency to find the exact dipole relaxation frequency. The complex dielectric function is given by

$$\varepsilon(\omega)^* = \varepsilon_2 + \frac{\varepsilon_0 - \varepsilon_1}{1 + (i\omega\tau_1)^{1-\alpha_1}} + \frac{\varepsilon_1 - \varepsilon_2}{1 + (i\omega\tau_2)^{1-\alpha_2}} \tag{6.1}$$

where ε_0 is the static dielectric permittivity, ε_i and τ_i are the frequency limits and relaxation times of the ith mode. α_i is the Cole-Cole distribution parameters of the respective modes.
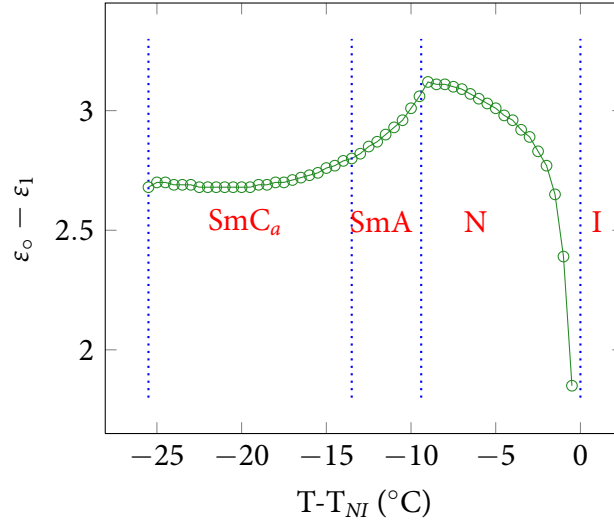
Figure 6.11: *Variation of dielectric strength ($\varepsilon_0 - \varepsilon_1$) with shifted temperature. Continuous line is drawn as a guide to the eye.*

It is found that both α_1 and α_2 are very small (< 0.01) at all temperatures and the relaxation time τ_2 is independent of temperature as expected. The temperature variations of dielectric strength ($\varepsilon_0 - \varepsilon_1$) and relaxation time τ_1 with temperature are shown
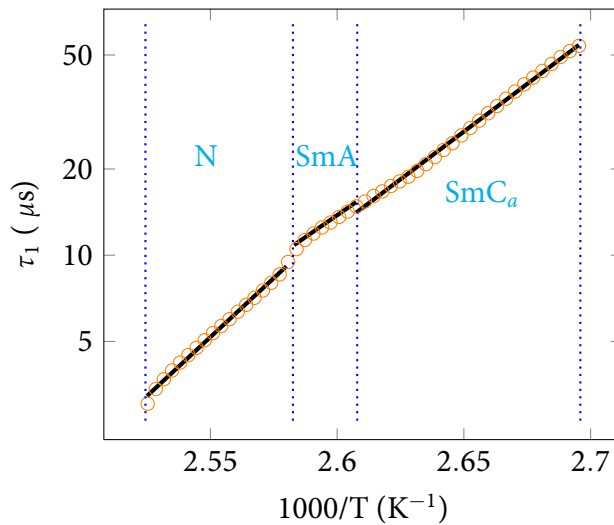
Figure 6.12: *Variation of relaxation time τ_1 as a function of $1/T$. Continious lines are theoretical fit to the equation $\tau_1 = \tau_0 exp(U/RT)$. Vertical lines indicate the phase transition temperatures.*

in figure 6.11 and figure 6.12. The dielectric strength increases rapidly in the nematic phase due to the increase in the orientational order and decreases sharply at the nematic-SmA transition (fig. 6.11). The sharp decrease below nematic-SmA transition is due to strong antiparallel correlation of the longitudinal components of the dipoles in the smectic phases as discussed earlier. τ_1 increases and varies linearly with the inverse of temperature (fig. 6.12) and can be fitted well with the Arrhenius equation, $\tau_1 = \tau_0 \exp(U/RT)$. The activation energy U of the nematic, SmA and SmC$_a$ phases are 158, 117 and 127 kJ/mol respectively. These values are comparatively higher than many calamitics in their respective phases [12, 13]. Similar behaviour is also reported very recently in a binary liquid crystal mixture (rod and bent-core) showing nematic-SmC$_a$ phase transition [11]. Since the activation energy represent the energy barrier associated with the flip-over of the long molecular axis it suggests that the flip-over motion is relatively uneasier in hockey-stick or bent-core systems than calamitic liquid crystals. Presumably this could arise due to the shape and larger rotational viscosity (fig. 6.7) of the hockey stick-shaped and bent-core compounds. However further investigations are needed to shine more light on this aspect.

6.3 Conclusions

In conclusion, we measured detailed physical properties of an unconventional liquid crystal with hockey stick-shaped molecules for the first time. All phase transitions are detected to be first order from optical and thermal (DSC) measurements. Dielectric measurements indicate that there exists an antiparallel dipolar correlation of both the longitudinal and transverse components of dipoles in the SmA and SmC$_a$ phases. Bend elastic constant is significantly lower than splay elastic constant as seen in other bent-core nematic liquid crystals. Rotational viscosity is comparatively larger than calamitics and are influenced by pretransitional smectic fluctuations. Dielectric relaxation of the longitudinal components of dipole moments is Debye type and the

relaxation frequency exhibits Arrhenius behaviour with comparatively higher activation energy. Finally it may be asserted that many physical properties of hockey stick-shaped compound are noticeably different than that of calamitic liquid crystals and that the shape is an important parameter for tuning the physical properties.

References

[1] S. Radhika, H. Srinivasa, and B. Sadashiva, "Anticlinic smectic c phase in new and novel five-ring hockey stick-shaped compounds," *Liquid Crystals*, vol. 38, no. 6, pp. 785–792, 2011.

[2] W. Maier and G. Meier, "A simple theory of the dielectric characteristics of homogeneous oriented crystalline-liquid phases of the nematic type," *Z. Naturforsch*, vol. 16a, p. 262, 1961.

[3] W. H. de Jeu, T. W. Lathouwers, and P. Bordewijk, "Dielectric properties of di-*n*-heptyl azoxybenzene in the nematic and in the smectic-*a* phases," *Phys. Rev. Lett.*, vol. 32, pp. 40–43, Jan 1974.

[4] P. Tadapatri, U. S. Hiremath, C. V. Yelamaggad, and K. S. Krishnamurthy, "Permittivity, conductivity, elasticity, and viscosity measurements in the nematic phase of a bent-core liquid crystal," *The Journal of Physical Chemistry B*, vol. 114, no. 5, pp. 1745–1750, 2010.

[5] C. Bailey, K. Fodor-Csorba, J. T. Gleeson, S. N. Sprunt, and A. Jakli, "Rheological properties of bent-core liquid crystals," *Soft Matter*, vol. 5, pp. 3618–3622, 2009.

[6] S. Stojadinovic, A. Adorjan, S. Sprunt, H. Sawade, and A. Jakli, "Dynamics of the nematic phase of a bent-core liquid crystal," *Phys. Rev. E*, vol. 66, p. 060701, Dec 2002.

[7] O. Francescangeli and E. T. Samulski, "Insights into the cybotactic nematic phase of bent-core molecules," *Soft Matter*, vol. 6, pp. 2413–2420, 2010.

[8] S. H. Hong, R. Verduzco, J. C. Williams, R. J. Twieg, E. DiMasi, R. Pindak, A. Jakli, J. T. Gleeson, and S. Sprunt, "Short-range smectic order in bent-core nematic liquid crystals," *Soft Matter*, vol. 6, pp. 4819–4827, 2010.

[9] O. Francescangeli, F. Vita, C. Ferrero, T. Dingemans, and E. T. Samulski, "Cybotaxis dominates the nematic phase of bent-core mesogens: a small-angle diffuse x-ray diffraction study," *Soft Matter*, vol. 7, pp. 895–901, 2011.

[10] M. Cifelli and V. Domenici, "Nmr investigation of the dynamics of banana shaped molecules in the isotropic phase: a comparison with calamitic mesogens behaviour," *Phys. Chem. Chem. Phys.*, vol. 9, pp. 1202–1209, 2007.

[11] P. Salamon, N. Éber, A. Buka, J. T. Gleeson, S. Sprunt, and A. Jákli, "Dielectric properties of mixtures of a bent-core and a calamitic liquid crystal," *Phys. Rev. E*, vol. 81, p. 031711, Mar 2010.

[12] B. S. Srikanta and N. V. Madhusudana, "Dielectric relaxation studies on two systems exhibiting the induced smectic a phase," *Molecular Crystals and Liquid Crystals*, vol. 108, no. 1-2, pp. 39–49, 1984.

[13] N. V. Madhusudana, B. S. Srikanta, and M. S. Raj Urs, "Comparative x-ray and dielectric studies on some structurally related smectogenic compounds," *Molecular Crystals and Liquid Crystals*, vol. 108, no. 1-2, pp. 19–37, 1984.

7

Optical, dielectric and elastic properties of a nematic liquid crystal with T-shaped molecules

7.1   Introduction

I N the last chapter we studied various physical properties of a liquid crystal with hockey stick-shaped molecules. In this chapter we present various physical measurements including X-ray diffraction study of a liquid crystal with T-shaped molecules, and show that elastic properties are significantly different than that of bent-core and rod-like molecules.

7.2 Results and Discussion

7.2.1 Sample and phase behaviour

The compound used in the present study was synthesized by M. C. Varia *et al.* [1]. The chemical structure of the compound is shown in figure 7.1. It has the following phase sequence: Cr 90 °C SmA 108 °C N 128 °C I.

Cr 90 °C SmA 108 °C N 128 °C I
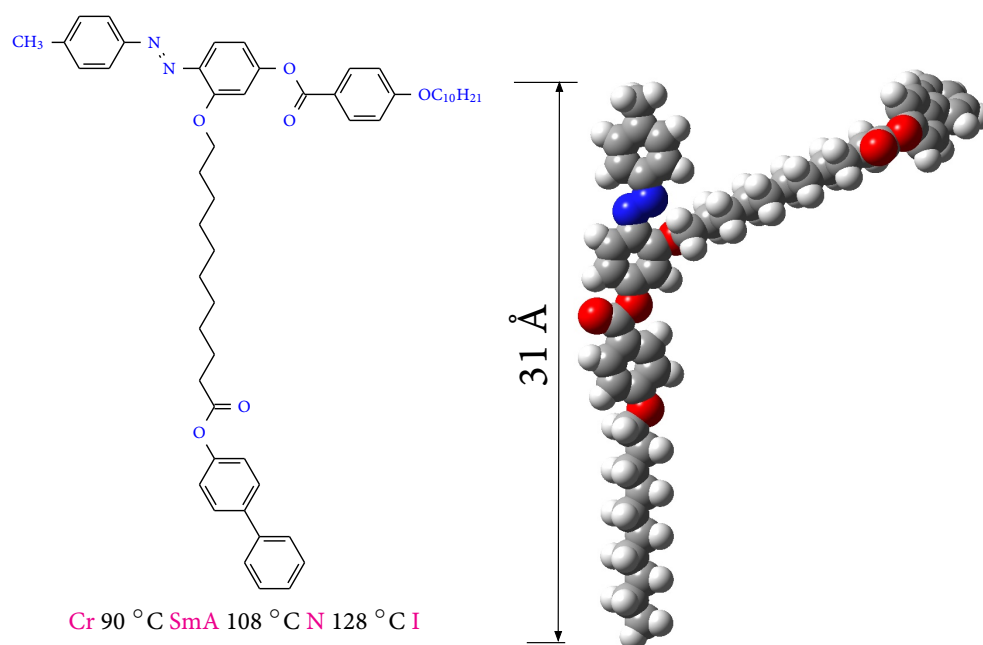
Figure 7.1: *Chemical structure and the energy minimized structure obtained from quantum chemical calculations using GAUSSIAN-03.*

A typical schlieren texture in the nematic phase at 123 °C and a focal conic texture in the SmA phase at 103 °C are shown in figure 7.2.

7.2.2 Optical and static dielectric measurements

The variation of birefringence (Δn) in the nematic and the SmA phases as a function of temperature is shown in figure 7.3. Δn develops sharply at the nematic-isotropic
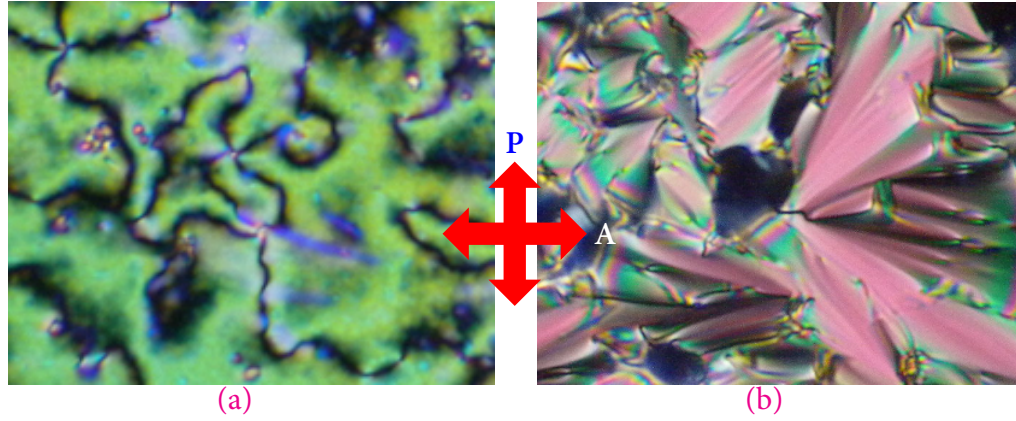
Figure 7.2: *(a) Schlieren texture in nematic phase (at 123 °C) and (b) Focal conic texture in SmA phase (at 103 °C).*
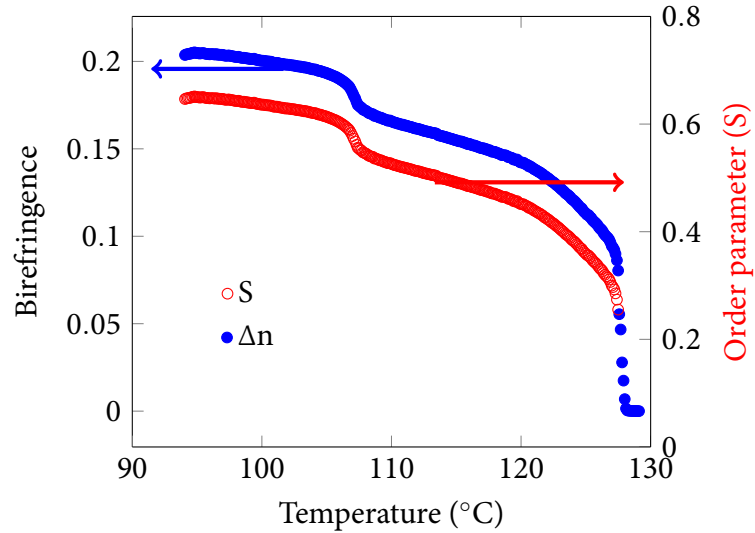
Figure 7.3: *Variation of birefringence (Δn) and order parameter (S) as a function of temperature.*

phase transition as expected and gradually increases as the temperature decreases in the nematic phase. A significant increase in Δn is also observed in the SmA phase (below 108 °C). The temperature dependent Δn in nematic liquid crystals can be approximated by the formula $\Delta n = \Delta n_{\circ}(1 - T/T^{**})^{\beta}$, where T^{**} and β are the adjustable fit parameters and $\Delta n_{\circ}$ is the birefringence of the perfectly aligned sample. The equation fits well in the entire nematic range with fit parameters $\Delta n_{\circ} = 0.31$ and $\beta = 0.21$. The order parameter S was estimated using the relation $S = \Delta n/\Delta n_{\circ}$. The temperature variation of the calculated order parameter is also shown in figure 7.3. The jump
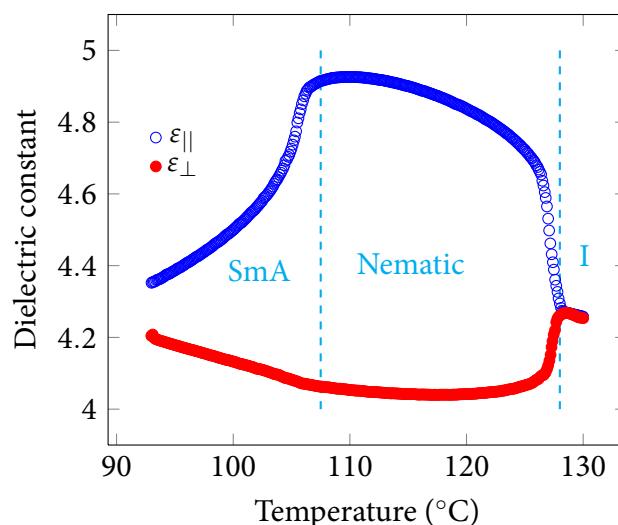
Figure 7.4: *Variation of parallel ($\varepsilon_{||}$) and perpendicular ($\varepsilon_{\perp}$) components of the dielectric constant as a function of temperature.*

in the order parameter at the nematic-isotropic transition was 0.25 and it increases to 0.65 (at 95 °C) with a significant increase $\Delta S_{SN} \simeq 0.06$ (at 107 °C) in the SmA phase. There have been many experimental and theoretical studies on the nematic to SmA (SN) transition in compounds with rod-like molecules. The coupling between the smectic order parameter ψ and the fluctuations in the nematic order parameter S can cause a crossover toward a tricritical point leading to a first order transition as the McMillan parameter α ($=T_{SN}/T_{NI}$) approaches to 1 [2]. The theoretical value of α for the crossover to the tricritical point is $\alpha \simeq 0.83$. However, the experimental value of α is not unique and is slightly higher [3], and it also depends on the type of the SmA phase [4–6]. The value of α for the present compound is 0.95 and is well above the tricritical point value. The large value of ΔS_{SN} ($\simeq 0.06$) in addition to large α suggests that the present nematic to SmA transition is first order in nature. A small increase in S in the nematic to SmA transition is also known in many other calamitic liquid crystals such as 8OCB (4-octyloxy 4'- cyanobiphenyl) [7], 8CB (4-octyl-4'-cyanobiphenyl) [8] and in some banana shaped compounds (chapter-5). In the case of 8CB the jump in the order parameter ΔS_{SN} is $\simeq 0.01$ and the nematic to SmA transition is considered to be weakly first order [9]. In the present compound ΔS_{SN} ($\simeq 0.06$) is much larger than that of 8CB. We also measured the enthalpies of isotropic-nematic (ΔH_{NI}) and

nematic-SmA transitions (ΔH_{SN}) using a differential scanning calorimeter. They are ΔH_{NI}=2.0 kJ/mol and ΔH_{SN}=1.6 kJ/mol, respectively. Thus enthalpies of both these transitions are *comparable* for present compound whereas ΔH_{SN} is $\sim$ 11 and $\sim$ 22 times smaller than ΔH_{NI} in case of 8CB and 8OCB, respectively [10]. The large values of ΔS_{SN} and enthalpy (ΔH_{SN}) further support first order nature of the nematic-SmA transition. The temperature variation of parallel ($\varepsilon_{||}$) and perpendicular ($\varepsilon_{\perp}$) components of the dielectric constant are shown in figure 7.4. The dielectric anisotropy is small and positive ($\Delta\varepsilon = 0.9$ at T=115 °C) in the nematic phase, and reduces in the SmA phase. The temperature dependent dielectric anisotropy is interpreted on the basis of the role of permanent dipoles and the molecular shape. The molecules have both longitudinal and transverse dipole components mainly due to the azo and ester linkages. The partial suppression of the transverse dipole moment in the nematic phase is made possible by largely unhindered rotations about the long molecular axis. This leads to a positive $\Delta\varepsilon$ in the nematic phase. In the SmA phase the dielectric anisotropy is reduced because the rotations about their long axes are more hindered due to the presence of a long side chain. This results in developing a quasi-macroscopic transverse dipole as suggested in previous chapters. Further, the increased in-layer dipolar correlation as reported by de Jeu *et al.* [11] has significant contribution in reducing the dielectric anisotropy in the SmA phase.

7.2.3   Splay, bend elastic constant measurements

Voltage dependent retardation is used to measure splay and bend elastic constants as described in chapter-2. The temperature dependent variation of both K_{11} and K_{33} is shown in figure 7.5. The variation of K_{33} near T_{NI} is proportional to S^2 and increases as the temperature is reduced similar to its variation as seen in many calamitic liquid crystals, diverging rapidly as the nematic-SmA transition is approached. Interestingly we find that the temperature dependence of K_{11} is the same as that of K_{33}. The ratio

$K_{33}/K_{11} \simeq 1$ at all temperatures except very close to the nematic-SmA transition. This ratio varies from 2 to 6 in case of rod-like molecules (e.g., 8OCB) as the temperature is reduced from the isotropic-nematic to the nematic-SmA transition. K_{33} shows strong pretransitional divergence as predicted and is given by $K_{33} = K_{33}^0 + A[(T/T_{NS}) - 1]^{-x}$ [12, 13], where K_{33}^0 is the background nematic contribution and x is the critical exponent. In the present compound $x=1\pm0.09$ which is similar to the value reported in 8CB [8].

Priest [14] showed that the Frank elastic constants may be expressed in terms of even-order Legendre polynomials averaged over the one-molecule orientational distribution function. It is found that

$$
\begin{aligned}
K_{11}/\bar{K} &= 1 + \Delta - 3\Delta'\bar{P}_4/\bar{P}_2 \\
K_{22}/\bar{K} &= 1 - 2\Delta - \Delta'\bar{P}_4/\bar{P}_2 \\
K_{33}/\bar{K} &= 1 + \Delta + 4\Delta'\bar{P}_4/\bar{P}_2
\end{aligned}
\tag{7.1}
$$

where $\bar{K} = (1/3)(K_{11} + K_{22} + K_{33})$, P_2 and P_4 are second and fourth order Legendre polynomials respectively, and Δ and Δ' are constants depending on molecular properties and are given by

$$
\begin{aligned}
\Delta &= (2R^2 - 2)/(7R^2 + 20) \\
\Delta' &= 9/16(3R^2 - 8)/(7R^2 + 20).
\end{aligned}
\tag{7.2}
$$

Here $R = (L - D)/D$, where L and D are the effective length and the width of spyro-cylindrical molecule.

Using equation 7.1 the ratio K_{33}/K_{11} can be written as

$$
K_{33}/K_{11} = (1 + \Delta + 4\Delta'\overline{P_4}/\overline{P_2})/(1 + \Delta - 3\Delta'\overline{P_4}/\overline{P_2}).
\tag{7.3}
$$

Since the molecules have long flexible lateral group, we calculated the radius of gyration along the long axis to estimate their width. It turns out that this effective width ($\simeq 9$ Å) is about a third of the experimentally measured length of the long axis (28.8 Å, discussed below), i.e., $L \simeq 3D$. Assuming $\overline{P_4}/\overline{P_2}$ is small ($\simeq 0.1$) and $L \simeq 3D$ (i.e., $R \simeq 2$) the estimated ratio of $K_{33}/K_{11} \simeq 1$ which is close to the experimental value (fig. 7.5).
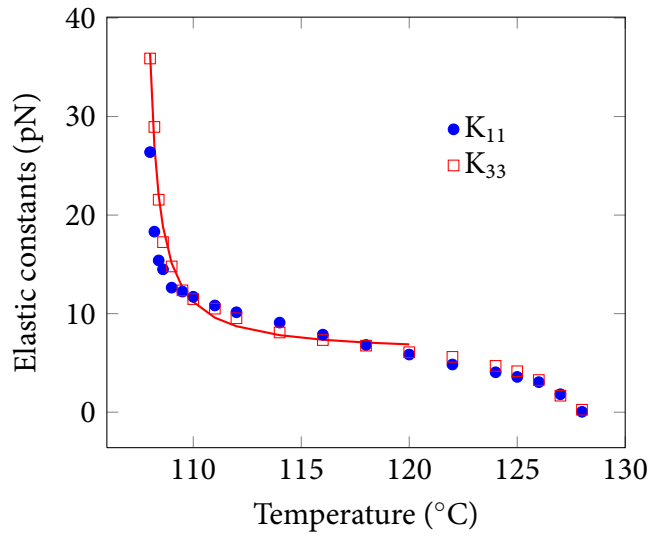
Figure 7.5: *Variation of K_{11} and K_{33} as a function of temperature. Solid line is a theoretical fit to $K_{33} = K_{33}^0 + A[(T/T_{NS}) - 1]^{-x}$.*
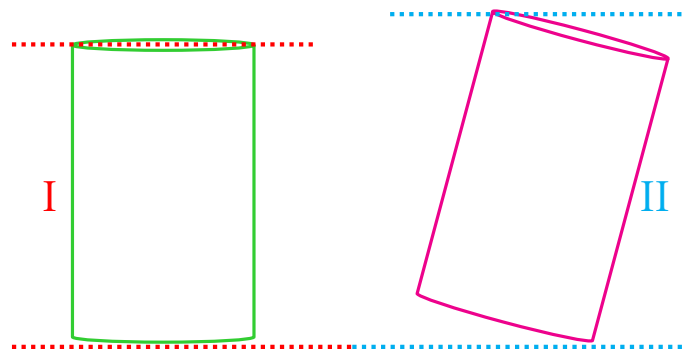
Figure 7.6: *Schematic of the splay fluctuations at the onset of short-range smectic order. Note the tilting of the molecule (splay deformation) is associated with a change in the layer spacing in II.*

The divergence of K_{11} is a consequence of suppression of splay fluctuations as SmA phase is approached. This looks unusual since the splay fluctuations are taken to be

compatible with the constant layer spacing requirement of smectics in conventional liquid crystals. However in the present case, the molecule has a long flexible lateral group and is undergoing largely unhindered rotations along the long axis. This seems to modify the aspect ratio of the molecules, effectively making it 3 (i.e., $L \simeq 3D$), depicted as a cylinder in figure 7.6(I). Splay fluctuations involving such objects lead to significant changes in the layer spacing as shown schematically in figure 7.6(II), necessitating relatively large elastic energy. Hence the splay fluctuations are considerably suppressed leading to the observed divergence in K_{11}. Further, compared to more rigid molecules the flexible terminal alkyl chains and long flexible lateral groups have the potential to partially hinder the mutual sliding of the molecules along each other. The consequent close proximity of aromatic cores of neighbouring molecules may also be responsible for larger effective width, thus supporting the experimental observations.

7.2.4 X-ray measurement
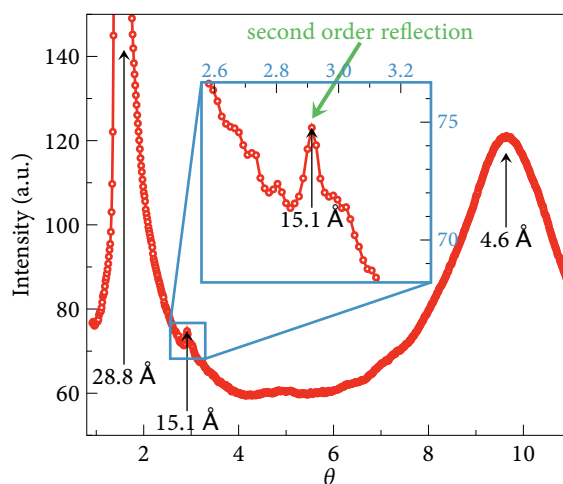
Figure 7.7: *X-ray intensity as a function of angle θ. (inset) A small second order reflection is shown.*

Finally we discuss the arrangement of T-shaped molecules in the smectic layers from the X-ray diffraction measurements. Typical intensity profile as a function of angle θ is
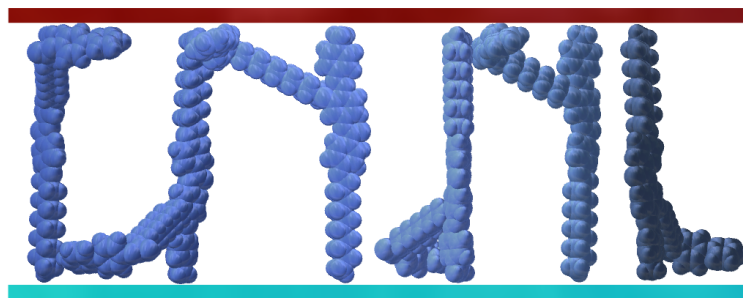
Figure 7.8: *Schematic arrangement of the molecules in the Sm-A phase.*

shown in figure 7.7. Two sharp reflections in the small-angle region with spacing 28.8 Å, 15.1 Å, as well as an additional broad diffuse wide-angle reflection at about 4.6 Å can be seen. Ratio of the first two spacings 1:1/2 clearly indicates a layered structure. Length of different segments of a single molecule were also estimated from energy minimized structure by considering different dihedral angles. The average length of the particular segment, containing three phenyl rings, azo and ester linkages with two terminal alkyl chains, is $L \simeq 31$ Å (fig. 7.1). This suggests that L is parallel to the smectic layer normal and the flexible chains are randomly oriented in the plane of the smectic layer as schematically shown in figure 7.8. Slightly lower value of the experimentally measured length (i.e., 28.8 Å), compared to the computed L value (= 31 Å) from the energy minimized structure, suggests that the molecules is not fully stretched in the SmA phase.

7.3 Conclusions

In conclusion, we for the fist time measured elastic constants K_{11} and K_{33} as a function of temperature in a liquid crystal with T-shaped molecules exhibiting *both* first order isotropic-nematic and nematic-SmA transitions. Our measurements show that $K_{33}/ K_{11} \simeq 1$ and *both* diverge as the SmA is approached. These results suggest that

the length to effective width ratio of the molecule is smaller than that of rigid rod-like molecules due to the presence of long flexible lateral group. Small angle X-ray diffraction and energy minimized structure suggest that the three phenyl rings and two linkages (azo and ester) and two terminal alkyl chains form the long axis. This axis is parallel to the the SmA layer normal and the flexible lateral groups are in the plane. This system may prove to be a convenient medium for testing theoretical models based on one elastic constant approximation.

References

[1] M. Varia, S. Kumar, and A. Prajapati, "T-shaped non-symmetrical twin liquid crystalline compounds," *Liquid Crystals*, vol. 39, no. 8, pp. 933–942, 2012.

[2] W. L. McMillan, "X-ray scattering from liquid crystals. i. cholesteryl nonanoate and myristate," *Phys. Rev. A*, vol. 6, pp. 936–947, Sep 1972.

[3] C. W. Garland and G. Nounesis, "Critical behavior at nematic-smectic-*A* phase transitions," *Phys. Rev. E*, vol. 49, pp. 2964–2971, Apr 1994.

[4] M. E. Huster, K. J. Stine, and C. W. Garland, "Calorimetric study of nematic-smectic-*A* tricritical behavior in mixtures of heptyloxypentylphenylthiolben-zoate and octyloxycyanobiphenyl," *Phys. Rev. A*, vol. 36, pp. 2364–2371, Sep 1987.

[5] J. Caerels, C. Glorieux, and J. Thoen, "Photopyroelectric ac calorimetric study of the nematic- smectic-*A* phase-transition line in binary liquid crystal mixtures with injected smectic- *A* phases," *Phys. Rev. E*, vol. 65, p. 031704, Feb 2002.

[6] J. Thoen, H. Beringhs, J. M. Auguste, and G. Sigaud, "Adiabatic scanning calorimetry of the nematic-smectic a1 and the smectic a1–smectic a transitions in frustrated smectic mixtures at low temperatures," *Liquid Crystals*, vol. 2, no. 6, pp. 853–863, 1987.

[7] B. Kundu, R. Pratibha, and N. V. Madhusudana, "Anomalous temperature dependence of elastic constants in the nematic phase of binary mixtures made of rodlike and bent-core molecules," *Phys. Rev. Lett.*, vol. 99, p. 247802, Dec 2007.

[8] S. W. Morris, P. Palffy-muhoray, and D. A. Balzarini, "Measurements of the bend and splay elastic constants of octyl-cyanobiphenyl," *Molecular Crystals and Liquid Crystals*, vol. 139, no. 3-4, pp. 263–280, 1986.

[9] I. Lelidis, "Experimental evidence of the halperin-lubensky-ma effect in liquid crystals," *Phys. Rev. Lett.*, vol. 86, pp. 1267–1270, Feb 2001.

[10] G. Oweimreen and M. Morsy, "Dsc studies on p-(n-alkyl)-p'-cyanobiphenyl (rcb's) and p-(n-alkoxy)-p'-cyanobiphenyl (rocb's) liquid crystals," *Thermochimica Acta*, vol. 346, no. 1-2, pp. 37 – 47, 2000.

[11] W. H. de Jeu, T. W. Lathouwers, and P. Bordewijk, "Dielectric properties of di-*n*-heptyl azoxybenzene in the nematic and in the smectic-*a* phases," *Phys. Rev. Lett.*, vol. 32, pp. 40–43, Jan 1974.

[12] T. C. Lubensky, "The nematic to smectic-a transition: a theoretical overview," *Journal de Chimie Physique et de Physico-Chimie Biologique*, vol. 80, pp. 31–43, 1983.

[13] P. G. De Gennes, "Some remarks on the polymorphism of smectics," *Molecular Crystals and Liquid Crystals*, vol. 21, no. 1-2, pp. 49–76, 1973.

[14] R. G. Priest, "Theory of the frank elastic constants of nematic liquid crystals," *Phys. Rev. A*, vol. 7, pp. 720–729, Feb 1973.

8

Large antagonistic flexoelectric response in liquid crystal mixture of bent-core and rod-like molecules

8.1 Introduction

ABOUT 40 years ago Meyer predicted that the nematic liquid crystals can exhibit microscope polarization due to the distortions in the director field [1]. This is known as flexoelectric effect. It was shown that the distortion induced polarization is given by

$$\vec{P} = e_1(\nabla . \hat{n})\hat{n} + e_3(\nabla \times \hat{n}) \times \hat{n} \qquad (8.1)$$

where e_1 and e_3 are the flexoelectric coefficients connected to the splay and bend distortions respectively. Since then a large number of experimental investigations are

reported and continuous efforts are made to enhance and understand this effect in various liquid crystalline systems such as chiral nematics [2, 3], blue phase liquid crystals [4, 5] and lipid bilayers [6]. It is well established that the origin of this effect is the molecular shape asymmetry such as seen in bent-core or wedge shaped molecules. Nematic liquid crystals with wedge shaped molecules and longitudinal dipole moments can induce flexoelectric polarization when splayed. Similarly bent-core molecules with transverse dipole moments can induce the flexoelectric polarization when it is subjected to a bend deformation. The flexoelectro-optic effect is linear with applied field and can be exploited to make switchable and bistable device with sub millisecond response time [7]. However their application is limited due to the small flexoelectric polarization in conventional liquid crystals with rod-like molecules. It was theoretically shown by Helfrich [8] that in liquid crystals with bent-core molecules $e_3 \propto \Theta(b/a)^{2/3}\mu$, where μ is the transverse dipole moment, Θ is the bend angle, a and b are the length and breadth of the molecule. In the recent past a giant flexoelectricity in pure bent-core liquid crystal was reported by Harden *et al.* [9]. This triggered various flexoelectric studies on pure [10–12] as well as on the binary mixture of rod-like and bent-core molecules [13–16]. There are also some reports on the flexoelectric studies in bimesogenic liquid crystals [3, 17–19] with *cis* form. In most of these studies a significant enhancement of flexoelectric effect has been observed and it is expected that apart from the bistable device it has the potential to be used in sensors and micro electric power generators.

8.2   Results and Discussion

8.2.1   Samples and phase behaviour

We prepared two mixtures with different concentrations namely 4.5 mol % and 7 mol % of bent-core compounds with the calamitic compound, RO (fig. 8.1). The phase

Cr 98.5 °C SmA$_2$ 109.5 °C N 125.0 °C I

Cr 114 °C B$_2$ 128.5 °C I

Cr 84.4 °C SmA 151.6 °C I
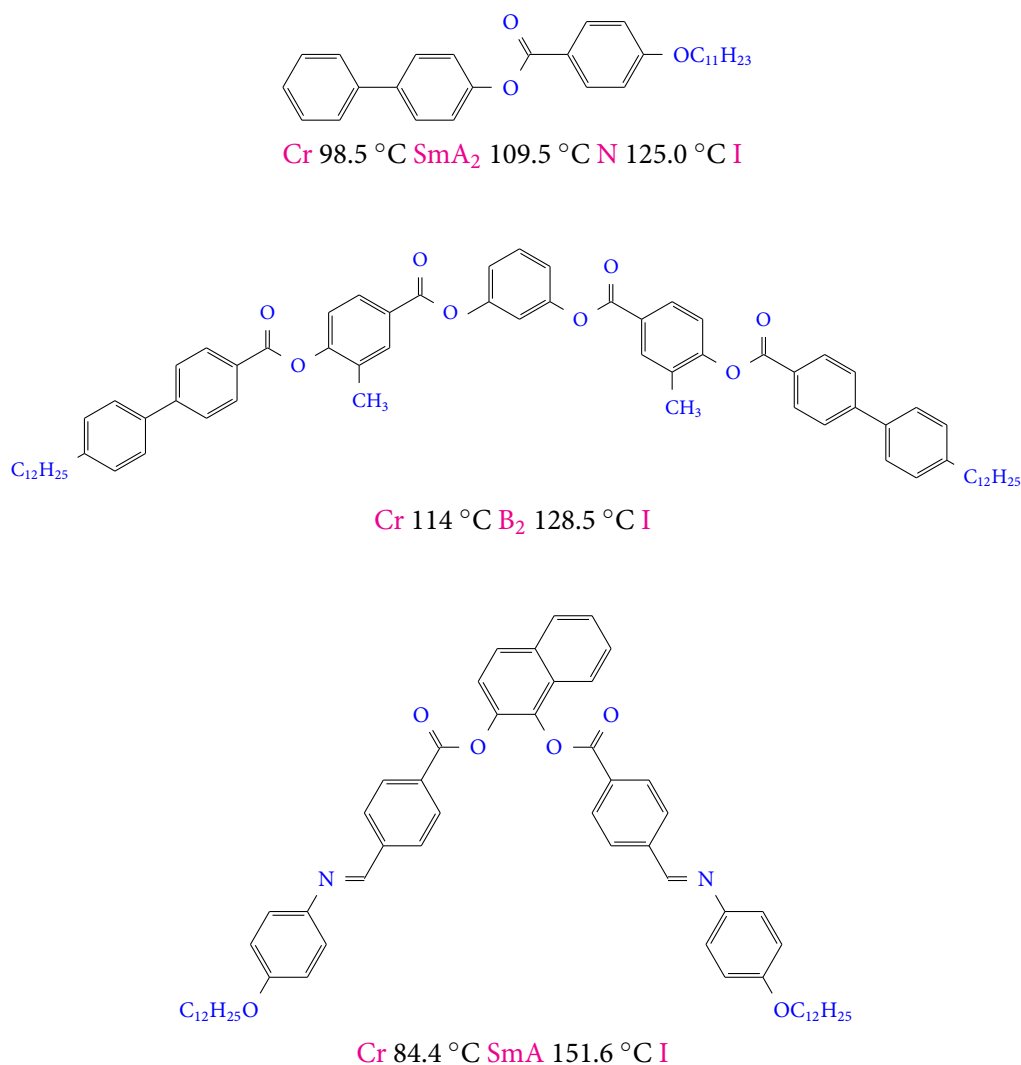
Figure 8.1: *Chemical structures and phase transition temperatures of the compounds. The first, second and third compounds are designated as RO, BC-120 and BC-60 respectively. The phase transition temperatures are indicated below each compounds.*

diagram of the binary mixture of BC-120 with RO is already reported [20]. The core of BC-120 is a resorcinol derivative substituted at the 1, 3 position and the bent angle is about 120°. The compound BC-60 has naphthalene core in which Schiff's based side wings are substitutes on 1, 2 positions. The synthesis and characterization of this compound was reported by Lee *et al.* [21]. It exhibits only liquid crystalline SmA phase and it was suggested from the X-ray studies that the arrow axis of the molecule is aligned *perpendicular* to the SmA layer. We found that the binary mixture of BC-60

and RO exhibits nematic phase in the low concentration range (< 10 mol %).

8.2.2 Flexoelastic measurements

We used a hybrid aligned nematic (HAN) cell as proposed by Dosov [22] to measure the flexo-elastic ratio e^*/K, where K is the average elastic constant of the nematic liquid crystal and $e^* = e_1 - e_3$. The experimental technique to measure e^*/K is explained earlier in chapter-2. In the present experiment $d = 20$ μm and the gap between the electrodes is 850μm. We used a motorized and computer controlled analyzer to measure azimuthal twist angle (φ) as a function of applied electric field and e^*/K was estimated from the best fit in the linear region. The error in the measurement is about 7% considering the errors from both the cell thickness measurement and the gradient of φ with electric field. It may be mentioned that we did not observe any domain formation in the cell within the range of applied field.
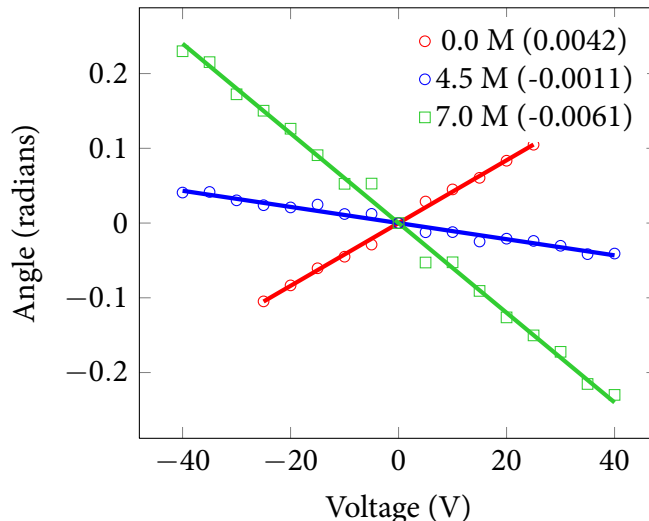
Figure 8.2: *Variation of field-induced azimuthal twist angle as a function of voltage in binary mixture of RO and BC-120 molecules. Solid lines represent the best fit to the equation $\varphi = e^* Ed/\pi$.*

We measured the azimuthal twist angle (φ) as a function of applied field for all the mixtures and the host compound. A representative variation of φ with the applied dc electric field in the mixtures with BC-120 molecule is shown in figure 8.2. It is
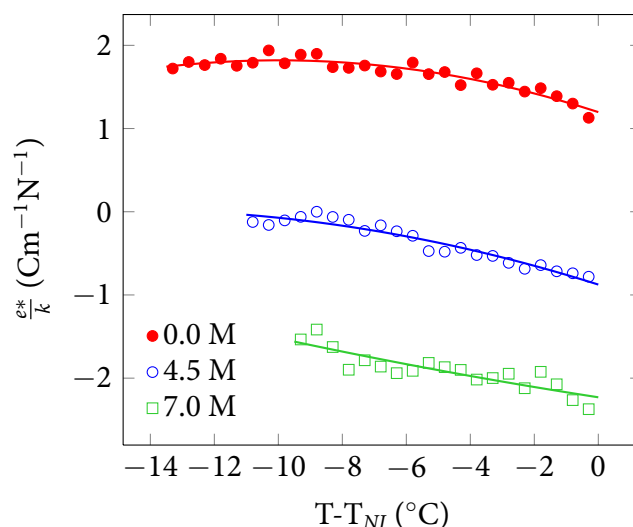
Figure 8.3: *Temperature variation flexo-elastic ratio e^*/K for mixtures with BC-120 for three different concentrations, 0, 4.5 and 7 mol %.*
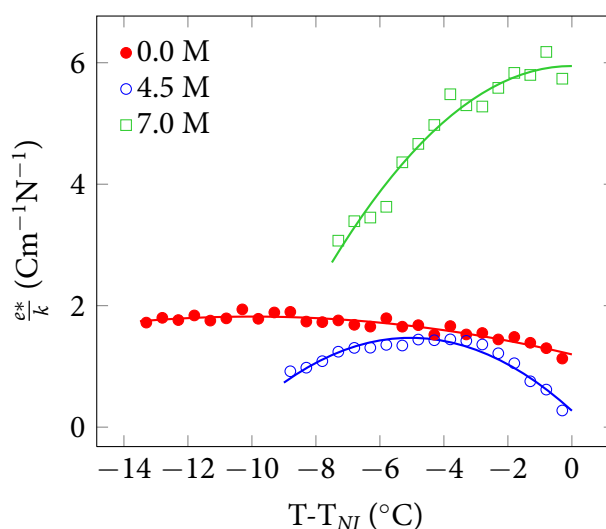
Figure 8.4: *Temperature variation flexo-elastic ratio e^*/K for mixtures with BC-60 for three different concentrations, 0, 4.5 and 7 mol %.*

noticed that the slope decreases and changes sign from positive to negative with increasing concentration of BC-120 molecules. The temperature variation of e^*/K of BC-120 is shown in figure 8.3. It is noticed that e^*/K decreases and changes sign with increasing concentration of BC-120 molecules (fig. 8.3). For example, in the host compound (RO), at a shifted temperature $T - T_{NI} = -5\,°C$, $e^*/K \simeq 1.7\ \mathrm{Cm^{-1}N^{-1}}$ and it reduces to $\simeq -0.48\ \mathrm{Cm^{-1}N^{-1}}$ when the concentration of BC-120 molecules

is 4.5 mol %. It changes sign and reduces to about -1.9 Cm^{-1}N^{-1} when the concentration is increased to 7 mol %. Assuming a linear variation, e^*/K of pure BC-120 liquid crystal is expected to be 30 times larger (negative) than the host compound. The temperature variation of e^*/K in the binary mixture of BC-120 and 8OCB (octyloxy cyanobiphenyl) was reported by Kundu *et al.*[15]. They found that e^*/K is negative and the magnitude increases significantly with increasing concentration of BC-120 molecules. They suggested that e^*/K in pure BC-120 compound could be 20 times larger than that of 8OCB. Thus in the present mixture the enhancement is significantly more than they reported. The compound RO appears to be a good host for BC-120 molecules for large flexoelectric response perhaps due to its partial structural similarity i.e., the aromatic and aliphatic parts of the rod are matched with one arm of the BC-120 molecule. Further it is observed that e^*/K is very weakly dependent on temperature (fig. 8.3). It is expected as both e^* and K is proportional to the square of the order parameter (S^2). e^* in the host compound RO is positive i.e., $e_1 > e_3$. Since the dopant molecule (BC-120) has large dipole moment along the arrow axis (i.e, transverse dipole), the bend distortion of the medium gives rise to a large e_3 with increasing concentration of BC-120 molecules and as a result e^*/K changes sign beyond a particular concentration. In figure 8.4 we show the temperature variation of e^*/K for the mixtures with BC-60 molecules. It remains positive but reduces slightly in the mixture (4.5 mol %) compared to the host compound (RO) and also exhibits weak temperature dependence. Interestingly it increases significantly in the mixture with 7 mol %. For example, at a shifted temperature $T - T_{NI} = -2\,^{\circ}$C, $e^*/K \simeq 1.5$ Cm^{-1}N^{-1} in host compound RO, and in the mixture it is $\simeq 5.8$ Cm^{-1}N^{-1} i.e., about 4 times larger and decreases rapidly with reducing temperature. Thus in the mixture (with BC-60), the sign of e^*/K is antagonistic in the sense that e^*/K is large positive compared to the large negative value at the same concentration with BC-120 molecules. Hence it is possible to tune significantly the magnitude and sign of flexoelectric coefficient by adding appropriate bent-core molecules.

8.2.3   Dielectric measurements
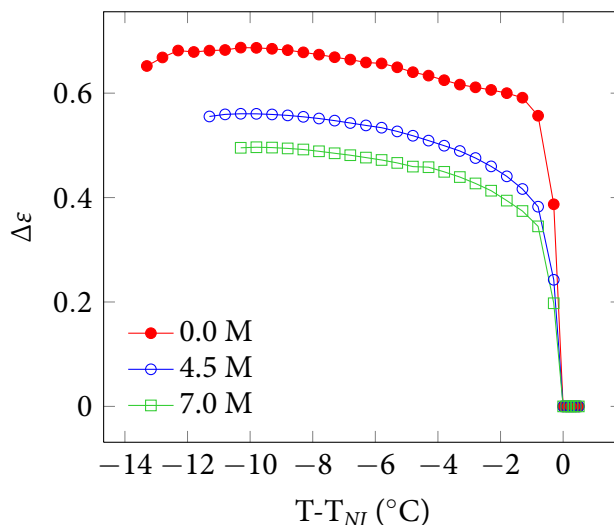
Figure 8.5: *Variation of dielectric anisotropy with temperature for mixtures with compound BC-120.*
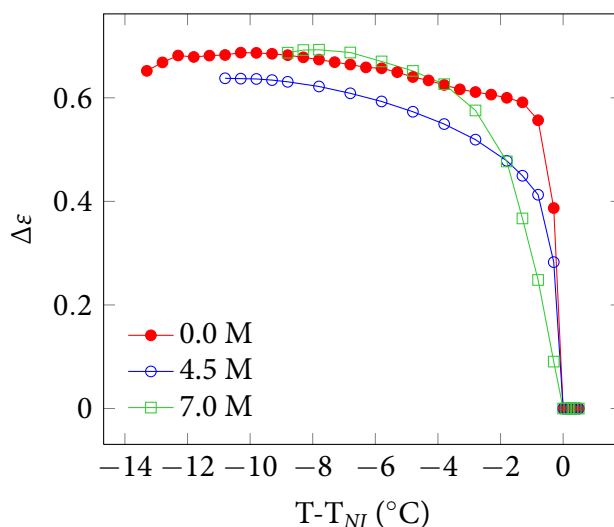
Figure 8.6: *Variation of dielectric anisotropy with temperature for mixtures with compound BC-60.*

To get an idea about the orientation of BC-60 and BC-120 molecules in the mixture we measured the dielectric anisotropy ($\Delta\varepsilon = \varepsilon_{||} - \varepsilon_{\perp}$) as a function of temperature at a frequency of 4111 Hz. The perpendicular component of dielectric constant ($\varepsilon_{\perp}$) was measured by using a LCR meter (Agilent 4980A) below the Freedericksz threshold voltage as a function of temperature. To estimate the parallel component ($\varepsilon_{||}$) ,
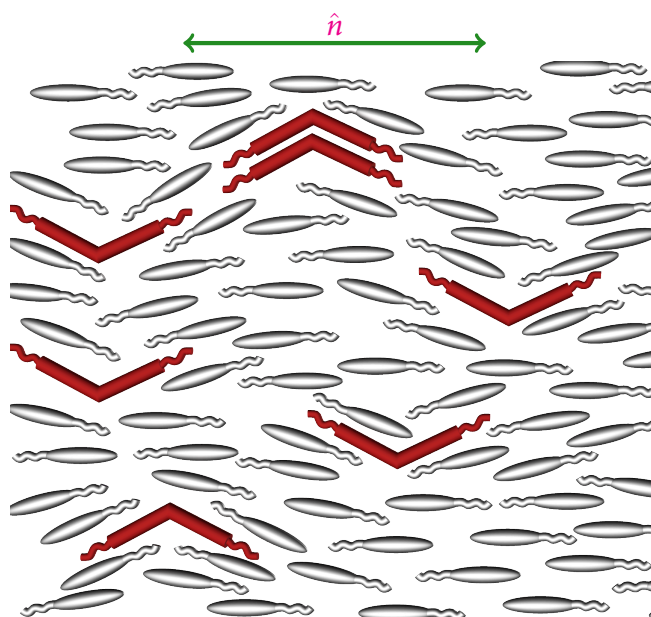
Figure 8.7: *Schematic representation of orientations of the bent-core molecules at higher concentration (7 mol %) for the BC-120 mixture*
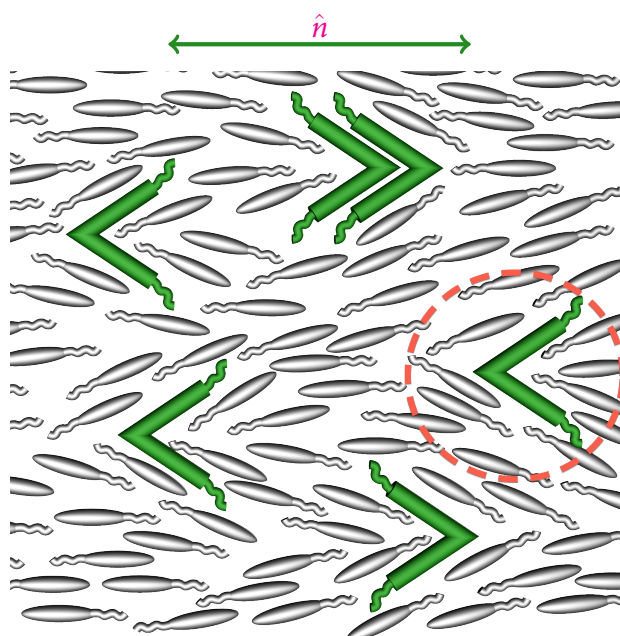
Figure 8.8: *Schematic representation of orientations of the bent-core molecules at higher concentration (7 mol %) for the BC-60 mixture*

we measured dielectric constant in the same cell as a function of voltage. Since the

dielectric anisotropy is positive, it increases with voltage and saturates at higher voltages. The linear part is plotted against $1/V$ and fitted to a straight line. The extrapolated value of dielectric constant at $1/V = 0$ provides $\varepsilon_{||}$. The temperature variation of $\Delta\varepsilon$ of all the samples are shown in figure 8.5 and figure 8.6. Measurement of viscoelastic properties and $\Delta\varepsilon$ of the mixtures with BC-120 was reported in chapter-3. It is observed that $\Delta\varepsilon$ is small and positive (fig. 8.5). At any shifted temperature it decreases with increasing concentration of BC-120 molecules. This indicates that the arrow axes are oriented perpendicular to the director as shown schematically in figure 8.5. The temperature variation of $\Delta\varepsilon$ of mixtures with BC-60 is not unique in the sense that it decreases at 4.5 mol % and then tends to increase at 7 mol % (fig. 8.6). The increase of $\Delta\varepsilon$ at 7 mol % suggests that the effective dipole moment along the director is increased i.e., the arrow axis of the molecule is orientated parallel to the director as the direction of dipole moment in the this molecule is along the arrow axis. On the other hand the decrease of $\Delta\varepsilon$ at 4 mol % can not be understood based on this model. However it may be noted that the terminal units of BC-60 molecules are alkoxy chains which have conformational freedom. As a result at low concentration of BC-60 molecules the transverse component of dipole moment can increase and hence $\Delta\varepsilon$ is reduced. Further, BC-60 can be considered as wedge shaped molecules that can generate substantial splay distortion in the host calamitic sample to reduce the steric interaction and can form a complex cluster [16] with increasing concentration (fig. 8.6). The longitudinal components of dipole moments can also get correlated and the conformational freedom of individual molecules in the cluster is reduced and as a result $\Delta\varepsilon$ can again increase. Presence of such clusters in the medium is expected to increase e_1 significantly than e_3 as a result e^*/K is large and positive (fig. 8.4). The effect of conformational freedom on the flexo-elastic coefficient in 8OCB liquid crystal was experimentally studied by Dosov *et al.*[23]. They reported that e^*/K decreases with reducing temperature. Using Landau de Gennes theory, Osipov [24] showed theoretically that it can be understood based on the average conformational degrees of freedom of alkoxy chains. The anomalous temperature dependence of e^*/K in the

present mixture is expected to originate from the similar conformational degrees of freedom of terminal alkoxy chains.

8.3   conclusions

In conclusion, we measured the flexoelectric coefficient of a binary mixture with bent-core molecules having two different bend angles. We showed that both the magnitude and sign can be tuned over a large range by adding small concentration of bent-core molecules with different bend angles. The arrow axes of the BC-120 molecules in the mixture are aligned perpendicular to the director whereas they are aligned parallel to the director in case of BC-60 molecules. Finally we showed that the appropriate selection of bent-core molecules in the binary mixture provides a viable route to greatly enhance and tune the sign of the flexoelectric properties for bistable liquid crystal displays.

References

[1] R. B. Meyer, "Piezoelectric effects in liquid crystals," *Phys. Rev. Lett.*, vol. 22, pp. 918–921, May 1969.

[2] J. S. Patel and R. B. Meyer, "Flexoelectric electro-optics of a cholesteric liquid crystal," *Phys. Rev. Lett.*, vol. 58, pp. 1538–1540, Apr 1987.

[3] H. J. Coles, M. J. Clarke, S. M. Morris, B. J. Broughton, and A. E. Blatch, "Strong flexoelectric behavior in bimesogenic liquid crystals," *Journal of Applied Physics*, vol. 99, no. 3, p. 034104, 2006.

[4] G. P. Alexander and J. M. Yeomans, "Flexoelectric blue phases," *Phys. Rev. Lett.*, vol. 99, p. 067801, Aug 2007.

[5] F. Castles, S. M. Morris, E. M. Terentjev, and H. J. Coles, "Thermodynamically stable blue phases," *Phys. Rev. Lett.*, vol. 104, p. 157801, Apr 2010.

[6] A. G. Petrov and F. Sachs, "Flexoelectricity and elasticity of asymmetric biomembranes," *Phys. Rev. E*, vol. 65, p. 021905, Jan 2002.

[7] C. V. Brown, L. Parry-Jones, S. J. Elston, and S. J. Wilkins, "Comparison of theoretical and experimental switching curves for a zenithally bistable nematic liquid crystal device," *Molecular Crystals and Liquid Crystals*, vol. 410, no. 1, pp. 417–425, 2004.

[8] W. Helfrich, "The strength of piezoelectricity in liquid crystals," *Z. Naturforsch*, vol. A26, pp. 833–835, 1971.

[9] J. Harden, B. Mbanga, N. Éber, K. Fodor-Csorba, S. Sprunt, J. T. Gleeson, and A. Jákli, "Giant flexoelectricity of bent-core nematic liquid crystals," *Phys. Rev. Lett.*, vol. 97, p. 157802, Oct 2006.

[10] J. Harden, R. Teeling, J. T. Gleeson, S. Sprunt, and A. Jákli, "Converse flexoelectric effect in a bent-core nematic liquid crystal," *Phys. Rev. E*, vol. 78, p. 031702, Sep 2008.

[11] K. Van Le, F. Araoka, K. Fodor-Csorba, K. Ishikawa, and H. Takezoe, "Flexoelectric effect in a bent-core mesogen," *Liquid Crystals*, vol. 36, no. 10-11, pp. 1119–1124, 2009.

[12] P. Kumar, Y. G. Marinov, H. P. Hinov, U. S. Hiremath, C. V. Yelamaggad, K. S. Krishnamurthy, and A. G. Petrov, "Converse flexoelectric effect in bent-core nematic liquid crystals," *The Journal of Physical Chemistry B*, vol. 113, no. 27, pp. 9168–9174, 2009. PMID: 19522471.

[13] J. H. Wild, K. Bartle, N. T. Kirkman, S. M. Kelly, M. O'Neill, T. Stirner, and R. P. Tuffin, "Synthesis and investigation of nematic liquid crystals with flexoelectric properties," *Chemistry of Materials*, vol. 17, no. 25, pp. 6354–6360, 2005.

[14] N. Aziz, S. M. Kelly, W. Duffy, and M. Goulding, "Banana-shaped dopants for flexoelectric nematic mixtures," *Liquid Crystals*, vol. 35, no. 11, pp. 1279–1292, 2008.

[15] B. Kundu, A. Roy, R. Pratibha, and N. V. Madhusudana, "Flexoelectric studies on mixtures of compounds made of rodlike and bent-core molecules," *Applied Physics Letters*, vol. 95, no. 8, p. 081902, 2009.

[16] J.-H. Lee, T.-H. Yoon, and E.-J. Choi, "Flexoelectric effect of a rod-like nematic liquid crystal doped with highly-kinked bent-core molecules for energy converting components," *Soft Matter*, vol. 8, pp. 2370–2374, 2012.

[17] C. Noot, M. J. Coles, B. Musgrave, S. P. Perkins, and H. J. Coles, "The flexoelectric behaviour of a hypertwisted chiral nematic liquid crystal," *Molecular Crystals and Liquid Crystals Science and Technology. Section A. Molecular Crystals and Liquid Crystals*, vol. 366, no. 1, pp. 725–733, 2001.

[18] C. Schott, S. P. Perkins, and H. J. Coles, "Physical properties of some novel nematic bimesogens for the flexoelectric effect," *Molecular Crystals and Liquid Crystals Science and Technology. Section A. Molecular Crystals and Liquid Crystals*, vol. 366, no. 1, pp. 715–724, 2001.

[19] D. S. Hermann, P. Rudquist, K. Ichimura, K. Kudo, L. Komitov, and S. T. Lagerwall, "Flexoelectric polarization changes induced by light in a nematic liquid crystal," *Phys. Rev. E*, vol. 55, pp. 2857–2860, Mar 1997.

[20] R. Pratibha, N. V. Madhusudana, and B. K. Sadashiva, "An orientational transition of bent-core molecules in an anisotropic matrix," *Science*, vol. 288, no. 5474, pp. 2184–2187, 2000.

[21] S. K. Lee, Y. Naito, L. Shi, M. Tokita, H. Takezoe, and J. Watanabe, "Mesomorphic behaviour in bent-shaped molecules with side wings at different positions of a central naphthalene core," *Liquid Crystals*, vol. 34, no. 8, pp. 935–943, 2007.

[22] Dozov, I., Martinot-Lagarde, Ph., and Durand, G., "Flexoelectrically controlled twist of texture in a nematic liquid crystal," *J. Physique Lett.*, vol. 43, no. 10, pp. 365–369, 1982.

[23] Dozov, I., Martinot-Lagarde, Ph., and Durand, G., "Conformational flexoelectricity in nematic liquid crystals," *J. Physique Lett.*, vol. 44, no. 19, pp. 817–822, 1983.

[24] Osipov, M.A., "The order parameter dependence of the flexoelectric coefficients in nematic liquid crystals," *J. Physique Lett.*, vol. 45, no. 16, pp. 823–826, 1984.

Curriculum Vitae

Paladugu Sathyanarayana

Curriculum Vitae

Contact   P. Sathyanarayana,

School of Physics,

University of Hyderabad,

Gachibowli, Hyderabad,

Andhra Pradesh, INDIA: 500 046

Phone: +91-99669 78238

Email: paladugu_sathya@me.com

Research Interests

My research interest lies in the field of Soft matter Physics. Mainly on structure-property correlation, visco-elastic, electro-optical properties and phase transitions of unconventional and nano particle

dispersed liquid crystals. I am also interested in the optical properties of various other soft materials.

Educational Qualifications

Doctor of Philosophy (Ph. D.)

School of Physics, University of Hyderabad, Andhra Pradesh, INDIA.

> Thesis title: "Investigation on the physical properties of unconventional nematic liquid crystals"
>
> Research Adviser: Dr. Surajit Dhara.

M. Sc., Physics, April 2007

Acharya Nagarjuna University, Nagarjuna Nagar, Guntur(dt), Andhra Pradesh.

> Percentage: 73.7 %
>
> Specialization: *Condensed matter physics*

B. Sc., Electronics, March 2005

T. J. P. S. College (Acharya Nagarjuna University), Guntur, Andhra Pradesh.

> Percentage: 85.5 %
>
> Other subjects: *Physics* and *Mathematics*

Publications

Journal Papers

1. **Antagonistic flexoelectric response in liquid crystal mixture of bent-core and rod-like molecules**
   P. Sathyanarayana and Surajit Dhara

PHYSICAL REVIEW E (*under review*)

2. **Structure-property correlation of a hockey stick-shaped compound exhibiting N-SmA-SmC$_a$ phase transitions**
   P. Sathyanarayana, S. Radhika, B. K. Sadashiva and Surajit Dhara
   Soft Matter, **8**, 2322 (2012)

3. **Viscoelasticity of ambient-temperature nematic binary mixtures of bent-core and rod-like molecules**
   P. Sathyanarayana, V. S. R. Jampani, Miha Skarabot, I. Musevic, K. V. Le, Hideo Takezoe and Surajit Dhara
   PHYSICAL REVIEW E **85**, 011702 (2012)

4. **Splay-bend elasticity and rotational viscosity of liquid crystal mixtures of rod-like and bent-core molecules**
   P. Sathyanarayana, B. K. Sadashiva and Surajit Dhara
   Soft Matter, **7**, 8556 (2011)

5. **Splay-bend elasticity of a nematic liquid crystal with T-shaped molecules**
   P. Sathyanarayana, M. C. Varia, A. K. Prajapati, B. Kundu, V. S. S. Sastry, and S. Dhara
   PHYSICAL REVIEW E **82**, 050701(R) (2010)

6. **Rotational Viscosity of a Bent-Core Nematic Liquid Crystal**
   Paladugu Sathyanarayana, Tatipamula Arun Kumar, Vanka Srinivasa Suryanarayana Sastry, Manoj Mathews, Quan Li, Hideo Takezoe, and Surajit Dhara
   Applied Physics Express **3**, 091702 (2010)

7. **Splay bend elasticity of a bent-core nematic liquid crystal**

   P. Sathyanarayana, M. Mathew, Q. Li, V. S. S. Sastry, B. Kundu, K. V. Le, H. Takezoe, and Surajit Dhara

   PHYSICAL REVIEW E **81**, 010702(R) (2010)

8. **Temperature- and electric-field-induced inverse Freedericksz transition in a nematogen with weak surface anchoring**

   T. Arun Kumar, P. Sathyanarayana, V. S. S. Sastry, Hideo Takezoe, N. V. Madhusudana, and Surajit Dhara

   PHYSICAL REVIEW E **82**, 011701 (2010)

Career Achievements

Qualified National Eligibility Test -2007 for Juniour research fellowship and lectureship conducted by Council of Scientific and Industrial Research and University Grants Commission (CSIR & UGC), Indian Government.

Qualified Joint Entrance Screening Test (*JEST is a common qualifying test for admissions to Ph.D. programmes in Physics at premier Indian research institutions*) in Feb 2008 and got All India Rank 563.

Qualified Graduate Aptitude Test in Engineering (*GATE is an all India examination administered and conducted jointly by the Indian Institute of Science and seven Indian Institutes of Technology on behalf of the National Coordination Board - GATE, Department of Higher Education, Ministry of Human Resource Development (MHRD), Government of India.*) in Feb 2007 and got All India Rank 473 in Physics.

Achieved Andhra Pradesh Association of Mathematics Teachers (APAMT), XXVIII MATHEMATICAL OLYMPIAD 2000, Merit Certificate of Senior level.

Computer Skills

LabVIEW, LaTeX and Mathematica.

Personal

Citizenship: Indian

Marital Status: Single

Date of Birth: 25-07-1985

December 2012

Publications

Publications

[1] P. Sathyanarayana and Surajit Dhara. Antagonistic flexoelectric response in liquid crystal mixture of bent-core and rod-like molecules. *Physical Review E* (under review).

[2] P. Sathyanarayana, S. Radhika, B. K. Sadashiva, and Surajit Dhara. Structure-property correlation of a hockey stick-shaped compound exhibiting N-SmA-SmC$_a$ phase transitions. *Soft Matter*, **8** (7), 2322, (2012).

[3] P. Sathyanarayana, V. S. R. Jampani, Miha Skarabot, I. Musevic, K. V. Le, Hideo Takezoe, and Surajit Dhara. Viscoelasticity of ambient-temperature nematic binary mixtures of bent-core and rodlike molecules. *Physical Review E*, **85**, 011702, (2012).

[4] P. Sathyanarayana, B. K. Sadashiva and Surajit Dhara. Splay-bend elasticity and rotational viscosity of liquid crystal mixtures of rod-like and bent-core molecules. *Soft Matter*, **7** (18), 8556, (2011).

[5] P. Sathyanarayana, M. C. Varia, A. K. Prajapati, B. Kundu, V. S. S. Sastry, and S. Dhara. Splay-bend elasticity of a nematic liquid crystal with T-shaped molecules. *Physical Review E*, **82**, 050701(R), (2010).

140

[6] Paladugu Sathyanarayana, Tatipamula Arun Kumar, Vanka Srinivasa Surya-narayana Sastry, Manoj Mathews, Quan Li, Hideo Takezoe, and Surajit Dhara Dhara. Rotational Viscosity of a Bent-Core Nematic Liquid Crystal. *Applied Physics Express*, **3** (9), 091 702, (2010).

[7] P. Sathyanarayana, M. Mathew, Q. Li, V. S. S. Sastry, B. Kundu, K. V. Le, H. Takezoe, and Surajit Dhara. Splay bend elasticity of a bent-core nematic liquid crystal. *Physical Review E*, **81**, 010702(R), (2010).

[8] T. Arun Kumar, P. Sathyanarayana, V. S. S. Sastry, Hideo Takezoe, N. V. Madhusudana, and Surajit Dhara. Temperature- and electric-field-induced inverse Freedericksz transition in a nematogen with weak surface anchoring. *Physical Review E*, **82**, 011701, (2010).